Chapter 2

Probing Individual Environmental Bacteria for Viruses Using Microfluidic Digital PCR

2.1 Abstract

Viruses may very well be the most abundant biological entities on the planet. Yet neither metagenomic studies nor classical phage isolation techniques have shed much light on the identity of the hosts of most viruses. We used a microfluidic digital PCR approach to physically link single bacterial cells harvested from a natural environment with a viral marker gene. When we implemented this technique on the microbial community residing in the termite hindgut, we found genus-wide infection patterns displaying remarkable intra-genus selectivity. Viral marker allelic diversity revealed restricted mixing of alleles between hosts indicating limited lateral gene transfer of these alleles despite host proximity. Our approach does not require culturing hosts or viruses and provides a method for examining virus-bacterium interactions in many environments.

2.2 Introduction

Despite the pervasiveness of bacteriophages in nature and their postulated impact on diverse ecosystems (*1*), we have a poor grasp of the biology of these viruses and their host specificity in the wild. Though significant progress has been made with certain host-virus systems such as cyanophages (*2-5*), this is the exception rather than the rule. Conventional plaque assays used to isolate environmental viruses are not applicable to >99% of microbes in nature since the vast preponderance of the microbial diversity on Earth has yet to be cultured *in vitro* (*6*). Given the magnitude of the problem, the development of high-throughput, massively-parallel sequencing approaches that do not rely on cultivation to identify specific virus-host relationships are required. While metagenomics has revolutionized our understanding of viral diversity on Earth (*7-9*), that approach has as yet done little to shed light on the nature of specific viral-host interactions, except in restricted cases (*10*).

2.3 Proposed method for phage-host co-localization

Recent advances in microfluidic technology have enabled the isolation and analysis of single cells from nature (*11-13*). Here we present an alternative to the classical phage enrichment technique where we propose to use an uncultured virus to capture its hosts from the environment using a microfluidic PCR approach called digital multiplex PCR (*12, 14*). To this end, microbial cells were harvested directly from the environment, diluted and loaded onto a digital PCR array panel containing 765 PCR chambers operating at single-molecule sensitivity. Samples were diluted such that the majority of chambers were ideally either empty or contained a single bacterium (Fig. 2.1), achieving a Poisson distribution (*15*). Because there is no universally conserved gene in viruses (*7, 16*), degenerate primers (*17*) were designed to target a subgroup of diverse phage-like elements (*18*). Concurrently, the small subunit ribosomal RNA (SSU rRNA) gene encoded by each bacterial cell was amplified using universal "all bacterial" primers (see Fig. 2.4 for experimental design). Possible genuine host-virus associations detectable by this assay are depicted in Fig. 2.1C. Free phages may also co-localize with hosts, however these events are not expected to lead to statistically significant co-localizations due to the random nature of these associations (*19*).

2.4 Hunting for phages in the termite hindgut

The system we chose to investigate was the termite hindgut. This microliter-in-scale environment contains ~10^7 prokaryotic cells per µl (*20*) with over 250 different species of bacteria (*21*), making it ideally suited to explore many potential, diverse phage-host interactions. To find a viral marker gene relevant to such an environment, the more abundant candidate viral marker genes present in the sequenced metagenome from a hindgut of a higher termite from Costa Rica collected in 2005 (*22*) were examined (Table 2.2; search algorithm described in the Materials and methods section). We then checked if any of these viral genes had homologous counterparts in the sequenced genomes of two spirochetes isolated in 1997 from a laboratory colony of a genetically and geographically distant termite originally collected in 1986 from Northern California (*23-24*). We identified two such genes encoding a large terminase subunit protein (homologous to the T4 associated pfam03237 Terminase_6) and a portal protein (homologous to pfam04860 Phage_portal) exhibiting about 70–78% amino acid identity to their closest homologs in the higher termite gut metagenome (Table 2.3). This finding is surprising given that typically, across biology, portal proteins and terminase proteins from different phages exhibit little overall sequence similarity (*25-28*). Further analysis revealed that the spirochete viral genes were part of a larger prophage-like element, with the majority of recognizable genes most closely related to *Siphoviridae* phage genes (*19*). The association of these genes with prophage-like elements is consistent with the fact that both the Terminase_6 pfam and the Phage_portal pfam describe proteins in known lysogenic and lytic phages.

As a viral marker gene for this prophage-like element we chose the large terminase subunit gene. This gene is a component of the DNA packaging and cleaving mechanism present in numerous double-stranded DNA phages (*26*) and is considered to be a signature of phages (*29*). We consequently designed degenerate primers based on the collection of fifty metagenome and treponeme-isolate alleles of this gene. The ~820bp amplicon spanned by these primers covered about two thirds of this gene and approximately 77% of the predicted N-terminal domain containing the conserved ATPase center (*26, 30*), the “engine” of this DNA packaging motor (*31*) (see alignments in Figs. 2.5 and 2.6). Testing these primers against the RefSeq viral database (*32*) did not yield any hits (Fig. 2.5). Indeed, the closest homolog of this gene in the RefSeq viral database displayed only 25% amino acid identity (Table 2.3). Thus, while this terminase gene was clearly associated with the Terminase_6 pfam, the termite related alleles appear to be part of a novel assemblage of terminase genes in this environment and not closely related to previously sequenced phages (Fig. 2.5).

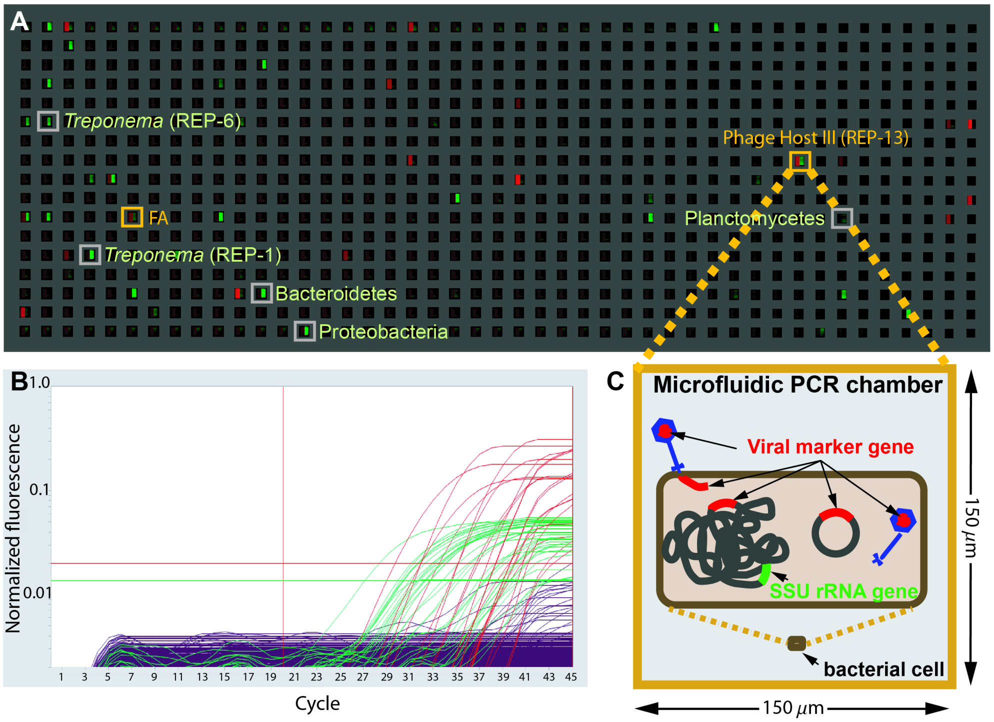

Figure 2.1. End-point fluorescence measured in a panel of a microfluidic digital PCR array. A. The measured end-point fluorescence from the rRNA channel (right half of each chamber) and the terminase channel (left half of each chamber) in a microfluidic array panel. Each panel in the array (one of twelve) consists of 765 150 x 150 x 270μm^3 (6 nL) reaction chambers. Retrieved co-localizations are outlined in orange and positive rRNA chambers randomly selected for retrieval are outlined in gray. FA indicates false alarm (a probable terminase primer-dimer). **B.** Normalized amplification curves of all chambers in (A) after linear derivative baseline correction (red/viral, green/rRNA). **C.** Specific physical associations between a bacterial cell and the viral marker gene resulting in co-localization include for example: an attached or assembling virion, injected DNA, an integrated prophage or a plasmid containing the viral marker gene.

Given that terminase genes of different phages often exhibit less sequence similarity (see above), the fact that we found such closely related terminase genes from such distantly related termites collected from well separated geographical locations (California and Costa Rica) and from specimens collected almost two decades apart led us to speculate that this family of viral genes and prophage-like elements might be ubiquitous in termites. Indeed, to date we have identified close homologs of the large terminase subunit gene in the gut communities of nine termite species belonging to seven families collected from five different geographical locations. We therefore wished to identify the bacterial hosts associated with this viral marker gene. To this end, we made collections of representatives of a third previously unexamined termite family (Rhinotermitidae; *Reticulitermes hesperus*, from a third geographical location in Southern California) over a span of six months (Table 2.4). We then performed seven independent experiments, where in each case the hindgut contents of three worker termites were pooled, diluted, and loaded onto a digital PCR array, screening in total ~3000 individual hindgut particles (i.e., individual cells or possibly clumps of cells positive for the SSU rRNA gene).

2.5 Identification of novel uncultured bacterial hosts

Of the 41 retrieved co-localizations, 28 were associated with just four phylotypes designated "Phage Hosts I, II, III and IV" (see Fig. 2.2, Table 2.1 and the phylogenetic analysis in Fig. 2.7 and Tables 2.5 and 2.6). Statistically, the reproducible co-amplifications were significant and cannot be explained by random co-localization of two unassociated genes (Table 2.1). Furthermore, these associations were independently reproduced in specimens from different colonies collected six months apart (Fig. 2.2), indicative that relationships between specific host bacteria and viral markers were being revealed.

All four of the phylotypes were members of the spirochetal genus *Treponema* and exhibited significant diversity within this genus (Table 2.5). No reproducible or statistically robust associations involving other bacteria were observed. The terminase alleles that associated with these cells shared ≥69.8% identity (average 81.9 ± 8.3% standard deviation, SD)(*33*) and were divergent from other currently known terminases

(Fig. 2.5), suggesting that the primer set amplifies elements exclusively found associated with termite gut treponemes. Analysis of the retrieved terminase gene sequences reveal that they are under substantial negative selection pressure with $\omega=\beta/\alpha=0.079$, where ω is the relative rate of non-synonymous, β, and synonymous, α, substitutions (*18*)(see Table 2.7 for additional estimates for individual hosts). Furthermore, none of the terminase sequences in Fig. 2.2 appeared to encode either errant stop codons or obvious frame shift mutations, and functional motifs appeared to be conserved (Fig. 2.5). Together, the sequence data suggest that these genes have been active in recent evolutionary history and are not degenerating pseudogenes (*19*).

Table 2.1 | Statistics of repeatedly co-localized SSU rRNA genes

Host	No. of repeated co-localizations[*] (*n*=41)	Occurrence in reference library[†] (*n*=118)	P value (one tailed, *n*=41)‡
Host I	13	5	$5.4\text{x}10^{-18}$
Host II	8	2	$7.6\text{x}10^{-13}$
Host III	4	1	$5.7\text{x}10^{-7}$
Host IV	3	1	$3.8\text{x}10^{-5}$

[*] Based on the DOTUR analysis described in Table 2.5
[†] Based on the DOTUR analysis described in Table 2.6. Reference library frequencies are roughly 1/3 of the co-localization frequencies indicating that sampling was unbiased.
‡The statistical test to determine the P value is explained in the supporting text.

Since the viral marker gene was present in hosts spanning a swath of species of termite gut treponemes, we were interested to see if this viral marker exhibited any selectivity within this genus. The relative frequency of free-living *Treponema* phylotypes was determined by randomly sampling chambers positive for the rRNA gene (*18*) (Fig. 2.3, Fig. 2.7). We found that Hosts I through IV were relatively infrequent, comprising 1.3% to 6.4% of the sampled *Treponema* cells (Table 2.1) and collectively about 9.8% of the sampled bacterial cells (correcting for reagent contaminants). Interestingly, the three most abundant

Treponema phylotypes in the survey constituting ~30, 10 and 9% of the free-swimming spirochetal cells (REPs 1, 2 and 3 in Fig. 2.3; see also Fig. 2.7 and Table 2.6) were never co-retrieved with the viral marker gene, to the extent that this target was spanned by our degenerate primers. Given that the degenerate core region (*17*) of each primer targets residues that were strictly conserved in gut microbes of highly divergent termite specimens (Fig. 2.5), and that these primers successfully amplified this gene from the guts of many different termite species (see above), it appears that these strains are most likely either insensitive to this virus or that only a small percentage are infected (*19*). Therefore we conclude that ~50% of the free-swimming spirochetal cells in the gut were likely not infected with an element encoding the targeted viral marker gene, whereas ~12% were hosts potentially infected (Fig. 2.3).

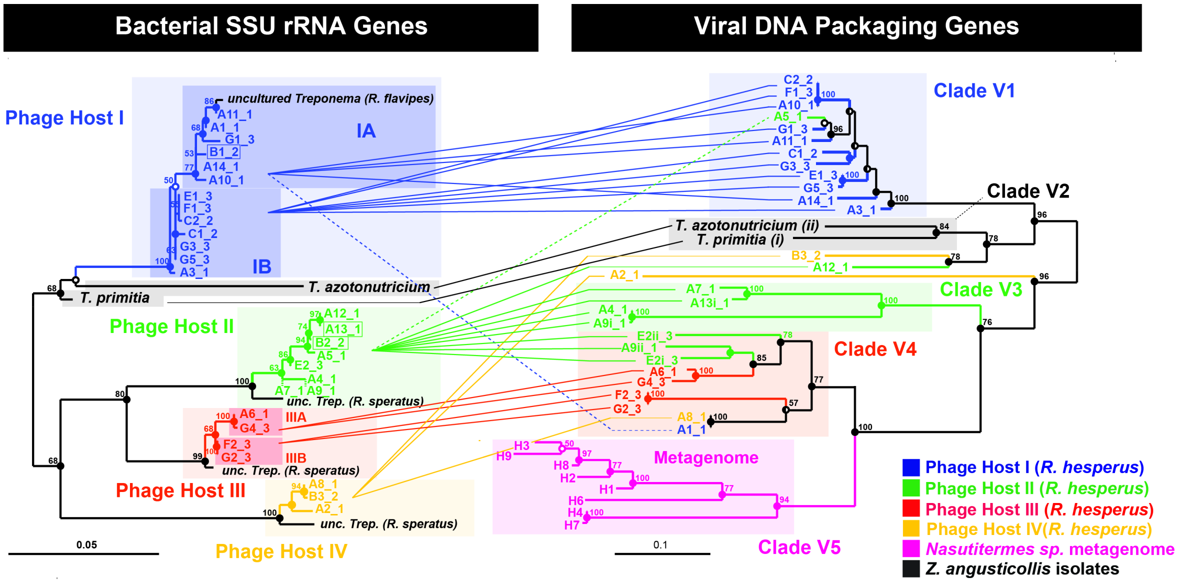

Figure 2.2. Phylogenetic relationship between cultured and uncultured bacterial host rRNA genes and their associated viral DNA packaging genes. Left: Maximum Likelihood (ML) tree of 898 unambiguous nucleotides of the SSU rRNA gene of ribotypes that repeatedly co-localized with the terminase gene, including the two isolated spirochetes *Treponema primitia* and *Treponema azotonutricium*. Shorter sequences (A7, 780bp and A9, 806bp) were added by parsimony (dashed branches). **Right:** ML tree of 705 unambiguous nucleotides of the large terminase subunit gene. Connecting lines represent co-localized pairs, revealing restricted mixing of terminase alleles between different bacterial hosts. For association of three additional recombinant sequences (boxed on the left) see Fig. 2.8. Statistically we estimate that an average of 0.6 co-localizations are false (~2% error (*19*)). The sequence error rate (*40*) for the rRNA and terminase genes was measured to be 0 (*n*=8) and <0.6±0.3% SD (*n*=9), respectively (*18*). Alleles are named by array (A–G) and retrieval index followed by an underscore and the colony number (colony 1 being sampled six months prior to colonies 2 and 3). Lower-case Roman numerals indicate multiple terminases per chromosome. Scale bars represent substitutions per alignment. For interpretation of node support refer to (*18*) and for accession numbers Table 2.11.

2.6 Phage-host cophylogeny

To elucidate the evolutionary relationship between the terminase alleles and their hosts we examined the phylogeny of the terminase genes associated with each bacterial host. Terminase alleles from *R. hesperus* formed separate clades from the clades of the two other termite species investigated in this study (Clades V2 and V5 in Fig. 2.2). Within *R.*

hesperus, different bacterial hosts exhibited different patterns of viral allelic diversity. Terminase sequences associated with Host I, for example, were highly clonal, with 11 out of 13 terminase alleles sharing 96.7 ± 1.7% SD identity (*n*=11, Clade V1) (*33*). Conversely, terminase alleles associated with Host II displayed marked diversity (79.1 ± 6.2% identity, *n*=11) (*33*), deep branches and divergent multiple alleles per bacterium for 3 out of 8 repetitions (with 15–31% divergence). The unique features of the terminase alleles associated with Host II compared with Host I may reflect a more ancient infection or possibly an infection by a phage replicating with a lower fidelity. Alternatively, Host II may be a more sensitive bacterial host susceptible to a wider range of phages. Overall, phage terminase alleles associated with different bacterial hosts were significantly divergent with only three exceptions (Table 2.8).

The tandem trees in Fig. 2.2 reveal multiple possible relations between bacterial hosts and terminase alleles: while Host I was associated almost exclusively with a single terminase clade (V1), Host II was associated with multiple terminase clades (primarily V3 and V4). Conversely, terminase Clade V1 was associated almost exclusively with Host I, while terminase Clade V4 was associated with all bacterial hosts. Overall, the terminase tree was highly structured and displayed specific bacterial host associated clades (e.g., Clades V1 and V3, see Fig. 2.8A). Applying the P Test (*34*) implemented in Fast UniFrac (*35*) to terminase alleles grouped by bacterial host indeed revealed significant differences between alleles associated with most pairs of hosts (Table 2.9). Grouping terminase alleles by colony, however, did not reveal significant differences between alleles (Table 2.10), indicating that sampling was not a factor in determining the observed host associated heterogeneity in terminase alleles. The highly non-random distribution of host associated terminase alleles therefore suggest that lateral gene transfer and/or host switching is limited in this system. This result, however, could also reflect the fact that the terminase gene does not appear to shuffle randomly among phages, possibly indicating a connection between DNA packaging and other characteristics of the phage (*36*). It remains to be seen whether other viral genes follow similar patterns.

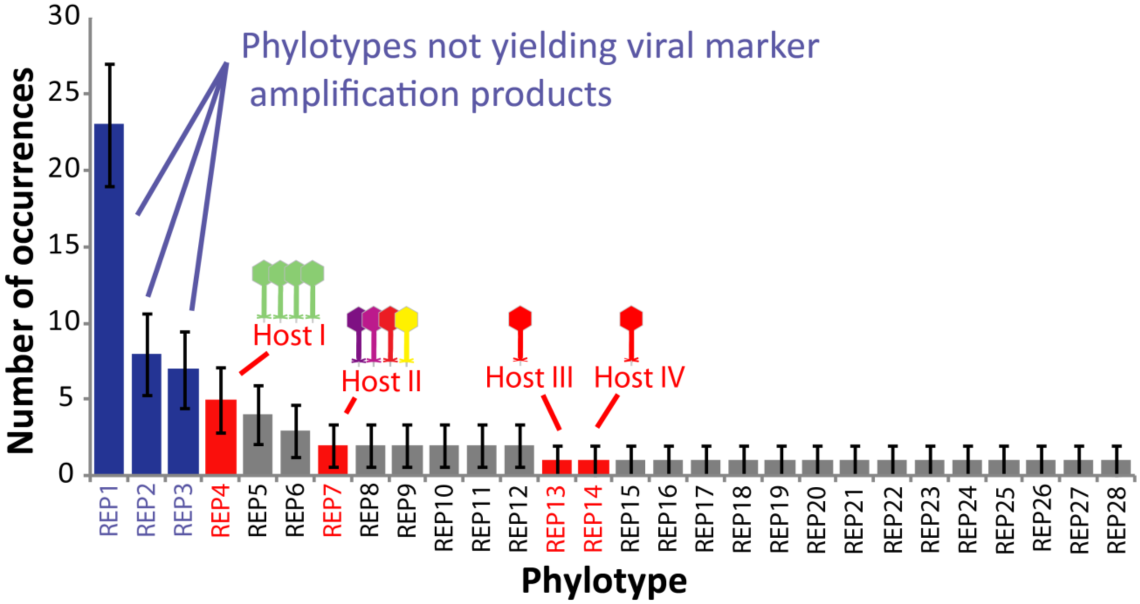

Figure 2.3. Rank abundance curve of free living *Treponema* spirochetes in *R. hesperus* termites identifying putative phage hosts. A library of 118 random chambers positive for the rRNA gene were retrieved, post-amplified, and sequenced. Of these, *n*=78 were related to the *Treponema* genus, corresponding to 28 different phylotypes using an operational taxonomical unit, OTU, cut-off set by DOTUR (*41*) at 3.1%. Here we show these 28 phylotypes, designated as *Reticulitermes* Environmental Phylotypes (REPs), ordered by their abundance. Phylotype abundance is expected to reflect true relative abundances in the gut, since single-cell amplification is not susceptible to primer bias or rRNA copy number bias. Phylotypes identified as phage hosts are marked by red bars (with the highly clonal marker associated with Host I depicted by green viruses and the divergent marker associated with Host II depicted by colored viruses). The most abundant free living *Treponema* in the gut — REPs 1, 2, and 3 (blue bars) were not associated with the viral marker. Remaining bars are gray. Error bars are estimated by the binomial SD. See Table 2.6 for OTU assignment. Note that the isolated spirochetes were not spanned by these REPs (see Fig. 2.7).

The fact that there was little mixing between terminase alleles associated with Host I (V1) and the more distantly related Hosts II (V3 and V4) and III (V4), whereas alleles of the more closely related Hosts II and III (Table 2.5) exhibited a certain degree of mixing (V4), supports the notion that the probability of cross-species transmission or lateral gene transfer decreases with the phylogenetic distance of the hosts (*37*). The rRNA gene of Hosts I through IV also exhibited patterns of microdiversity that may have physiological relevance (*38-39*), however, mirrored only by the terminase alleles of Host III. Host I and II terminase alleles appeared to be indifferent to the bacterial host at the sub-species level.

2.7 Conclusions

Our results show that, in a marked departure from classical phage enrichment techniques, specific viral-host relationships can be revealed in uncultivated cells harvested straight from the environment. We found that variants of a viral packaging gene appear to have infected bacterial hosts across an entire genus of bacteria. Furthermore, despite the significant potential for lateral gene transfer and/or host switching in this well-mixed, small-volume system, the terminase tree was highly structured and displayed specific bacterial host associated clades. It will be interesting to continue to monitor the host-virus interactions within this ecosystem as a function of space and time and across the termite community at large, shedding further light on host-virus co-evolution in this unique ecosystem. More broadly, the method we have developed enables a highly parallel analysis of host-virus interactions in environmental samples from virtually any environment in nature.

2.8 References and notes

1. C. Suttle, *Nat. Rev. Microbiol.* **5**, 801 (2007).
2. M. Sullivan et al., *Environ. Microbiol.* **12**, 3035 (2010).
3. D. Lindell et al., *Nature* **449**, 83 (2007).
4. F. Angly et al., *PLoS Biol* **4**, e368 (2006).
5. S. Williamson et al., *PLoS ONE* **3**, 1456 (2008).
6. P. Hugenholtz, *Genome Biol.* **3**, reviews0003 (2002).
7. R. Edwards, F. Rohwer, *Nat. Rev. Microbiol.* **3**, 504 (2005).
8. E. Dinsdale et al., *Nature* **452**, 629 (2008).
9. D. Kristensen, A. Mushegian, V. Dolja, E. Koonin, *Trends Microbiol.* **18**, 11 (2009).
10. A. Andersson, J. Banfield, *Science* **320**, 1047 (2008).
11. R. N. Zare, S. Kim, *Annu. Rev. Biomed. Eng.* **12**, 187 (2010).
12. E. Ottesen, J. Hong, S. Quake, J. Leadbetter, *Science* **314**, 1464 (2006).
13. Y. Marcy et al., *Proc. Natl. Acad. Sci. USA* **104**, 11889 (2007).
14. L. Warren, D. Bryder, I. L. Weissman, S. R. Quake, *Proc. Natl. Acad. Sci. USA* **103**, 17807 (2006).
15. S. Dube, J. Qin, R. Ramakrishnan, *PLoS ONE* **3**, doi:10.1371/journal.pone.0002876 (2008).
16. F. Rohwer, R. Edwards, *J. Bacteriol.* **184**, 4529 (2002).
17. T. Rose et al., *Nucleic Acids Res.* **26**, 1628 (1998).
18. See Materials and methods in the Appendix.
19. See Supporting text in the Appendix.
20. A. Tholen, B. Schink, A. Brune, *FEMS Microbiol. Ecol.* **24**, 137 (1997).

21. Y. Hongoh, M. Ohkuma, T. Kudo, *FEMS Microbiol. Ecol.* **44**, 231 (2003).

22. F. Warnecke et al., *Nature* **450**, 560 (2007).

23. J. Leadbetter, T. Schmidt, J. Graber, J. Breznak, *Science* **283**, 686 (1999).

24. T. Lilburn et al., *Science* **292**, 2495 (2001).

25. S. D. Moore, P. E. Prevelige Jr, *Curr. Biol.* **12**, R96 (2002).

26. V. Rao, M. Feiss, *Annu. Rev. Genet.* **42**, 647 (2008).

27. S. Chai et al., *J. Mol. Biol.* **224**, 87 (1992).

28. K. Eppler, E. Wyckoff, J. Goates, R. Parr, S. Casjens, *Virology* **183**, 519 (1991).

29. S. Casjens, *Mol. Microbiol.* **49**, 277 (2003).

30. M. Mitchell, S. Matsuzaki, S. Imai, V. Rao, *Nucleic Acids Res.* **30**, 4009 (2002).

31. S. Sun et al., *Cell* **135**, 1251 (2008).

32. K. Pruitt, T. Tatusova, D. Maglott, *Nucleic Acids Res.* **33**, D501 (2005).

33. Percent identity was measured across 235 unambiguous aligned amino acids.

34. A. P. Martin, *Appl. Environ. Microbiol.* **68**, 3673 (2002).

35. M. Hamady, C. Lozupone, R. Knight, *The ISME journal* **4**, 17 (2009).

36. S. Casjens et al., *J. Bacteriol.* **187**, 1091 (2005).

37. N. Wolfe et al., *Global Change & Human Health* **1**, 10 (2000).

38. L. Moore, G. Rocap, S. Chisholm, *Nature* **393**, 465 (1998).

39. J. Thompson et al., *Appl. Environ. Microbiol.* **70**, 4103 (2004).

40. S. Acinas, R. Sarma-Rupavtarm, V. Klepac-Ceraj, M. Polz, *Appl. Environ. Microbiol.* **71**, 8966 (2005).

41. P. Schloss, J. Handelsman, *Appl. Environ. Microbiol.* **71**, 1501 (2005).

2.9 Appendix

2.9.0 Contents

2.9.1 Materials and methods

2.9.2 Supporting text

- 2.9.2.1 Statistical analysis of co-localization in digital PCR microfluidic arrays
- 2.9.2.2 The viral marker gene and its genetic context

2.9.3 Supporting figures

- **Figure 2.4.** Workflow using the microfluidic digital PCR array for host-virus co-localization in a novel environmental sample
- **Figure 2.5.** Multiple alignment of termite related terminase sequences and closest homologs
- **Figure 2.6.** Multiple alignment of pfam03237 with a ZAS-associated terminase
- **Figure 2.7.** Phylogenetic analysis of retrieved *Treponema* SSU rRNA sequences and close relatives
- **Figure 2.8.** NeighborNet network of termite-related terminase alleles
- **Figure 2.9.** Example of microfluidic array panel readout after thresholding
- **Figure 2.10.** Agarose gel electrophoresis analysis of all FAM hits in a microfluidic array panel
- **Figure 2.11.** Schematic diagram of a Monte Carlo simulation of microfluidic array loading and sampling

2.9.4 Supporting tables

- **Table 2.2.** Abundance of homologs of known viral genes in the higher termite metagenome
- **Table 2.3.** Similarity analysis of the termite-associated terminase gene and portal protein gene with close homologs
- **Table 2.4.** Sample collection and analysis information
- **Table 2.5.** Estimated evolutionary distance between bacterial host SSU rRNA phylotypes
- **Table 2.6**. Retrieved *Treponema* phylotypes from the microfluidic arrays
- **Table 2.7.** Selection pressure analysis of the terminase gene
- **Table 2.8.** Similar terminase sequences associated with different bacterial hosts
- **Table 2.9.** P values for the P Test comparing terminase alleles by bacterial host
- **Table 2.10.** P values for the P Test comparing terminase alleles by colonies
- **Table 2.11.** Sequences analyzed in this study
- **Table 2.12.** Analysis of all FAM hits for a number of microfluidic array panels
- **Table 2.13.** Definition of variables used in the microfluidic array statistical model
- **Table 2.14.** Statistics for all sampled panels

2.9.5 References

2.9.1 Materials and methods

Termite collection

Reticulitermes hesperus specimens were collected from Chilao Flats Campground in the Angeles National Forest (Table 2.4). Throughout the experiment, starting in the field, different colonies were kept in separate tip boxes and never came in contact with each other. Colonies thereafter were maintained in the laboratory (*S1*). Microfluidic array experiments were carried out days to weeks (<4 weeks) thereafter.

PCR on the microfluidic array

Microfluidic array multiplex PCR reactions contained Perfecta multiplex qPCR master mix (Quanta Biosciences), 0.1% Tween 20 (Sigma Aldrich Incorporated), 100nM ROX (Quanta Biosciences). Universal 16S SSU rRNA primers and probes used were (*S1*): forward 357F 5’-CTCCTACGGGAGGCAGCAG-3’ (300nM), reverse 1492RL2D 5’-TACGGYTACCTTGTTACGACTT-3’ (300nM), 1389 probe HEX-GTGCCAGCMGCCGCGGTAA-BHQ1 HPLC purified (300nM). Unprobed terminase primers used were: forward ter7F 5’-CATTTGATTTGCCGTTACCGIGCYAARGAYGC-3’ (200nM) and reverse ter5eR 5’-CICCWCCAGCCGGATCRCARTAMAC-3’ (100nM). The probed terminase reverse primer used was: ter5eR.L 5'- CAGCCACACICCWCCAGCCGGATCRCARTAMAC-3' (100nM). The universal probe used for the terminase primer set was: Roche Universal Probe #5 (250 nM). The primers and the rRNA probe were ordered from Integrated DNA Technologies and resuspended in sterile TE buffer (10 mM Tris-HCl, 1 mM EDTA, pH 8) filtered with a 0.02 µm sterile Anotop syringe filter (Whatman). Primers and probes were diluted in DEPC-treated sterile filtered water (Sigma) and then sterile filtered again (prior to dilution) with a 0.02 µm syringe filter.

Preparation of termite hindguts

In each experiment three *Reticulitermes hesperus* worker termites from the same colony (and same tip box) were incubated for several minutes at 4°C to immobilize the specimens and whole guts were subsequently extracted using sterilized forceps on a disposable sterile petri dish. Guts were resuspended in 897 µL of 4°C "synthetic gut fluid" (SGF) salt solution (*S2*) pre-filtered with a 0.02 µm sterile syringe filter containing 0.5 µg/mL final concentration of DNase free RNase (Roche) to prevent inhibition by ribosomal RNA. Guts were repeatedly disrupted with a sterile 1 ml filter pipette tip and suspensions were briefly vortexed and allowed to settle for 30 seconds to sediment large particles. Samples were then diluted to working concentrations using the SGF diluent. For microfluidic arrays C through G the resuspended gut fluid was further filtered with an Acrodisc 5 µm sterile syringe filter (Pall Life Sciences) to remove inhibiting large particles such as wood fragments and protists. Samples were then mixed 1:10 with the PCR reaction mix (above) for immediate loading onto the primed microfluidic array once the dilutions were completed. Termite bodies were frozen for later analysis of their COII sequences (see below).

Microfluidic array thermocycling and fluorescence analysis

BioMark 12.765P peelable microfluidic arrays from Fluidigm were loaded with the samples described above and PCR was performed using the BioMark system (Fluidigm Corporation) as recommended by Fluidigm. The cycling protocol was 95ºC 5 min, (95ºC 15 s, 60ºC 90 s) x 45, 10 min at 60ºC, 20ºC 10 sec. Amplification curves were evaluated using BioMark Digital PCR analysis software (Fluidigm, v.2.0.6) applying ROX normalization and a linear baseline correction. FAM fluorescence threshold was set to detect any increase in fluorescence, while the HEX threshold was set above the fluorescence leakage of the FAM channel into the HEX channel, detectable in both a no-16S rRNA-primer control panel (dedicated for this purpose) and the no-template-control panel. Both panels were included in every microfluidic array. To minimize diffusion from neighboring chambers after pressure release, only chambers displaying fluorescence in both channels that were flanked by chambers displaying no fluorescence in both channels were selected for retrieval. An example of end-point fluorescence of an array panel is shown in Fig. 2.1A. In this figure only fluorescence from within chambers is shown, detected based on the reference dye fluorescence measurement. To illustrate the nature of co-localizations, we mask the chambers in such a way that half of each chamber shows one fluorescence channel and the other half shows the other. This way the left half of each chamber showed only the FAM/viral channel fluorescence and the right half of each chamber showed only the HEX/SSU rRNA channel fluorescence. Fluorescence is shown on a logarithmic scale with background subtracted.

Sample retrieval

Microfluidic arrays were peeled shortly after the end of the PCR run and pressure in the arrays was released by depressing the pressure valves. Samples were retrieved into 10µl TE buffer (that was pre-filtered with a 0.02µm sterile Anotop syringe filter) using disposable sterile 30.5G needles (*S1*) (one disposable needle per chamber) and subsequently evaluated for the presence of target genes via conventional simplex PCR. In addition, for each array, with the exception of array B, at least five chambers were also retrieved from the no-template-control panel to test for possible cross-contamination (all control retrievals were negative - see below). The PCR reaction mix consisted of perfecta qPCR multiplex master mix with the SSU rRNA primers at 300nM concentration and terminase primers at 200nM concentration. The SSU rRNA probe, the Universal Probe #5 and the probe binding primer ter5eR.L were omitted from these reactions. The cycling protocol for conventional PCR for the simplex terminase reaction was 95ºC 3 min, (95ºC 15 s, 60ºC 60 s, 72ºC 60

s) x 40, 72ºC 10 min and for the simplex SSU rRNA reaction was the same but with 32 cycles of amplification to prevent amplification of contaminates associated with the Taq master mix. The presence or absence of product was evaluated using agarose gel electrophoresis. Samples that displayed a band at the expected fragment size for both simplex reactions were deemed successful.

The majority of successful retrievals from the microfluidic arrays were amplified for cloning and/or sequencing in two 30 µL reactions using 3.5 U of EXPAND high fidelity polymerase (Roche), Fail-Safe PCR PreMix D (Epicentre), and primers and cycling conditions as above. In the case of microfluidic array A, terminase sequences were amplified with Perfecta qPCR multiplex master mix instead. For each reaction 1.5 µL of retrieved sample was used. PCR products were purified using the Qiagen PCR purification kit, and sequenced using the terminase ter7F and ter5eR primers and SSU rRNA gene internal primers 1100R (3'-AGGGTTGCGCTCGTTG-5') and 533F (3'-GTGCCAGCMGCCGCGGTAA-5'). Sequencing reactions of microfluidic array amplicons were carried out by the USC DNA core facility (Los Angeles, CA) using an annealing temperature of 50 or 55ºC.

Sequences that contained a mixture of SSU rRNA sequences were discarded from further analysis. Sequences that contained a mixture of terminase sequences, or in which the trace quality was poor were cloned for sequencing using the TOPO TA cloning kit (Invitrogen). At least eight colonies from each cloning reaction were picked and used as templates for PCR reactions. PCR reaction mix included Fail-Safe PCR PreMix H (Epicentre), Taq polymerase (New England Biolabs) and standard T3/T7 primers at 250 nM. Cycling conditions were 95ºC 3 min, (95ºC 15 s, 55ºC 30 s, 72ºC 60 s) x 35, 72ºC 10 min. Sequences with different restriction fragment length polymorphism (RFLP) patterns were chosen for sequencing. For the RFLP analysis, 6 μl of each reaction was digested at 37ºC for 4 hr with 3 units HinPI1 from New England Biolabs followed by an inactivation step at 65ºC for 20 min. A representative of each RFLP type (with the correct product band) was sequenced with the high fidelity polymerase and standard T3 and T7 primers. PCR products were purified using the Qiagen PCR purification kit and sequenced with standard T3/T7 primers. Sequencing reactions for cloning were carried out by Laragen Inc. (Los Angeles, CA).

Identification of termite species

The mitochondrial cytochrome oxidase II (COII) gene was used to identify the termite specimens analyzed in this study (*S3*-*S5*). For each of the three colonies that were collected, either heads or bodies of three to five worker termites frozen on the day of the microfluidic array experiments were used as a template for a PCR amplification of the COII gene. Primers used were A-tLeu (5'-ATGGCAGATTAGTGCAATGG -3') and B-tLys (5'-GTTTAAGAGACCAGTACTTG-3')(*S6*-*S7*). For colonies 1 and 2 the PCR product was cloned and sequenced. For colony 3 the product was directly sequenced. Colonies 1, 2, and 3 shared 99.3% nt identity with 0 gaps (0.003% SD; *n*=3 over 680 unambiguous nt) and 100% amino acid identity (over 226 residues) with the COII sequence of *Reticulitermes hesperus* isolate LBL2 (accession# AY623445.1).

Sequence analysis

Sequence traces were converted into a nucleotide sequence using Lasergene SeqMan Pro v8.1.2. Representatives of the SSU rRNA nucleotide sequence of Hosts I through IV were then screened for chimeras using Pintail (*S8*) and Bellerophon (*S9*), the latter implemented in Greengenes (*S10*), returning negative results. All terminase sequences from all 41 co-localizations were also tested for amplification related chimeras using Bellerophon (*S9*). Cases where both chimera parents belonged to the same PCR batch (E2iii) were eliminated from further analysis.

SSU rRNA sequences were aligned by SILVA (*S11*) incremental aligner SINA and subsequently analyzed in ARB (*S12*) version 07.12.07org using SILVA release 100 (SSURef_100_SILVA_02_08_09_opt). jModelTest 0.1.1 (*S13-S14*) was used to find the optimal nucleotide substitution model for the rRNA sequences in Fig. 2.2, testing 40 different models on an alignment of 898 unambiguous nucleotides without gaps, estimating a maximum likelihood (ML) tree for each model. The optimal nucleotide substitution model (based on the AICc criterion with sample size set to the number of sites in the alignment) was a Tamura-Nei model (*S15*) +I+Γ with unequal base frequencies. A maximum likelihood tree was then computed for this alignment with PhyML 2.4.5 (*S14*) implemented in ARB using the Tamura-Nei model +I+Γ (nCat=4), with all parameters estimated from the data and with 1000 non-parametric bootstrap iterations. Other treeing methods such as Phylip DNAPARS v3.6a3 (*S16*) and Fitch-Margoliash (*S17*) distance method implemented in ARB predicted very similar topologies (Fig. 2.2). In Fig. 2.2 solid circles represent significant nodes supported by ML, parsimony (Phylip DNAPARS v3.6a3 (*S16*)), and distance (Fitch-Margoliash (*S17*)) methods. Half circles represent nodes supported by ML and either parsimony or distance methods. Open circles represent nodes supported by only ML. In addition, support values greater than 50% for 1000 bootstrap iterations are shown. We note that the topological relation between Phage Host clades I–IV appeared to be sensitive to the addition of other *Treponema* sequences from public databases, and to the particular outgroup chosen as well, and therefore the topology in Fig. 2.2, though robust, may not be definitive.

Nucleotide sequences of the large terminase subunit gene present in *R. hesperus*, Z. *angusticollis* and *Nasutitermes* sp. termites were translated in reading frame and aligned with ClustalW (*S18*) in MEGA4 (*S19*) (the alignment used in the analysis was straightforward and involved a single insertion event of a highly conserved five amino acid sequence in some of the sequences). Subsequently 705 unambiguous aligned nucleotides without gaps were tested for the presence of recombination with RDP3 v3.44 (*S20*). Methods used to scan for recombinant sequences included Geneconv (*S21*), Maxchi (*S22*), and RDP (*S23*) (as recommended in the RDP3 manual and shown to be the preferable tests for non-redundant sequences (*S24-S25*)) as well as the Bootscan method (*S26*). Since each recombination detection method individually is error prone (*S24-S25, S27*) several methods are required to explore recombination (*S24, S27*). Similar sequences≤(3.3%) were removed prior to analysis as recommended in the RDP3 manual. The first two events found by RDP3 implicated by all four methods alleles A13ii and B1 as recombinants, confirmed by manual phylogenetic inspection in RDP3. A NeighborNet analysis with SplitsTree4 (*S28*) using optimal substitution parameters estimated by FindModel (*S29*) confirmed the reticulate nature of these alleles and consequently these alleles were excluded from the phylogenetic tree in Fig. 2.2 (see Fig. 2.8). The following two events detected by RDP3 (H5, B2) were only supported by Maxchi, however the NeighborNet network showed these putative recombinants were also associated with significant reticulate patterns, which were eliminated upon removal of these sequences. Consequently these two samples were also excluded from the phylogenetic tree. The remaining events detected by RDP3 with lower confidence exhibited either a small degree of local reticulate patterns or no reticulate patterns and were therefore kept in the analysis. Eliminating potential recombinant alleles resulted in a largely tree-like network suitable for phylogenetic analysis (Fig. 2.8B). A likelihood-mapping analysis (*S30-S31*) with TREE-PUZZLE 5.0 using 10000 quartets and the optimal model found by jModelTest (see below) showed that 95.7% percent of the quartets fell in the triangle corners (A_1,A_2,A_3) suggesting that a phylogenetic tree should fit the data (*S31*).

After recombinant sequences were removed, jModelTest was used to find the optimal nucleotide substitution model testing 40 different models, estimating a ML tree for each model. The optimal model (based on the AICc criterion as described above) was a Tamura-Nei model (*S15*) +I+Γ with the base frequencies having little effect on the AICc score. A ML tree was then computed with PhyML 2.4.5 implemented in ARB using the Tamura-Nei model with +I+Γ (nCat=4), with all parameters estimated from the data and with 1000 non-parametric bootstrap iterations. Other treeing methods such as DNAPARS v3.6a3 and Fitch-Margoliash distance method implemented in ARB predicted very similar topologies (Fig. 2.2). Tree topology was also similar to the ML estimated tree topology of the corresponding 235 amino acid residues, with the main differences being a slight repositioning of the higher termite clade and sequence A2. Since the terminase gene is comprised of two functional domains, an ATPase domain and a nuclease domain (see Fig. 2.6), we also compared the ML estimated topology of 495 unambiguous aligned nucleotides of the N-terminal domain of the gene (see Fig. 2.5 for alignment) with the nucleotide tree of the entire gene and found the topologies to be nearly identical. p-distances were measured in MEGA4 and standard deviations were calculated in Matlab.

Survey of SSU rRNA ribotypes on the microfluidic array

In order to assess the frequency of putative host ribotypes I through IV on the microfluidic array as well as the frequency of other rRNA ribotypes, we constructed a library of 118 randomly sampled rRNA hits from the microfluidic arrays. To this end, for two microfluidic arrays (F and G) and for every panel on these arrays (except the two control panels), 10 chambers for which the HEX (rRNA) fluorescence exceeded the detection threshold (irrespective of florescence in the FAM/terminase channel) were randomly selected for retrieval. The identities of the chambers for retrieval were obtained by a random number generator implemented in Matlab 7.4. These sequences were then post-amplified for sequencing using Perfecta multiplex qPCR master mix (Quanta Biosciences) as described in the Methods section. Sequencing was performed by the USC DNA core facility using internal SSU rRNA primers 533F and 1100R (see Methods). A total of 118 sequences were successfully sequenced and assembled using Lasergene SeqMan Pro v8.1.2. In Fig. 2.3 we plot the rank abundance curve of just *Treponema* phylotypes from the reference library. The frequency of each phylotype is given in Table 2.6. Each column in Fig. 2.3 can be thought of as a random variable sampled from a binomial distribution with mean $n \cdot p$ and standard deviation $SD = \sqrt{n \cdot p \cdot (1-p)}$, where *p* is the probability to sample this phylotype and *n* is the total number of trials (here *n*=78 trials). The error bars in Fig. 2.3 are ±SD, with *p* estimated for each phylotype as the number of occurrences of that phylotype divided by *n*.

Degenerate primer design and testing

Terminase phage primers were designed to target several conserved regions of the large terminase subunit gene found in the four prophage-like elements in *Treponema primitia* (ZAS-2) (*S32*) and *Treponema azotonutricium* (ZAS-9) (*S33*), and in 46 contigs found in the metagenome of a *Nasutitermes* species termite (*S5*). The primers were designed with CODEHOP (*S34*), selecting candidates with melting temperatures matching the all-bacterial SSU rRNA primer set (primer candidates were required to be different by at least five base pairs to be considered different candidates). The primer sequences in both the degenerate core region and the clamp region were manually tweaked to offer the best coverage for the conserved region (matching the codon bias in these sequences) and to minimize primer dimers. In addition, inosines were incorporated at certain positions instead of mixed bases to reduce primer degeneracy. Several forward and reverse primer candidates were chosen and the nucleotide regions were further adjusted to minimize forward/reverse primer-dimers and dimers with the all-bacterial primers and probe. Multiplex PCRs for various forward and reverse primers were performed on a dilution series of purified genomic DNA from ZAS-2 and ZAS-9. PCR products were analyzed by agarose gel electrophoresis and primers yielding the strongest bands and having the lowest detection limit (<100 copies) were selected. The chosen primers were further screened on genomic DNA extracted from *Zootermopsis nevadensis* by agarose gel electrophoresis.

To allow us to do quantitative PCR (qPCR) with these primers without having to design a degenerate probe we implemented a universal-template probe strategy first suggested by Zhang et al. (*S35*) and adapted for degenerate primers by Ottesen et al. (*S2*). In this method a short universal nondegenerate probe sequence is attached to the 5’ end of the forward and/or reverse primers. The probe-binding sequence is incorporated into the amplicon during the first round of amplification, allowing the probe to detect amplification of that product. A short nondegenerate 8 base probe incorporating locked nucleic acids (LNAs) then binds to the probe-binding sequence and is subsequently cleaved by the DNA polymerase like in a standard TaqMan chemistry. The locked nucleic acids increase the melting temperature of the probe allowing usage of a very short probe. A probe yielding the minimal interaction with the SSU rRNA amplicon and other oligos in the master mix was chosen for this task. A linker sequence was incorporated between the probe-binding sequence and the degenerate primer to further reduce dimers.

Multiplex qPCR standard curves were obtained for all probe binding sequence combinations (probe binding sequence on the forward primer, probe binding sequence on the reverse primer and probe binding sequence on both the forward and the reverse primers) and for all the candidate primer sets. In all cases, primers with LNA probe binding sequences were mixed 50% with primers lacking the probe binding sequence as this seemed to enhance the PCR reaction. Primer sets yielding the best standard curves, highest end-point amplification for positive templates and highest Cts for the no-template-controls were selected. Primer sequences for the best candidates were fine tuned to further reduce dimers and then screened again using the same metric described above. The best candidates were then tested on ZAS DNA on the digital PCR microfluidic array. Primers yielding the best amplification curves, highest end-point amplification, and lowest number of no-template-control hits were selected. Finally, primer and probe concentrations were optimized on the microfluidic array for the chosen primer set. All benchtop qPCRs were performed on a Stratagene Mx3000P. Cycling conditions were as described in the Methods section.

Measures to prevent and test for contamination

To prevent contamination from the environment, from termites and from post-PCR products, several precautions were taken. Experiments were conducted in five different laboratories that were physically separated (different laboratories within the same building or different buildings). All PCR master mixes for dPCR runs, PCR master mixes for post-amplification of retrieved microfluidic array samples, and tubes loaded with 10 µl TE buffer for retrieved sample resuspension were prepared in laboratory #1 that never came in contact with termites or related samples thereafter. In addition, pipettes and benches were always thoroughly cleaned with EtOH or EtOH and bleach prior to setup. Termite handling and microfluidic array loading were conducted in laboratory #2, where each of these two procedures took place in well-separated designated areas. Sample retrieval was performed in a separate room within laboratory #2 using disposable syringes. Sample loading for post-amplification was performed in laboratory #3. Master mixes for cloning related PCR reactions were prepared in laboratory #3 (which was designated as a PCR cloning "clean area") and loading of samples for cloning-related PCR was performed in laboratory #4. All subsequent manipulations of samples or cloned PCR products (such as RFLP analysis, agarose gel electrophoresis, PCR purification, etc.) were performed in laboratory #5.

To test that no contamination occurred, every microfluidic array contained a no-template control panel and for each array (except B) at least five chambers from the no-template-control panel on the array were retrieved and processed with the rest of the samples to insure there was no cross-contamination during the retrieval process. No-template-control chambers retrieved for this purpose were selected such that these chambers and their flanking chambers on either of their sides did not exhibit fluorescence in both the FAM and HEX channels (this was done to prevent possible diffusion of targets from adjacent chambers into the sampled chamber after pressure release). All no-template-control samples that were retrieved from the microfluidic arrays were post-amplified with the rest of the retrievals and tested by agarose gel electrophoresis. All negative controls were always negative for both channels[1]. Background amplification in the no-template-control-panels never exceeded 2.6% of positive chambers for both channels (1.25 ± 0.75% SD for the terminase channel and 1.35 ± 0.7% SD for the SSU rRNA channel). Some background amplification using all-bacterial SSU rRNA primers is expected (*S1*) and is commonly attributed to DNA fragments present in commercial enzyme preparations (*S36*). The positive hits for the FAM channel in the microfluidic panels are expected to be

[1] One of the five SSU rRNA control chambers in array G was positive in a diagnostic post-amplification (not for sequencing), however this turned out to be an artifact of the diagnostic run as post-amplification of the same sample a second time was negative (with the positive control being positive).

a consequence of the modified TaqMan chemistry employed: since the universal LNA probe can spuriously bind to a terminase primer, primer-dimers will lead to amplification of a spurious product and fluorescence (similar to primer-dimers observed in SYBR Green assays), however no actual contaminating target is present, verified by agarose gel electrophoresis (see Fig. 2.10, Table 2.12, and supporting text for further discussion). Finally, every post-array amplification was always executed with several no-template-controls.

Measurement of PCR and cloning error rates

To measure the sequence error rate of samples retrieved from the microfluidic dPCR array, genomic DNA from ZAS-9 was used as a reference template in a microfluidic dPCR array. Vortexed genomic DNA from ZAS-9 was loaded onto a microfluidic dPCR array and cycled as described in the Methods section. Samples were then retrieved and the rRNA and terminase gene fragments were post-amplified using EXPAND high fidelity polymerase (Roche) as described in the Methods section. To measure the error rate, sequenced array retrievals were aligned against the known sequence of ZAS-9 rRNA and terminase genes. The error rate of the rRNA gene was 0 with 0 gaps (*n*=8, 905 ± 20bp SD) and the error rate of the terminase gene was 0 with 0 gaps (*n*=16, 711 ± 14bp SD). Post-amplification of the terminase gene fragment with the Quanta master mix resulted in a small number of ambiguous bases, however correcting these artifacts resulted in perfect matches. To test cloning associated errors, a retrieved ZAS-9 terminase sequence post-amplified with Roche high fidelity polymerase was cloned and several colonies were picked, amplified with the Roche high fidelity polymerase and sent for sequencing, as described in the Methods section. The measured error rate was 0.59 ± 0.29% SD (*n*=9, 759 ± 4bp SD) with 1 gap for 1 out of 9 cases. A similar cloning error rate was found when comparing the nucleotide sequences of 12 terminase amplicons in Fig. 2.2 sequenced directly from retrieved samples with their corresponding TOPO clones (0.55% ± 0.32% SD, *n*=12). In some cases single nucleotide deletions were also observed (see below). To check that clone errors were not sequencing related, five samples of the same terminase clone were amplified and sent for sequencing, however all sequences were found to be identical. To check that these errors are not introduced by *E. coli* during the growth phase, a single terminase colony was re-streaked and five colonies were amplified and sent for sequencing. All colonies yielded 100% identical sequences. Consequently, the origin of the terminase sequence errors appears to be the cloning step.

Out of 31 terminase sequences in Fig. 2.2, 10 were sequenced from the original retrieval, 12 were sequenced from a combination of the original retrieval and a TOPO clone, and 9 were sequenced from the TOPO clone alone. When sequences from the original retrieval were available and unambiguous, to minimize cloning errors these sequences were used in the consensus sequence in overlapping regions. Therefore for these sequences the error rate is expected to be lower. TOPO clones A9ii and E2i initially contained a frame shift mutation and E2i contained in addition an errant stop codon. These mutations were suspected to be cloning-related errors, confirmed by sequencing additional TOPO clones for each sample and calling base pairs by majority consensus. TOPO clone A11 also contained a frame shift mutation outside the alignment region considered in Fig. 2.2. This frame shift mutation also appears to be a cloning artifact as similar (though not identical) clones from the same retrieval did not contain this frame shift mutation. Consequently an N was inserted at this position. In the absence of TOPO clones, if an ambiguous base was declared (one such case) the degeneracy was arbitrarily broken to facilitate translation.

Measurement of primer efficiency

To measure SSU rRNA primer efficiency, five panels of a microfluidic dPCR array were loaded with ZAS-9 genomic DNA. Genomic DNA was titrated to achieve a final expected number of 400 (*n*=1), 300 (*n*=2), and 200 (*n*=2) SSU rRNA targets that were uniformly distributed across a panel containing 765 microfluidic chambers. Expected number of targets was estimated based on genomic DNA concentration measured using a Hoefer DynaQuant 200 fluorimeter. Digital PCR chemistry and cycling conditions were as described in the Methods section. The genomic DNA was vortexed upon extraction and therefore the genome is expected to be sheared to 10–20kb fragments. Since the two copies of the rRNA and terminase genes were located 689 kbs and 939 kbp apart, respectively, each genome was assumed to contribute two separate copies of each gene. After subtraction of noise, estimated from the no-template-control panels, the average rRNA and terminase primer efficiencies were calculated to be 59 ± 6% SD (*n*=5) and 74 ± 7% SD (*n*=5).

Selection pressure analysis

The program HyPhy 2.0 (*S37*) was used to estimate the relative rate of non-synonymous (β) and synonymous (α) substitutions (ω=β/α) for all 28 retrievals associated with Hosts I through IV using a maximum likelihood approach with a codon substitution model (*S38*). An alignment comprising 705 unambiguous nucleotides without gaps was used to generate a maximum likelihood (ML) tree with phyml assuming a TN93 (*S15*) nucleotide substitution model +Γ(nCat=4)+I+F. Given the above alignment and ML tree, HyPhy was used to find an optimal nucleotide substitution model out of all possible time-reversible models using the AIC criterion for selection. Finally, HyPhy was used to obtain the ML estimates of the independent model parameters of an MG94(*S39*)xREV_3X4(*S38*) substitution model with the optimal constraints found above (012032) assuming global parameters, the above ML tree, and the above in-frame alignment. Equilibrium frequencies were estimated from the partition. The global estimated ω was found to be 0.079. The 95% profile likelihood confidence interval was 0.071 to 0.088. This range is significantly lower than ω=1 (the case of neutral evolution) indicating that the terminase gene is under substantial negative selection pressure. A likelihood ratio test (LRT) comparing the null hypothesis model (ω=1) to the above alternative model strongly rejects the null hypothesis of neutral evolution with LR=754 and a P value (likelihood ratio test) predicted by HyPhy to be 0. In Table 2.7 the selection pressure was estimated for individual bacterial hosts using several additional methods and resulted in the same conclusion.

Analysis of viral genes in the metagenome

We were interested in finding the more abundant viral genes in the metagenome to identify a viral marker gene for this environment. In order to make this method widely accessible we designed an automated tool called MetaCAT that screens all gene objects in a metagenome and clusters them based on homology to genes in a reference database of known viral genes. The number of metagenome gene objects in a given cluster is then interpreted as the relative frequency of the corresponding known viral reference gene in the metagenome. This method is capable of assessing the relative frequency of viral-related metagenome gene objects in an annotation independent way. We refer to the implementation of this algorithm as the Metagenome Cluster Analysis Tool (MetaCAT), available upon request.

The MetaCAT algorithm is as follows: we first BLAST a list of known (viral) reference genes against all metagenome gene objects using BLAST v2.2.22+ (*S40*) (wrapped by Matlab) with a cutoff E value of 10^{-3}. As a reference list of known viral genes we use NCBI's viral RefSeq database v37 (*S41*). The number of metagenome gene objects homologous to each of the known reference genes is defined to be the *abundance* of that known reference gene in the metagenome. Since the list of known reference genes is long (~80,000 genes) we wished to filter this list based on several criteria. First, we retain only known reference genes whose best E value score is$\leq 10^{-7}$. This filtering step is performed to retain only known reference genes that yield reasonable alignments to metagenome gene objects. The second filtering step, implemented in Matlab, was designed to take out redundancy in the RefSeq database itself with respect to the metagenome using a dedicated clustering algorithm. For example, if two known reference genes are homologous to similar lists of metagenome gene objects, we would like to report only one of the two known reference genes, choosing the one with the lower E value. More generally, we wish to find for every known reference gene all the other known reference genes to which it is *related* (a known reference gene is always *related* to itself; see definition below). Therefore each known reference gene belongs to a *group* of *related* known reference genes. Finally, for each *group* of *related* known reference genes we only report the known reference gene with the lowest E value to represent that *group*. The combined list of reported known reference genes is then the final list of viral genes. The frequency of each reported viral gene is defined as the *abundance* of that known reference gene in the metagenome (see above). To complete the definitions: two known reference genes are said to be *related* if the *signatures* of both known reference genes is *similar*. A *signature* of a known reference gene is defined as the list of metagenome gene objects to which that known reference gene is homologous ($E \leq 10^{-3}$). Two signatures are then said to be *similar* if they share 50% of the elements in their lists. That is, if list A has L_i elements and list B has L_j elements, lists A and B are said to be similar if $50\% \geq 100 \cdot \min\left(L_i \cap L_j / L_i , L_i \cap L_j / L_j\right)$, with the symbol $\cap$ denoting the intersection between the two lists.

Note that the final reported known reference genes can still be *related*. Nevertheless, this filtering step is effective at removing a considerable amount of redundancy in the RefSeq database. A third manual filtering step is applied to retain only viral genes related to building a virion. Such genes are considered to be virus-specific genes (*S42*). Examples of such genes include capsid proteins, portal proteins, terminase proteins, tail proteins, baseplate proteins, and so on (*S42*). The list of the most abundant viral genes in the metagenome (*abundance* ≥10) is given in Table 2.2.

2.9.2 Supporting text

2.9.2.1 Statistical analysis of co-localization in digital PCR microfluidic arrays

Origin of a random co-localization component

We wish to see if *k* repeated co-localizations of a particular 16S rRNA ribotype with the terminase gene can be explained by chance co-localization on the microfluidic array (referred hereto as a "chip"). The reason there is a finite probability for chance co-localization is that typical array panels usually contain a certain fraction of FAM hits (the channel of the terminase marker) that are not co-localized with HEX hits (the channel of the 16S rRNA marker) as is shown in Fig. 2.9. If a fraction of these non-co-localized FAM hits contains the terminase target there is finite probability they may co-localize by random chance with a 16S rRNA gene and be mistaken for a true (host/terminase) co-localization. The number of these types of chance events determines the probability for false co-localization. Non co-localized FAM hits (which do not always contain an actual terminase product) can arise for several reasons:

(1) Since the universal LNA probe binds to a terminase primer, primer-dimers can lead to amplification and spurious fluorescence, i.e., fluorescence in the absence of a terminase target. These types of hits are apparent in the no-template-control panel and can account for roughly half of the non co-localized hits on a typical panel (see Table 2.12 and Table 2.14 discussed below). To verify that FAM hits in the no-template-control panel do not contain a target and are not the result of a contamination, four positive FAM chambers were retrieved from a no-template-control panel, post amplified for the terminase gene and analyzed by agarose gel electrophoresis, however no bands were detected. In addition, for several panels for two chips all FAM hits (both co-localized and non-co-localized) were retrieved, post amplified for the terminase gene and analyzed by agarose gel electrophoresis (Table 2.12). For each panel there were several samples that did not display any band (see Fig. 2.10 for a representative example), a finding that is consistent with the presence of spurious products observed in the no-template-control (NTC) panel. Furthermore, the average number of samples that did not display a band agreed well with the number of FAM hits in the no-template-control panels for these chips (Table 2.12), confirming that there is a noise component of spurious amplification on the panels similar to the no-template-control panel. For the seven chips in this study the average number of FAM hits in the no-template-control panel was 9.6±5.7. These types of non-co-localized FAM hits will not lead to chance co-localization with a 16S rRNA gene since there is no actual terminase target present.

(2) If the end-point fluorescence generated by a 16S rRNA target did not exceed the HEX threshold, this chamber would seemingly appear as a non-co-localized event (even though there is a 16S product present). Since the HEX threshold is set high enough to filter out cross-talk from the FAM channel into the HEX channel, some potential HEX hits may have been omitted. Indeed, when retrieving all FAM hits from a panel and amplifying all retrievals for the 16S rRNA gene, usually some wells whose HEX end point fluorescence did not pass the detection threshold did have a 16S rRNA band (data not shown). These types of non co-localized FAM hits should not contribute to false co-localization or contribute minimally because samples with mixed/chimera 16S rRNA traces are discarded from analysis and the probability of repeatedly amplifying the same wrong 16S rRNA is negligibly small (see discussion below).

(3) The 16S rRNA qPCR efficiency was measured to be ~60% for ZAS-9 genomic DNA (see Materials and methods). These types of events could potentially lead to false co-localization if a 16S rRNA amplification product is not generated (but the terminase gene in this cell was amplified) and this target co-localized by chance with another bacterial cell whose 16S rRNA gene was amplified. If an amplicon was generated (but for some reason fluorescence was inhibited) then these types of non-co-localized FAM hits will not contribute to false co-localization because samples with mixed 16S rRNA traces are discarded.

(4) Some cells may potentially prematurely lyse and their DNA may get sheared (for example when crushing the gut or during the loading process onto the chip). If this happens there is a possibility that free floating terminase targets are released into the mix.

(5) There may be assembled viruses present or free floating viral DNA, which can be regarded as free floating terminase targets.

As mentioned above, approximately half of the non co-localized FAM hits on a given panel can be explained by the spurious noise and do not contribute to random co-localization. Of the remaining non-co-localized FAM hits, the fraction relating to (2), if present, will not lead to false co-localization. Therefore the probability for false co-localization estimated below, which is based on fluorescence measurements alone, is an upper bound on the true probability for false co-localization.

Statistical model of random co-localization (P value estimation)

In Fig. 2.2 we see that certain 16S rRNA ribotypes are repeatedly co-localized, giving rise to 16S rRNA clades I–IV. The null hypothesis is that these 16S rRNA ribotypes are not true hosts and that the observed repeated co-localizations are due to chance associations, that is, these 16S rRNA ribotypes are simply co-localized many times by chance with free floating terminase targets. We therefore wish to estimate the probability (P value) that out of n=41 successful retrievals from the chip, i.e., retrievals that resulted in obtaining a 16S rRNA and terminase sequence after post-amplification, we will retrieve k or more instances of a particular ribotype $\boldsymbol{S}$ co-localized with a terminase (any terminase). This probability is given by

$$\text{Prob}\left(\text{number of chance co-localizations of } \boldsymbol{S} \text{ with a terminase } \geq k \,|\, n \text{ successful retrievals}\right) =$$

$$= \sum_{k'=k}^{n} \text{Prob}\left(\text{number of chance co-localizations of } \boldsymbol{S} \text{ with a terminase } = k' \,|\, n \text{ successful retrievals }\right) =$$

$$= 1 - \sum_{k'=0}^{k-1} \text{Prob}\left(\text{number of chance co-localizations of } \boldsymbol{S} \text{ with a terminase } = k' | \, n \text{ successful retrievals}\right) =$$

$$= 1 - \sum_{k'=0}^{k-1} \text{Prob}\left(\text{succeed } k' \text{ times with probability } p_F | \, n \text{ trials}\right) =$$

$$= 1 - \sum_{k'=0}^{k-1} \binom{n}{k'} p_F^{k'} \left(1 - p_F\right)^{n-k'} = 1 - \textbf{binocdf}(k-1, n, p_F)$$

where **binocdf** is the cumulative distribution function of the binomial distribution and p_F is the probability that when we successfully retrieve a co-localized well from a panel it contains the particular ribotype $\boldsymbol{S}$ and any terminase gene by pure chance. Given k, n and p_F (estimated below) the P value can be calculated. We find that the P values (n=41; one-tailed) for Hosts I–IV are all highly statistically significant (P < 10^{-4}; see Table 2.1 and Table 2.14) allowing us to reject the null hypothesis.

A model for a typical panel

Each panel loaded with a template is assumed to have the following species: Y HEX hits ("blue" hits), X FAM hits ("red" hits) out of which "*noise"* FAM hits are due to spurious amplification (no actual target). We assume that out of the X FAM hits there is a fraction of FAM hits that are free floating targets, that is a DNA fragment coding for a terminase gene but not for a 16S rRNA gene. The number of free floating targets is defined to be $X_T - noise$. These free floating targets would be the source of false co-localizations events. Thus co-localization events observed on the chip can be due to three possible causes: **(1)** genuine co-localization of a host SSU rRNA with its terminase, **(2)** chance co-localization of a free floating terminase gene with a 16S rRNA gene, **(3)** chance co-localization of a spurious FAM amplification (no actual terminase amplicon present) with an rRNA gene. See Table 2.13 for a definition of all the variables used in the model.

Estimation of p_F

To calculate the P value above, one must estimate p_F, i.e., the probability that a successful retrieval from a panel contains our particular ribotype $\boldsymbol{S}$ and any terminase gene by pure chance. This probability can be estimated as follows: let X_T be defined as the sum of the total number of free floating terminase targets and spurious targets leading to spurious FAM amplification (i.e., noise). We will see how to estimate X_T later on but for the time being let's assume it is given. The average number of free floating terminase targets to co-localize with a *particular* 16S rRNA ribotype $\boldsymbol{S}$ on a panel, defined as I_{S}, is given by multiplying the number of wells on a panel (765) by (a) the probability that a given well will contain a free floating terminase target p_{ter} and (b) the probability that that well will also contain ribotype $\boldsymbol{S}$**.** The probability that a given well will contain a free floating terminase target is

(S1)
$$p_{ter} = \left(\frac{X_T - noise}{765} \right).$$

where *noise* is the number of FAM hits that are due to spurious amplification and are not associated with an actual terminase target. Thus $X_T - noise$ is the number of free floating terminase targets on the panel. Note that $X_T - noise$ will lead to an upper bound on the number of free floating terminase targets (leading to an upper bound on p_F) since $X_T - noise$ may include wells with a genuine 16S rRNA amplicon that simply did not pass the HEX detection threshold and are thus wrongly labeled as free-floating terminase targets (as described above). The value for *noise* can be estimated from the no-template-control panel for a given chip (see for example Table 2.12).

The average number of free floating terminase targets to co-localize with a *particular* 16S rRNA ribotype ***S*** on a panel is therefore given by

(S2a)
$$I_S = 765 \cdot p_{ter} \cdot \left(\frac{f_S \cdot Y}{765} \right) = p_{ter} \cdot f_S \cdot Y.$$

where *Y* is the total number of HEX hits on a panel, f_S is the frequency of ribotype ***S*** on the chip so that $f_S Y$ is the number of ribotypes ***S*** on a given panel. I_S is an estimate of the number of false co-localizations on a panel. This number is smaller than the number of observed co-localization on the panel, which we designate by *I* (=number of HEX and FAM intersections on a given panel). The number actual co-localizations on a panel of any 16S rRNA target with any terminase target (i.e., the total pool from which we draw successful retrievals) would be on average

(S2b)
$$I_{\text{all 16S-ter}} = I - \frac{noise \cdot Y}{765}.$$

taking out random co-localization of spurious FAM hits from *I*. The probability p_F is therefore given by the ratio of the number of random co-localization on a panel, I_S, and $I_{\text{all 16S-ter}}$, the number of actual co-localizations on the panel (i.e., of any 16S rRNA and any terminase target, both true and false co-localizations). Thus

(S3)
$$p_F = \frac{I_{\text{S}}}{I_{\text{all 16S-ter}}} = f_{\text{S}} \cdot \frac{p_{ter} \cdot Y}{I_{\text{all 16S-ter}}}.$$

Since $p_{ter} \cdot Y / I_{\text{all 16S-ter}}$ can vary somewhat from panel to panel, to calculate p_F we use Bayes' theorem:

$$p_F = P(\text{false} \mid \text{panel A}) P(\text{panel A}) + P(\text{false} \mid \text{panel B}) P(\text{panel B}) + \ldots$$

We therefore replace $p_{ter} \cdot Y / I_{\text{all 16S-ter}}$ in Eq. S3 by its panel averaged value, weighted by the number of times each panel was sampled (making at total of *n*=41 trials). The estimated values of p_F per host type are given in Table 2.14.

Estimation of X_T

Let us assume that a given panel has X FAM hits, Y HEX hits, and I intersections. The number of non-co-localized terminase hits is then $X_f = X - I$. X_T is slightly larger than X_f since some of the free floating targets or spurious targets may have co-localized with HEX hits. This difference ($X_T - X_f$) is estimated by multiplying the number of wells on a panel by (a) the probability that a well will contain a free floating target *or* a spurious target and (b) the probability that that well will contain *any* HEX hit. Thus $X_T - X_f = (765 \text{ wells})\left(\frac{X_T}{765}\right)\left(\frac{Y}{765}\right)$, or

$$X_T = X_f + (765 \text{ wells})\left(\frac{X_T}{765}\right)\left(\frac{Y}{765}\right).$$

Solving for X_T we find that

(S4)
$$X_T = X_f\left(1-\frac{Y}{765}\right)^{-1} = (X-I)\left(1-\frac{Y}{765}\right)^{-1}.$$

Note that since typically Y~50, $X_T \approx X - I$.

Estimation of f_s

f_s, the frequency of ribotypes ***S*** on the chip, is estimated based on the number of the particular REP ribotypes that grouped with the corresponding host ***S*** (e.g., five REP4 ribotypes out of 118 grouped with Host I in Fig. 2.7, therefore f_s=5/118). Operational taxonomical units for REP/host clades were determined by a DOTUR analysis (Table 2.6 and Fig. 2.7).

Given f_S and X_T (Eq. S4) we can calculate p_F (Eq. S3), and given k (Table 2.1) we can calculate the P value. Table 2.14 summarizes the frequencies f_S, probabilities p_F and P values for Hosts I though IV. As mentioned in the beginning of this section, the P values calculated for Hosts I through IV were very small ($P < 10^{-4}$) allowing us to reject the null hypothesis, i.e., the repeated ribotypes I–IV cannot be explained by random co-localization of these ribotypes with free floating terminase targets.

Bound on false co-localization in the dataset

We would like to estimate the average number of retrievals where one of the observed hosts co-localized by chance with a terminase (resulting in either two terminases — the host's and the free floating terminase, or, in the case the host's terminase did not amplify or was not present, one wrong terminase). The probability that we retrieve from a given panel any of the host ribotypes with the wrong terminase is given by summing the individual false co-localization probabilities for each host -

$p_{F,tot} = \sum_{\text{host I-IV}} p_F = \left(p_{ter} \cdot \sum_{\text{host I-IV}} f_S \cdot Y \right) \Big/ I_{\text{all 16S-ter}}$. The average number of false co-localizations in a dataset of n=41 retrievals would therefore be

$$N_{false} = p_{F,tot} \cdot n. \qquad \text{(S5)}$$

We find that N_{false} =0.6. Thus out of 28 repeated co-localizations of our hosts, on average ~0.6 are expected to be false (an error of 2%). The fact that no co-localized pairs were retrieved with the most abundant phylotypes on the array (see Table 2.6 and Fig. 2.7) and that the three most abundant phylotypes on the array comprising 49% of all treponemes in only one out of 38 cases co-localized with an rRNA gene (see discussion on non-hosts below) confirms that erroneous co-localization was indeed very rare.

Numerical simulation to test the statistical model

To check our statistical analysis (Eq. S1-S7) we conducted a Monte Carlo simulation of retrieval from the microfluidic panels based on the model presented above (Fig. 2.11). The numerical simulation results were predicted precisely by the statistical model described above.

Model for Monte Carlo simulation

In the simulation Y rRNA templates were loaded randomly onto a panel of 765 chambers (Y~U[Y_{min},Y_{max}]). Each panel was also randomly loaded with *noise* spurious FAM hits (*noise*~U[$noise_{min}$,$noise_{max}$]) and *free* free floating terminase targets (*free*~U[$free_{min}$, $free_{max}$]). A fraction f (i.e., probability) of the Y rRNA templates was assumed to be genuine hosts (i.e., hosts that genuinely harbor a terminase gene). The terminase gene within these hosts was assumed to be amplified with probability e_{ter}. Each retrieval trial consisted of loading a single panel of 765 chambers with the above elements and retrieving one sample that contained both a 16S rRNA sequence and a terminase sequence. If the retrieval failed (i.e., the rRNA was co-localized with a spurious FAM target) a new retrieval trial would be attempted until successful (these mute trials would not be counted as successful iterations). For each successful retrieval trial it was registered if the retrieval was a false co-localization (i.e., a host 16S rRNA sequence was co-localized with a free floating terminase). In addition for each successful retrieval trial the probability of false co-localization p_F was calculated. This probability is given by the ratio of number of false-co-localizations on the panel (i.e., a 16S rRNA gene that co-localized with a free-floating terminase) and the total number of co-localization on the panel (any 16S and any terminase gene). A single Monte Carlo iteration ended when $N_{retrievals}$ (=41) successful retrievals were obtained. At the end of each Monte Carlo iteration, the total number of false co-localizations (N_{false}) was tallied and the average value for p_F was calculated. In total there were 1000 Monte Carlo iterations.

To compare with the statistical model above, after each Monte Carlo iteration, p_F and N_{false} were estimated based on Eq. S3 and Eq. S5 assuming $f=f_S$ and given the random values for X, Y, I and *noise* generated for each of the 41 panels in the simulation. At the end of the simulation the average value of p_F and N_{false} (averaged over 1000 iterations) was compared to the predicted values of p_F and N_{false} based on the statistical analysis.

Simulation parameters

Simulation parameters were chosen to mimic the experiments in this study as closely as possible: $N_{retrievals}=41$; all hosts were assumed to be indistinguishable so that f_S was given as the sum of all the rates f_S in Table 2.14 (i.e., $f_S=9/118$, where 9 is the total number of occurrences of Hosts I–IV phylotypes in the reference library, and 118 is the size of the reference library — see Table 2.1). All other parameters followed the distributions in Table 2.14 with $Y \sim U(20,80)$, $noise \sim U(5,15)$, $free \sim U(0,20)$ and $e_{ter}=0.74$ (see Materials and Methods).

Simulation results

We found that the predictions for p_F (Eq. S3) and N_{false} (Eq. S5) closely matched the numerical simulation:

$$\begin{cases} p_F\text{(simulation)=0.014}\pm 0.011 \\ \hat{p}_F\text{(Eq. S3)=0.018}\pm 0.022 \end{cases} \quad \begin{cases} N_{false}\text{(simulation)=0.6}\pm 0.8 \\ \hat{N}_{false}\text{(Eq. S5)=0.7}\pm 0.9 \end{cases}$$

The errors are standard deviations. The simulation presented here shows that the statistical model presented above (Eq. S1-S7) is consistent with the numerical simulations.

Chambers with multiple cells

Since the average number of targets loaded per panel was small (~50), the chance of obtaining multiple cells in a given chamber was small (1.7 chambers out of 50 on average (*S43*)). However cells can also potentially "stick" together upon loading as well. If a chamber contains multiple 16S rRNA genes and more than one gene is amplified then the sequence trace will be mixed. Such samples were automatically discarded in this study. If a 16S rRNA chimera is formed, chimera products are screened with Pintail (*S8*) and Bellerophon (*S9*) and discarded from further analysis (no such chimeras were found in this study). The chance however that the same ribotypes would repeatedly co-localize and either form a chimera or amplify the wrong rRNA gene are extremely small. To estimate the chance for such an event, we shall consider the case where the host 16S rRNA gene, ***S***, repeatedly co-localized with the same rRNA gene ***S'***, and that the foreign 16S rRNA gene (***S'***) was amplified while the host 16S rRNA gene (***S***) was not amplified. The average number of such chance events per panel where the host terminase was also amplified is given by $I_{SS'} = \varepsilon_{ter}\varepsilon_{16S}(1-\varepsilon_{16S})(f_sY)(f_{s'}Y)/765$, where ε_{ter} and ε_{16S} are the amplification efficiencies of the terminase gene and the 16S rRNA gene, respectively (see Materials and methods for an estimation of these efficiencies), $f_{s'}$ is the frequency of the ***S'*** ribotype, and $(f_sY)(f_{s'}Y)/765$ is the number of chance co-localizations of ***S*** and ***S'*** cell types on a given panel. The probability therefore of retrieving such events is $p_F^{mixed} = I_{SS'} / I_{\text{all 16S-ter}}$. Assuming $f_{s'} \sim 0.2$ (corresponding to the worst case scenario of co-localizing with the most frequent ribotype on the chip, REP1) then based on Table 2.14 we have $p_F^{mixed} << p_F$ (where p_F is given in Eq. S3) and therefore these events can be neglected (the P values for such events would be much smaller than those in Table 2.1).

Uniformity of panel loading

On a few occasions, panels were loaded by the NanoFlex somewhat nonuniformly. This has the consequence of reducing the effective number of wells available for the cells. The samples affected for Host I were C2 and G1. The terminases of samples C2 and G1 fell in the main clade of Host I of highly similar terminases (Clade V1 in Fig. 2.2) lending support for these co-localizations. Sample G2 (Host III) was taken from a slightly nonuniform panel, however the terminase of sample G2 was 100% identical at the amino acid level (235 aa alignment) to F2 also associated with Host III, lending support for this co-localization. Samples affected for Host II were A4 and A7, however the terminase of A4 was 99.6% identical at the amino acids level (235 aa alignment) to the terminase of A9i also of Host II, lending support for this sample. The terminase of A7 was 95.3% identical at the amino acids level to the terminase of A13i also of Host II, lending support for this sample.

Estimation of the P value for putative *Treponema* non-host (REPs1-3)

The phylotypes REP1, REP2, and REP3 were highly repeated in the random rRNA reference library ($f_{\mathrm{S}} = 23/118, 8/118, 7/118$, respectively) but were never sampled in the co-localization library (n=41). The null hypothesis is therefore that ribotype ***S*** is a genuine host but was not sampled n=41 times by chance. We wish to calculate the probability for this event. The fraction of co-localizations in a given panel that contain host ***S*** is given on average by

(S6)
$$p_S = \frac{\varepsilon_{ter} \cdot f_{\mathrm{S}} \cdot Y}{I_{\text{all 16S-ter}}}.$$

where ε_{ter} is the efficiency of amplification for the terminase gene (see Materials and methods), f_{S} the frequency of host ***S*** on the chip, Y the number of 16S rRNA hits on a given panel, and $I_{\text{all 16S-ter}}$ is the number co-localizations on a panel of a 16S rRNA target with an actual terminase target (Eq. S2b). Therefore $\varepsilon_{ter} \cdot f_{\mathrm{S}} \cdot Y$ is the number of expected genuine co-localizations for ribotype ***S****,* and $\varepsilon_{ter} \cdot f_{\mathrm{S}} \cdot Y / I_{\text{all 16S-ter}}$ would be the probability to sample this co-localization. The probability (P value, one tailed, n=41) for not retrieving ***S*** (k=0) after n=41 trials is given by

$$\text{P value} = \text{Prob}\left(k = 0 \,|\, n = 41 \text{ successful retrievals}\right) = (1 - p_S)^n$$

where p_S is averaged using Bayes' theorem as described above (i.e., a panel-weighed average based on Table 2.14 for all 41 retrievals). For $\varepsilon_{ter} \approx 0.8$ (measured value) we find that the P value (one tailed test with *n*=41) for not retrieving a host with a frequency of $f_S \geq 7/118$ is $\leq 4.8 \cdot 10^{-20}$ allowing us to reject this hypothesis. If REPs-1, 2, and 3 are infected in only >5%, 14%, and 16% of the cases respectively, then the P value for not retrieving these infected strains is 0.01 (one tailed test with *n*=41). Therefore based on statistical grounds we conclude that the majority of REP1–3 cells are not infected. Furthermore 21 out of 23 REP-1 ribotypes, 8 out of 8 REP-2 ribotypes, and 7 out of 7 REP-3 ribotypes were not associated with a terminase hit on the microfluidic chips. Of the two positive hits for REP-1, post-amplification followed by agarose gel electrophoresis showed that just one of these samples contained a terminase target. Statistically, out of *n*=38 occurrences of REPs1-3, $p_{ter} \cdot n$ should randomly co-localize with a terminase target on the chip, or 0.4±0.2 random co-localizations, as observed. This is consistent with the hypothesis that REPs1-3 are indeed non-hosts.

2.9.2.2 The viral marker gene and its genetic context

Requirements for a viral marker gene

Since certain viral genes can be of bacterial origin, and some viral genes may not be associated with an actual functional virus, a genuine viral marker should satisfy certain requirements (*S42*). We were therefore interested in choosing as a viral marker a gene that (a) was unique to viruses, (b) was present in a larger viral context, (c) was prevalent in the ecosystem we were investigating, (d) contained multiple conserved regions that could be used to design degenerate primers, and (e) is active or has been active in recent evolutionary history in this system. The large terminase subunit chosen as a viral marker gene fulfilled all of the above requirements:

(1) The large terminase subunit is considered to be one of the most universally conserved phage genes and best phage identifiers (*S42*), exhibiting certain conserved residues and motifs (see Figs.

2.5 and 2.6). Furthermore, since typically different phages exhibit little overall sequence similarly (see main text), the terminase gene also appears to be system specific (*S44*), thereby potentially serving as a good differentiating marker (*S45*).

(2) Bioinformatic analysis of the ZAS-2 and ZAS-9 genomes revealed four prophage-like elements (two in each genome) that were related to tailed phages based on their sequence homology. The largest of these elements (ZAS-2A) spanned 43.5 kb, which is a typical size for tailed phages (*S46*). Furthermore, all four copies of the terminase gene in the ZAS genomes had homologs in the higher termite metagenome with 77–79% amino acid identity. The largest of these elements, ZAS-2A, appeared to be associated with the *Caudovirales* order: When BLASTing each of the 41 identified genes in this prophage-like element against NCBI's viral RefSeq (v37) database, 16 genes had significant hits ($E < 0.005$), with 15 out of the 16 genes being associated with homologs present in viruses belonging to the *Caudovirales* order. The viral genes also follow a typical tailed-phage gene organization pattern (*S47*). For example genes ZA3, ZA4, ZA5, ZA7, ZA8 are the head related genes (homologous to the small and large terminase subunit genes, portal protein gene, prohead protease gene, and capsid protein gene, respectively), whereas genes ZA32 and ZA33 towards the end of the cassette exhibited a weak homology to a tail fiber gene and a tail tape measure protein gene, respectively ($E = 0.16$, 0.29, respectively). Among the 15 hits above, 11 were associated with the *Siphoviridae* family, two with the *Podoviridae* and two with the *Myoviridae* family. The last four genes appear to be less diagnostic than the *Siphoviridae* related genes as they are not signature phage genes and the E value for three of these genes was low ($E \geq 0.001$). Although it is possible that the prophage-like elements are mosaics of

Caudovirales families (*S48*), based on the above analysis it appears that these elements are mostly closely related to the *Siphoviridae* family.

(3) Bioinfomratic analysis of the metagenome (Table 2.2) identified the large terminase subunit as one of the most abundant viral-unique genes in the metagenome (though this may not reflect absolute abundance in the sample due to assembler bias). In addition, more generally, the ZAS prophage-like elements appear to be ubiquitous to the termite environment as certain cassettes within the ZAS prophage-like elements were found to be abundant in the higher termite metagenome. For example, the large terminase subunit and its adjacent portal protein from ZAS-2A had a maximum percent amino acid identity of 78% and 70%, respectively, when BLASTed against the metagenome (Table 2.3) and were homologous to 46 and 43 metagenome gene objects respectively, ($E \leq 1e\text{-}5$). Furthermore, these two genes, that are adjacent to each other in the ZAS genomes (a typical organization in viruses (*S42*)) were also found to be next to each other in the metagenome contigs.

(4) Alignment of the terminase alleles from the ZAS genomes and the higher termite metagenome revealed multiple conserved regions that could be used for primer design (Fig. 2.5).

(5) Viral-specific genes encoded by ZAS-2 and ZAS-9 prophage-like elements (the portal protein, the capsid protein, the large terminase subunit and the prohead protease protein) exhibited substantial negative selection pressure (data not shown). In addition, the terminase genes retrieved from *R. hesperus* specimens also exhibited substantial negative selection pressure (see Materials and methods and Table 2.7). This evidence suggests that the terminase gene in the termite system if not functional, has been functional in recent evolutionary history (see discussion below). In addition, there is some anecdotal evidence suggesting the terminase is part of an active viral entity. In one of the earlier experiments with the microfluidic arrays (prior to execution of arrays A through G from which samples were retrieved), where chilling of samples to 4°C was not strictly enforced, a dilution series of a *Zootermopsis nevadensis* termite hindgut fluid was loaded onto a microfluidic array. The panel on the array corresponding to the largest gut dilution exhibited 34.9 times the number of expected terminase hits (384 observed verus 11 expected), where the expected number of hits was estimated based on the number of hits from more concentrated dilutions loaded onto the same microfluidic array. At the same time, the rRNA channel displayed the expected number of hits (72 observed versus 74 expected) for this dilution. Since the degenerate terminase primers that were used in the qPCR chemistry were designed based on the terminase alleles in the ZAS-2 and ZAS-9 prophage-like elements (among other alleles), this induction event is specific to the terminase gene investigated in this study. This result indicates that a lytic event associated with the prophage-like element may have taken place in the tube containing the largest gut dilution, suggesting that this putative prophage is functional. We note that earlier experiments to induce the ZAS-2 and ZAS-9 cultures using mitomycin C were not successful, suggesting that mitomycin C may not be the inducing agent of this element.

Functionality of the terminase gene

Given the fact that the terminase gene is under negative selection pressure and in the absence of obvious frame shift mutations or errant stop codons in the alignment, there are several options regarding the nature of the prophage-like element in which it resides and the functionality of the terminase gene within these elements: **(1)** the terminase is part of an active prophage (for which there is some evidence, as discussed in point 5 above) **(2)** the terminase is part of a defective prophage but it remained functional because there was not enough time for point mutations to have accumulated. This can happen because "prophage-debilitating deletions can accumulate more rapidly than gene-inactivating point mutations" (*S42*). **(3)** The prophage indeed decayed and the terminase gene degraded over time, but was subsequently repaired by a recombination event with another phage that was likely functional (since it infected the cell in the first place)(*S42*). Finally, **(4)** the terminase was recruited by the bacterium because it confers on the bacterium some competitive advantage and is therefore under negative selection pressure.

To further elaborate on the last point (4), phage genes that are adopted by the cell are typically lysogenic conversion genes (*S42*) — genes that change the phenotype of the cell and confer some selective advantage to the cell. In this context, known possibilities may be (*S42*) tail-like bacteriocins and genetic transfer agents (GTAs). Bacteriocins are devices that kill other bacteria and some bacteria can produce bacteriocins that resemble phage tails (*S42, S49*). However since these entities do not have heads or package DNA it seems unlikely they would encode a terminase gene. For example, type F and type R tail-like bacteriocins of *Pseudomonas aeruginosa* PAO1 do not appear to encode a terminase gene or any other head related proteins (*S50-S51*). GTAs are tailed phage-like particles that encapsidate random fragments of the bacterial genome and can transfer them to other bacteria of the same species (*S42*). GTAs are thought to be adopted by the host cell to facilitate genetic exchange under the control of the host (*S52-S54*). The GTA coding region is typically short (~14–16 kb (*S54*)) and appears to contain the genes required for assembly of the GTA head and tail structures and the genes required for DNA packaging (including a terminase gene) (*S52, S54*). Phage DNA-specific replication functions and phage DNA-specific integration or excision functions are in principle not required by the GTA (*S52*). Although it cannot be ruled out that the terminase genes retrieved from *R. hesperus* are part of a GTA, this possibility appears to be unlikely since the predicted prophage-like element identified in ZAS-2 spans ~43.5 kb (a typical length for a functional phage), which is much longer than a typical GTA length (14–16 kb — see above). In addition, unlike GTAs, the ZAS-2 prophage-like element encodes both integration genes and several DNA replication machinery genes.

To summarize, the fact that the *R. hesperus* terminase alleles are under substantial negative selection pressure suggests that this terminase is either active or has been active in recent evolutionary history and was the direct or indirect result of a viral infection (options 1, 2, or 3 above). The possibility that the terminase was adopted by the cell and is part of a GTA appears to be unlikely. Thus the associations between the hosts and the terminase genes revealed by the microfluidic assay should be a valid proxy for interaction of these hosts with genuine infecting phages, reflecting either current or recent infections.

2.9.3 Supporting figures

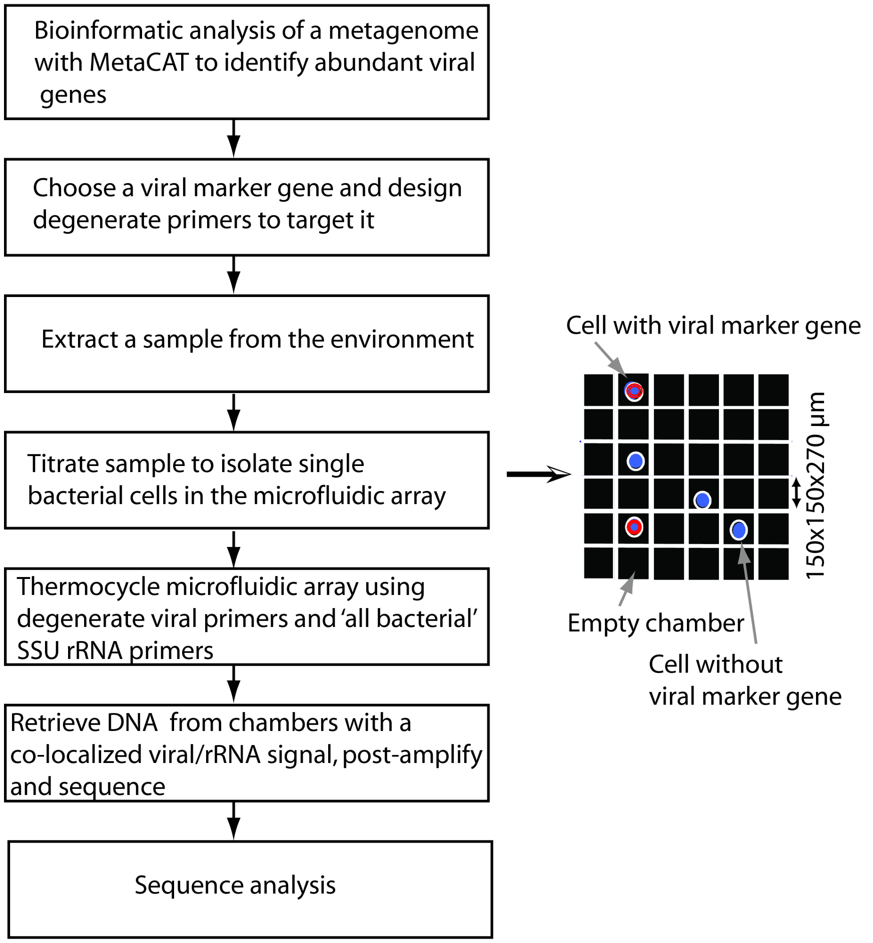
Bioinformatic analysis of a metagenome with MetaCAT to identify abundant viral genes
Choose a viral marker gene and design degenerate primers to target it
Extract a sample from the environment
Titrate sample to isolate single bacterial cells in the microfluidic array
Thermocycle microfluidic array using degenerate viral primers and 'all bacterial' SSU rRNA primers
Retrieve DNA from chambers with a co-localized viral/rRNA signal, post-amplify and sequence
Sequence analysis
Cell with viral marker gene
150x150x270 µm
Empty chamber
Cell without viral marker gene

Figure 2.4. Workflow using the microfluidic digital PCR array for host-virus co-localization in a novel environmental sample. See Materials and methods for further details.

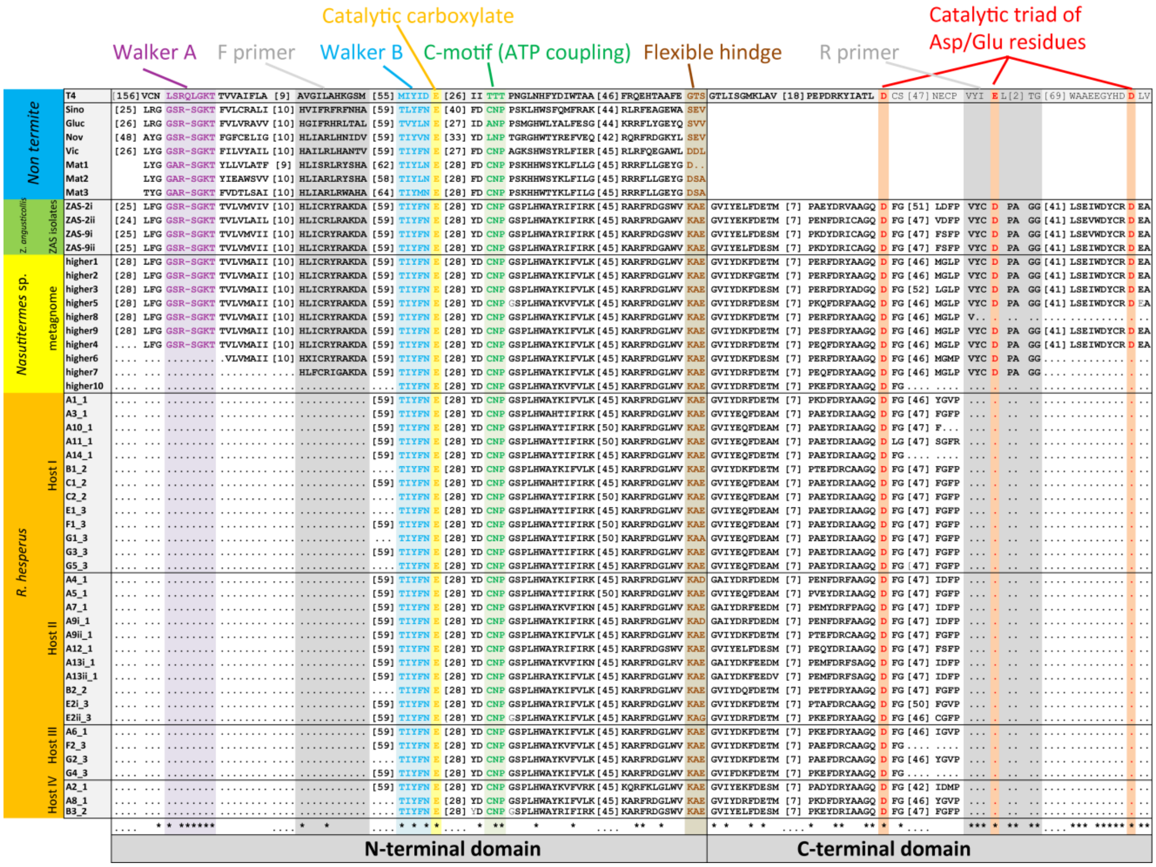

Figure 2.5. Multiple alignment of termite related terminase sequences and closest homologs. Here we show a multiple alignment of terminase genes of both termite and non-termite origin highlighting putative functional motifs. Terminase sequences included are (1) terminase sequences retrieved from *R. hesperus* termites using the digital PCR, (2) homologous terminases from the metagenome of a *Nasutitermes* sp. termite, (3) homologous terminases from *Treponema* isolates obtained from a *Z. angusticollis* termite, and (4) homologous terminases from non-termite related bacteria found in public databases (NCBI's protein RefSeq database and the Joint Genome Institute database). Also highlighted are putative conserved functional motifs for the N-terminal ATPase center and the C-terminal nuclease center (see Fig. 2.6). When searching for homologs for the ZAS2-i terminase gene in public databases, the N-terminal ATPase domain of this gene (amino acids 1-234 — see Fig. 2.6) appeared to be much more conserved (47% identity) than the entire gene (29% identity). Consistent with this fact, the ATPase domain of the large terminase subunit has been shown to be conserved in a wide variety of dsDNA (*S55*) viruses and even shows certain conserved motifs with the putative herpesvirus terminase (*S55-S56*) suggesting it is an ancient viral domain (*S55, S57-S58*). We therefore show here only the N-terminal domain alignment of non-termite homologous terminases.

N-terminal alignment: The boundary of the N-terminal domain for the terminase alleles was determined based on its location in T4 (residue 360)(*S59*) by aligning the amino acid sequences of the ZAS2-i terminase and all non-termite related terminases with RPS-BLAST against pfam03237 (*S59*) in the CDD (*S60*) (see Fig. 2.6 for ZAS2-i alignment). The N-terminal domain of other termite related sequences was then determined by a MUSCLE alignment to the ZAS2-i terminase (*S61*). All N-terminal domains were then MUSCLE aligned. **C-terminal alignment:** maximum length termite related terminases were MUSCLE aligned and then only their C-terminal regions were juxtaposed to the N-terminus alignment found above (the overlap with the N-terminus alignment was identical).

Functional motifs were identified based on an RPS-BLAST alignment of ZAS-2i against pfam03237 (Fig. 2.6). This figure demonstrates that the termite related terminase sequences exhibit terminase-like functional motifs. Putative functional motifs include (1) Walker A motif G/A-XXXXGK(T/S) (purple) with a single residue X deletion, (2) Walker B ZZZZD motif with D replaced by N — a relatively common substitution for this residue (blue), (3) catalytic carboxylate group motif — E (orange), (4) putative ATP coupling motif (green), and (5) catalytic Asp/Glu triad motif — here a conserved D (red)(*S62-S63*). Also highlighted is the putative flexible hinge motif (brown)(*S63*) based on the RPS-BLAST alignment. Numbers in brackets correspond to aligned residues not shown. Stars indicate conserved residues excluding T4. Dots indicate end of available sequence. X residues in the higher termite sequences are due to ambiguous base pairs in the nucleotide sequence. The RPS-BLAST ZAS2-i alignment with T4 (Fig. 2.6) was superimposed to guide the eye and was not part of the MUSCLE alignment. Also shown are the primer binding sites. The degenerate core region of the CODEHOP primers (*S34*) that is required to be conserved consists of 4 amino acids at the 3' end of the primer. Out of the 50 ZAS and higher termite gut alleles, 31 alleles included the forward primer motif and 26 alleles included the reverse primer motif. In all cases, the degenerate core region of the primers was strictly conserved. In one additional allele, the sequence began from the center Asp residue in the conserved catalytic Asp/Glu triad motif. This residue was mutated in this allele from an Asp residue to a Gly residue suggesting this partial allele encodes a nonfunctional terminase. Thus, all functional alleles of the terminase gene exhibited a strictly conserved degenerate core region. Note that the Walker A motif was not chosen for a forward primer binding site due to the high degeneracy involved with this amino acid sequence.

To check what diversity of terminase genes are expected to be amplified, we BLASTed the core region of the forward (ter7F) and reverse (ter5eR) terminase primers against all viral genes in NCBI's viral RefSeq database v37. Only the core region of the primer was used in the BLAST analysis (a more general search) because the primers are CODEHOP primers and therefore while the degenerate core region (11–12 bases in the 3' region of the primer) must base pair with the target, homology of the clamp region is less critical for initial amplification. We then crossed the list of hits for the forward and reverse primers searching for mutual hits present in the same gene within the same bacteriophages, however no such solutions were found. Based on this result we anticipate that the degenerate terminase primers target the unique diversity of terminase genes currently known to exist only in termite and possibly related insect species.

Non-termite related terminases (Vic, Sino, Gluc, and Nov) are gram negative isolates belonging to the Lentisphaerae and Proteobacteria phyla. These bacteria grow in a variety of habitats (human gut, soil, fresh water, plants, etc.) and can either be free living or symbiotic, anaerobic or aerobic. Mat1, Mat2, and Mat3 were found to be present in the metagenome of a hypersaline microbial mat from Mexico (see Table 2.11 for accession numbers).

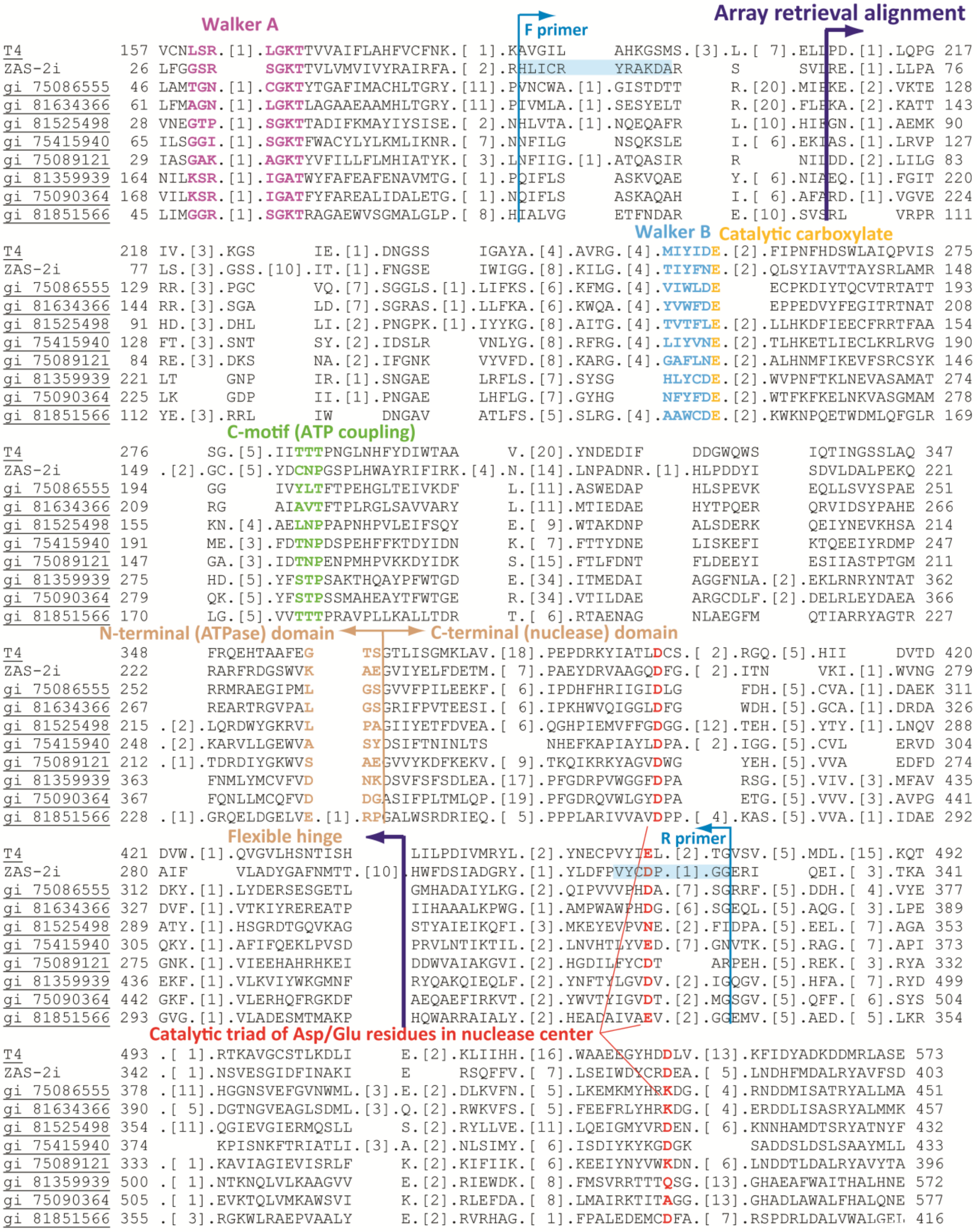
Walker A
F primer
Array retrieval alignment
Walker B
Catalytic carboxylate
C-motif (ATP coupling)
N-terminal (ATPase) domain
C-terminal (nuclease) domain
Flexible hinge
R primer
Catalytic triad of Asp/Glu residues in nuclease center

```
T4           157 VCNLSR.[1].LGKTTVVAIFLAHFVCFNK.[ 1].KAVGIL      AHKGSMS.[3].L.[ 7].ELIPD.[1].LQPG 217
ZAS-2i        26 LFGGSR      SGKTTVLVMVIVYRAIRFA.[ 2].RHLICR      YRAKDAR      S       SVIRE.[1].LLPA 76
gi 75086555   46 LAMTGN.[1].CGKTYTGAFIMACHLTGRY.[11].PVNCWA.[1].GISTDTT      R.[20].MIEKE.[2].VKTE 128
gi 81634366   61 LFMAGN.[1].LGKTLAGAAEAAMHLTGRY.[11].PIVMLA.[1].SESYELT      R.[20].FLEKA.[2].KATT 143
gi 81525498   28 VNEGTP.[1].SGKTTADIFKMAYIYSISE.[ 2].NHLVTA.[1].NQEQAFR      L.[10].HIEGN.[1].AEMK 90
gi 75415940   65 ILSGGI.[1].SGKTFWACYLYLKMLIKNR.[ 7].NNFILG      NSQKSLE      I.[ 6].EKIAS.[1].LRVP 127
gi 75089121   29 IASGAK.[1].AGKTYVFILLFLMHIATYK.[ 3].LNFIIG.[1].ATQASIR      R       NIIDD.[2].LILG 83
gi 81359939  164 NILKSR.[1].IGATWYFAFEAFENAVMTG.[ 1].PQIFLS      ASKVQAE      Y.[ 6].NIAEQ.[1].FGIT 220
gi 75090364  168 VILKSR.[1].IGATFYFAREALIDALETG.[ 1].NQIFLS      ASKAQAH      I.[ 6].AFARD.[1].VGVE 224
gi 81851566   45 LIMGGR.[1].SGKTRAGAEWVSGMALGLP.[ 8].HIALVG      ETFNDAR      E.[10].SVSRL      VRPR 111

T4           218 IV.[3].KGS      IE.[1].DNGSS      IGAYA.[4].AVRG.[4].MIYIDE.[2].FIPNFHDSWLAIQPVIS 275
ZAS-2i        77 LS.[3].GSS.[10].IT.[1].FNGSE      IWIGG.[8].KILG.[4].TIYFNE.[2].QLSYIAVTTAYSRLAMR 148
gi 75086555  129 RR.[3].PGC      VQ.[7].SGGLS.[1].LIFKS.[6].KFMG.[4].VIWLDE     ECPKDIYTQCVTRTATT 193
gi 81634366  144 RR.[3].SGA      LD.[7].SGRAS.[1].LLFKA.[6].KWQA.[4].YVWFDE     EPPEDVYFEGITRTNAT 208
gi 81525498   91 HD.[3].DHL      LI.[2].PNGPK.[1].IYYKG.[8].AITG.[4].TVTFLE.[2].LLHKDFIEECFRRTFAA 154
gi 75415940  128 FT.[3].SNT      SY.[2].IDSLR      VNLYG.[8].RFRG.[4].LIYVNE.[2].TLHKETLIECLKRLRVG 190
gi 75089121   84 RE.[3].DKS      NA.[2].IFGNK      VYVFD.[8].KARG.[4].GAFLNE.[2].ALHNMFIKEVFSRCSYK 146
gi 81359939  221 LT      GNP      IR.[1].SNGAE      LRFLS.[7].SYSG      HLYCDE.[2].WVPNFTKLNEVASAMAT 274
gi 75090364  225 LK      GDP      II.[1].PNGAE      LHFLG.[7].GYHG      NFYFDE.[2].WTFKFKELNKVASGMAM 278
gi 81851566  112 YE.[3].RRL      IW      DNGAV      ATLFS.[5].SLRG.[4].AAWCDE.[2].KWKNPQETWDMLQFGLR 169

T4           276       SG.[5].IITTTPNGLNHFYDIWTAA      V.[20].YNDEDIF      DDGWQWS      IQTINGSSLAQ 347
ZAS-2i       149 .[2].GC.[5].YDCNPGSPLHWAYRIFIRK.[4].N.[14].LNPADNR.[1].HLPDDYI      SDVLDALPEKQ 221
gi 75086555  194       GG      IVYLTFTPEHGLTEIVKDF      L.[11].ASWEDAP      HLSPEVK      EQLLSVYSPAE 251
gi 81634366  209       RG      AIAVTFTPLRGLSAVVARY      L.[11].MTIEDAE      HYTPQER      QRVIDSYPAHE 266
gi 81525498  155       KN.[4].AELNPPAPNHPVLEIFSQY      E.[ 9].WTAKDNP      ALSDERK      QEIYNEVKHSA 214
gi 75415940  191       ME.[3].FDTNPDSPEHFFKTDYIDN      K.[ 7].FTTYDNE      LISKEFI      KTQEEIYRDMP 247
gi 75089121  147       GA.[3].IDTNPENPMHPVKKDYIDK      S.[15].FTLFDNT      FLDEEYI      ESIIASTPTGM 211
gi 81359939  275       HD.[5].YFSTPSAKTHQAYPFWTGD      E.[34].ITMEDAI      AGGFNLA.[2].EKLRNRYNTAT 362
gi 75090364  279       QK.[5].YFSTPSSMAHEAYTFWTGE      R.[34].VTILDAE      ARGCDLF.[2].DELRLEYDAEA 366
gi 81851566  170       LG.[5].VVTTTPRAVPLLKALLTDR      T.[ 6].RTAENAG      NLAEGFM      QTIARRYAGTR 227

T4           348       FRQEHTAAFEG      TSGTLISGMKLAV.[18].PEPDRKYIATLDCS.[ 2].RGQ.[5].HII      DVTD 420
ZAS-2i       222       RARFRDGSWVK      AEGVIYELFDETM.[ 7].PAEYDRVAAGQDFG.[ 2].ITN      VKI.[1].WVNG 279
gi 75086555  252       RRMRAEGIPML      GSGVVFPILEEKF.[ 6].IPDHFHRIIGIDLG      FDH.[5].CVA.[1].DAEK 311
gi 81634366  267       REARTRGVPAL      GSGRIFPVTEESI.[ 6].IPKHWVQIGGLDFG      WDH.[5].GCA.[1].DRDA 326
gi 81525498  215 .[2].LQRDWYGKRVL      PAGIIYETFDVEA.[ 6].QGHPIEMVFFGDGG.[12].TEH.[5].YTY.[1].LNQV 288
gi 75415940  248 .[2].KARVLLGEWVA      SYDSIFTNINLTS      NHEFKAPIAYLDPA.[ 2].IGG.[5].CVL      ERVD 304
gi 75089121  212 .[1].TDRDIYGKWVS      AEGVVYKDFKEKV.[ 9].TKQIKRKYAGVDWG      YEH.[5].VVA      EDFD 274
gi 81359939  363       FNMLYMCVFVD      NKDSVFSFSDLEA.[17].PFGDRPVWGGFDPA      RSG.[5].VIV.[3].MFAV 435
gi 75090364  367       FQNLLMCQFVD      DGASIFPLTMLQP.[19].PFGDRQVWLGYDPA      ETG.[5].VVV.[3].AVPG 441
gi 81851566  228 .[1].GRQELDGELVE.[1].RPGALWSRDRIEQ.[ 5].PPPLARIVVAVDPP.[ 4].KAS.[5].VVA.[1].IDAE 292

T4           421 DVW.[1].QVGVLHSNTISH      LILPDIVMRYL.[2].YNECPVYIEL.[2].TGVSV.[5].MDL.[15].KQT 492
ZAS-2i       280 AIF      VLADYGAFNMTT.[10].HWFDSIADGRY.[1].YLDFPVYCDP.[1].GGERI      QEI.[ 3].TKA 341
gi 75086555  312 DKY.[1].LYDERSESGETL      GMHADAIYLKG.[2].QIPVVVPHDA.[7].SGRRF.[5].DDH.[ 4].VYE 377
gi 81634366  327 DVF.[1].VTKIYREREATP      IIHAAALKPWG.[1].AMPWAWPHDG.[6].SGEQL.[5].AQG.[ 3].LPE 389
gi 81525498  289 ATY.[1].HSGRDTGQVKAG      STYAIEIKQFI.[3].MKEYEVPVNE.[2].FIDPA.[5].EEL.[ 7].AGA 353
gi 75415940  305 QKY.[1].AFIFQEKLPVSD      PRVLNTIKTIL.[2].LNVHTLYVED.[7].GNVTK.[5].RAG.[ 7].API 373
gi 75089121  275 GNK.[1].VIEEHAHRHKEI      DDWVAIAKGVI.[2].HGDILFYCDT      ARPEH.[5].REK.[ 3].RYA 332
gi 81359939  436 EKF.[1].VLKVIYWKGMNF      RYQAKQIEQLF.[2].YNFTYLGVDV.[2].IGQGV.[5].HFA.[ 7].RYD 499
gi 75090364  442 GKF.[1].VLERHQFRGKDF      AEQAEFIRKVT.[2].YWVTYIGVDT.[2].MGSGV.[5].QFF.[ 6].SYS 504
gi 81851566  293 GVG.[1].VLADESMTMAKP      HQWARRAIALY.[2].HEADAIVAEV.[2].GGEMV.[5].AED.[ 5].LKR 354

T4           493 .[ 1].RTKAVGCSTLKDLI      E.[2].KLIIHH.[16].WAAEEGYHDDLV.[13].KFIDYADKDDMRLASE 573
ZAS-2i       342 .[ 1].NSVESGIDFINAKI      E      RSQFFV.[ 7].LSEIWDYCRDEA.[ 5].LNDHFMDALRYAVFSD 403
gi 75086555  378 .[11].HGGNSVEFGVNWML.[3].E.[2].DLKVFN.[ 5].LKEMKMYHRKDG.[ 4].RNDDMISATRYALLMA 451
gi 81634366  390 .[ 5].DGTNGVEAGLSDML.[3].Q.[2].RWKVFS.[ 5].FEEFRLYHRKDG.[ 4].ERDDLISASRYALMMK 457
gi 81525498  354 .[11].QGIEVGIERMQSLL      S.[2].RYLLVE.[11].LQEIGMYVRDEN.[ 6].KNNHAMDTSRYATNYF 432
gi 75415940  374       KPISNKFTRIATLI.[3].A.[2].NLSIMY.[ 6].ISDIYKYKGDGK      SADDSLDSLSAAYMLL 433
gi 75089121  333 .[ 1].KAVIAGIEVISRLF      K.[2].KIFIIK.[ 6].KEEIYNYVWKDN.[ 6].LNDDTLDALRYAVYTA 396
gi 81359939  500 .[ 1].NTKNQLVLKAAGVV      E.[2].RIEWDK.[ 8].FMSVRRTTTQSG.[13].GHAEAFWAITHALHNE 572
gi 75090364  505 .[ 1].EVKTQLVMKAWSVI      K.[2].RLEFDA.[ 8].LMAIRKTITAGG.[13].GHADLAWALFHALQNE 577
gi 81851566  355 .[ 3].RGKWLRAEPVAALY      E.[2].RVRHAG.[ 1].FPALEDEMCDFA.[ 7].RSPDRLDALVWALGEL 416
```

Figure 2.6. Multiple alignment of pfam03237 with a ZAS-associated terminase. Multiple sequence alignment of pfam03237 (Terminase_6) with the ZAS-2 terminase sequence (ZAS-2i) aligned with RPS-BLAST in the CDD (*S60*) (E value 1.2e-19). Conserved functional motifs (*S62-S63*) are indicated as well as the boundary between the N-terminal ATPase domain (T4: amino acids 1–360 (*S63*)) and C-terminal nuclease domain (T4: amino acids 361–610 (*S63*)) based on T4 (*S59, S62*). Conserved functional motifs for the N terminal ATPase center include (*S62-S63*) a Walker A motif G/A-XXXXGK(T/S) (purple), a Walker B motif ZZZZD where Z represents a

hydrophobic amino acid (blue), a catalytic carboxylate group motif (usually) Glu (orange), and an ATPase coupling motif (T/S-G/A-T/S(N)) (green). The functional motif for the C-terminal nuclease center is a catalytic triad of Asp/Glu residues (red)(*S62-S63*). The forward primer (upper light blue box) targeted a conserved region between the putative Walker A and Walker B motifs in the ATPase domain and the reverse primer targeted a conserved region that included the central aspartic acid residue in the catalytic triad (lower light blue box). Also indicated is the 235 residue alignment region (without gaps) used for phylogenetic analysis. The alignment shows the 10 most diverse members (out of 43) of the pfam with the T4 large terminase subunit gene gp17 being the representative sequence. Numbers in brackets are unaligned residues. ZA2-2i was chosen for the alignment because this gene was found to be present in the largest (43.5 kb) prophoage-like element of the ZAS genome (see supporting text).

Figure 2.7. Phylogenetic analysis of retrieved *Treponema* SSU rRNA sequences and close relatives. Maximum likelihood tree of 39 retrieved *Treponema* SSU rRNA sequences from co-localized pairs (red), 78 reference library *Treponema* SSU rRNA sequences (black) and close relatives found in the SILVA (*S11*) database v100 (green). Also highlighted are Phage Hosts I through IV, Reticulitermes Environmental Phylotypes (REPs) 1 through 7 (comprising 67% of all treponemes found on the array; see Table 2.6), previously identified clades of traditional treponemes (known as subgroups 1 and 2)(*S64-S66*) and the so called "Termite Cluster" (*S65*). Many *R. hesperus* SSU rRNAs retrieved from the microfluidic array (including Phage Hosts I through IV) were similar to previously characterized SSU rRNAs from other *Reticulitermes* species. The overall diversity of *R. hesperus* treponeme SSU rRNAs was phylogenetically similar to that of other *Reticulitermes* species (*S64*). The tree was constructed based on 743 aligned unambiguous nucleotides excluding gaps using PhyML 2.4.5 (*S14*) implemented in ARB (*S67*). An optimal substitution model was estimated with jModelTest 0.1.1 (*S13-S14*) using the AICc criterion and was found to be the Tamura-Nei model (*S15*) +I+Γ (nCat=4) with unequal base pair frequencies. Shorter sequences (A7, A9, rF79, rG41 and rG53) were added by parsimony. Support values greater than 50% for 1000 bootstrap iterations are shown. Scale bar represents 0.1 nucleotide changes per alignment position. See Table 2.11 for a list of all sequences. Note that reference library sequences begin with the letter "r".

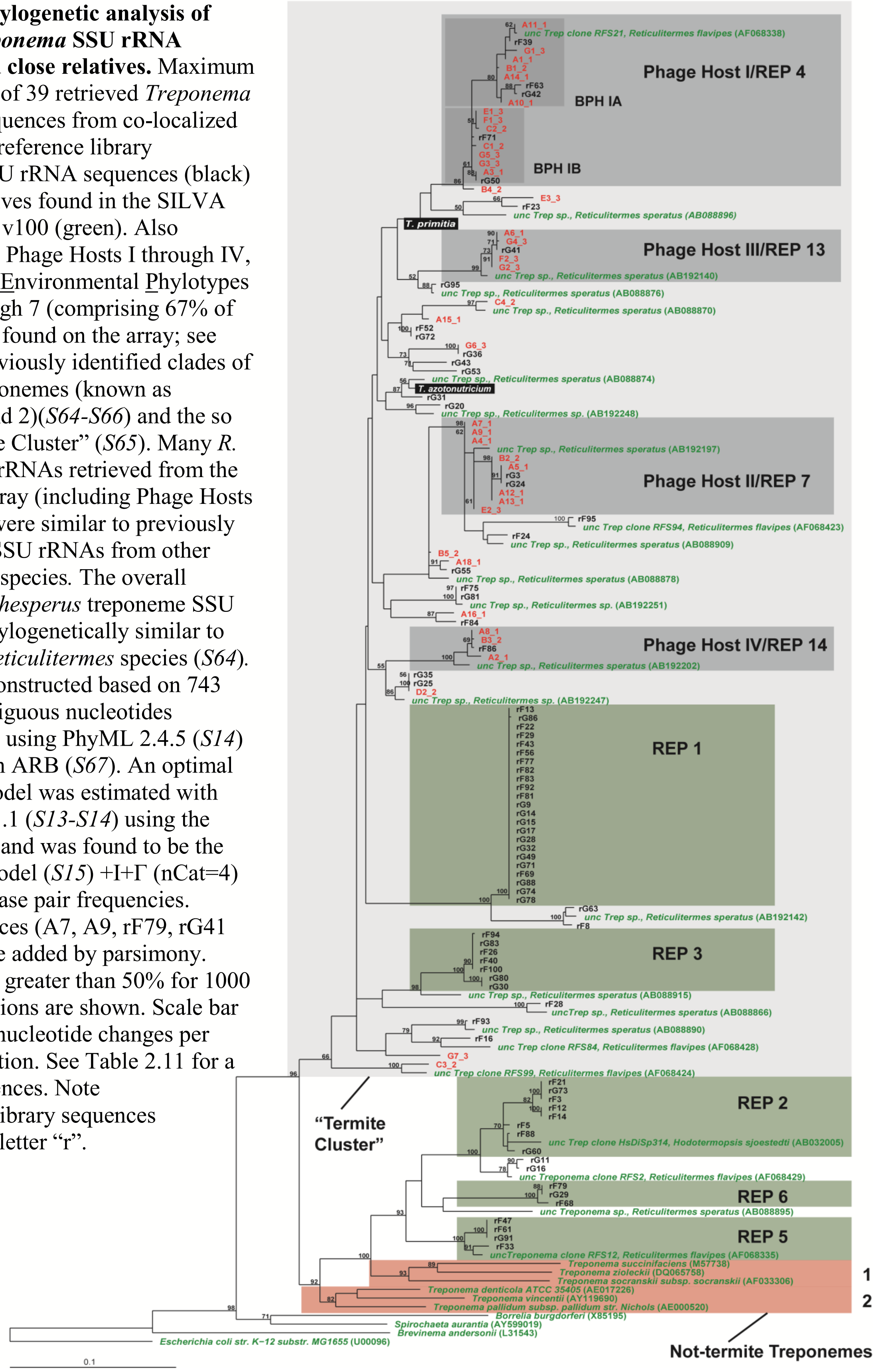
Phage Host I/REP 4
BPH IA
BPH IB
A11_1
unc Trep clone RFS21, Reticulitermes flavipes (AF068338)
rF39
G1_3
A1_1
B1_2
A14_1
rF63
rG42
A10_1
E1_3
F1_3
C2_2
rF71
C1_2
G5_3
G3_3
A3_1
rG50
B4_2
E3_3
rF23
unc Trep sp., Reticulitermes speratus (AB088896)
T. primitia
Phage Host III/REP 13
A6_1
G4_3
rG41
F2_3
G2_3
unc Trep sp., Reticulitermes speratus (AB192140)
rG95
unc Trep sp., Reticulitermes speratus (AB088876)
C4_2
unc Trep sp., Reticulitermes speratus (AB088870)
A15_1
rF52
rG72
G6_3
rG36
rG43
rG53
unc Trep sp., Reticulitermes speratus (AB088874)
T. azotonutricium
rG31
rG20
unc Trep sp., Reticulitermes sp. (AB192248)
Phage Host II/REP 7
A7_1
A9_1
A4_1
unc Trep sp., Reticulitermes speratus (AB192197)
B2_2
A5_1
rG3
rG24
A12_1
A13_1
E2_3
rF95
unc Trep clone RFS94, Reticulitermes flavipes (AF068423)
rF24
unc Trep sp., Reticulitermes speratus (AB088909)
B5_2
A18_1
rG55
unc Trep sp., Reticulitermes speratus (AB088878)
rF75
rG81
unc Trep sp., Reticulitermes sp. (AB192251)
A16_1
rF84
Phage Host IV/REP 14
A8_1
B3_2
rF86
A2_1
unc Trep sp., Reticulitermes speratus (AB192202)
rG35
rG25
D2_2
unc Trep sp., Reticulitermes sp. (AB192247)
REP 1
rF13
rG86
rF22
rF29
rF43
rF56
rF77
rF82
rF83
rF92
rF81
rG9
rG14
rG15
rG17
rG28
rG32
rG49
rG71
rF69
rG88
rG74
rG78
rG63
unc Trep sp., Reticulitermes speratus (AB192142)
rF8
REP 3
rF94
rG83
rF26
rF40
rF100
rG80
rG30
unc Trep sp., Reticulitermes speratus (AB088915)
rF28
uncTrep sp., Reticulitermes speratus (AB088866)
rF93
unc Trep sp., Reticulitermes speratus (AB088890)
rF16
unc Trep clone RFS84, Reticulitermes flavipes (AF068428)
G7_3
C3_2
unc Trep clone RFS99, Reticulitermes flavipes (AF068424)
"Termite Cluster"
REP 2
rF21
rG73
rF3
rF12
rF14
rF5
rF88
unc Trep clone HsDiSp314, Hodotermopsis sjoestedti (AB032005)
rG60
rG11
rG16
unc Treponema clone RFS2, Reticulitermes flavipes (AF068429)
REP 6
rF79
rG29
rF68
unc Treponema sp., Reticulitermes speratus (AB088895)
REP 5
rF47
rF61
rG91
rF33
uncTreponema clone RFS12, Reticulitermes flavipes (AF068335)
Treponema succinifaciens (M57738)
Treponema zioleckii (DQ065758)
Treponema socranskii subsp. socranskii (AF033306)
1
Treponema denticola ATCC 35405 (AE017226)
Treponema vincentii (AY119690)
Treponema pallidum subsp. pallidum str. Nichols (AE000520)
2
Borrelia burgdorferi (X85195)
Spirochaeta aurantia (AY599019)
Brevinema andersonii (L31543)
Escherichia coli str. K−12 substr. MG1655 (U00096)
Not-termite Treponemes
0.1

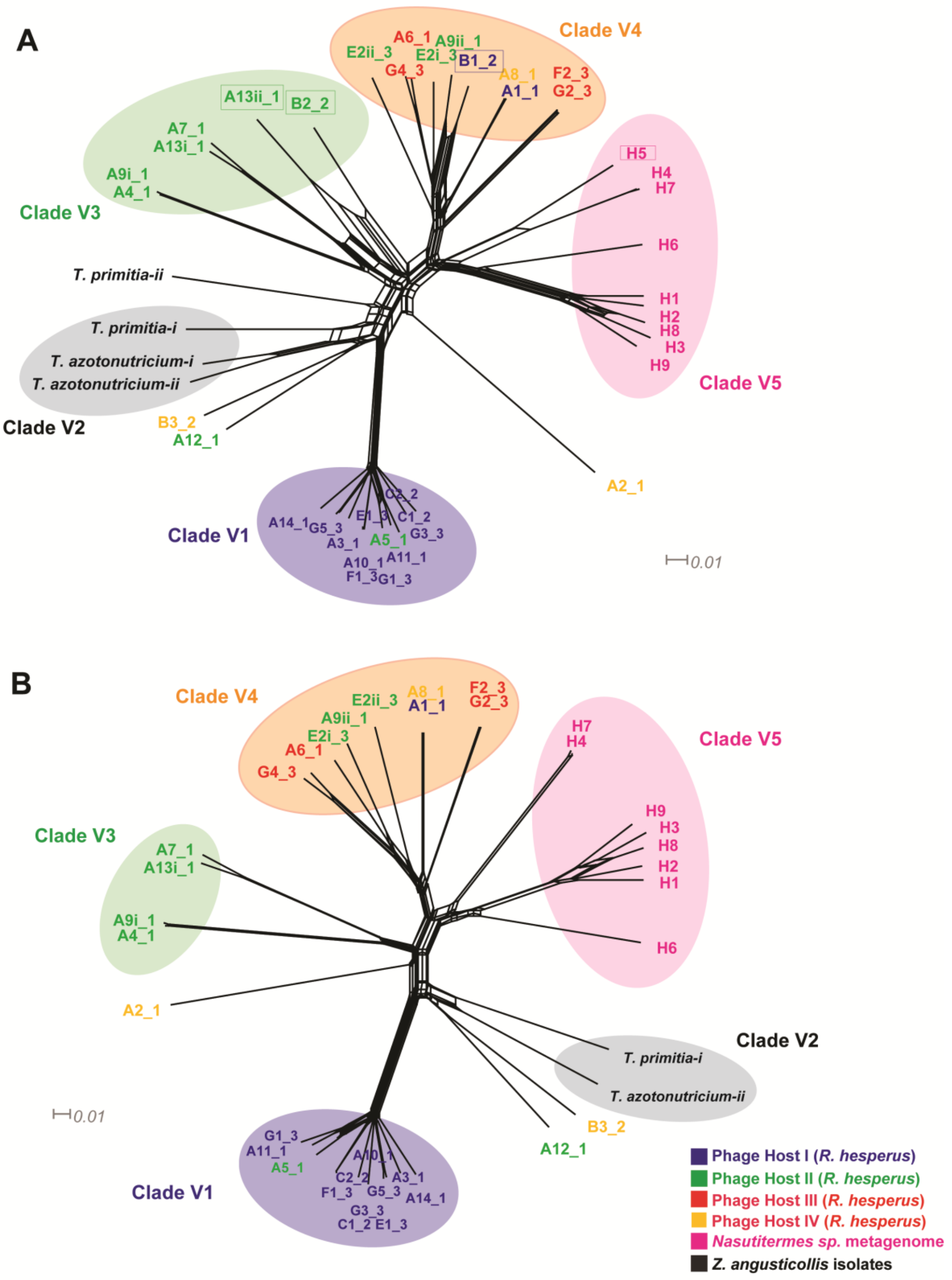

Figure 2.8. NeighborNet network of termite-related terminase alleles. (A) NeighborNet (*S68*) of **(1)** all terminase alleles that were retrieved with Phage Hosts I through IV, **(2)** terminases genes present in Z. *angusticollis* isolates, *Treponema primitia* (ZAS-2), and *Treponema azotonutricium* (ZAS-9), and **(3)** terminase alleles found in the metagenome of the hindgut of an *Nasutitermes sp.* termite. Boxed sequences are the first four events identified by RDP3 as recombinant (see Methods). **(B)** Same as (A) but excluding **(1)** RDP3 identified recombinant sequences, **(2)** ZAS terminases alleles associated with most likely defunct phage cassettes. ZAS-2 and ZAS-9 both have two copies of the terminase gene. Each copy resides in a region coding for

other viral genes, however only a single one of these copies in each genome appears to be present in a large enough contiguous region of putative viral genes (~36–43 kbp) that could constitute a viable phage and therefore only this copy was included. After removal of recombinant sequences (B1, B2, A13ii, H5) there remains some residual reticulate patterns at the base of the network, however the network largely appears to be tree-like (confirmed by likelihood mapping; see Methods). These sequences were used to generate the terminase tree in Fig. 2.2. The network structure shown here is consistent with the topology shown in Fig. 2.2. The network was calculated using SplitsTree4 (*S28*) on 705 aligned unambiguous nucleotides without gaps using the optimal model found by FindModel (*S29*), a K80 substitution model (*S69*) +Γ with $\alpha \simeq 0.5$. The LSfit score for networks A and B was 99.97% and 99.94%, respectively. Note that sample B1 associated with Host I in (A) was found by RDP3 to be a chimera of A1 (Host I) and A9ii (Host II), possibly indicating a lateral gene transfer event between these two distinct subpopulations of viruses. Alternatively, since only one such event was observed, it could also be due to an unlikely experimental artifact. Sample notation is as described in Fig. 2.2.

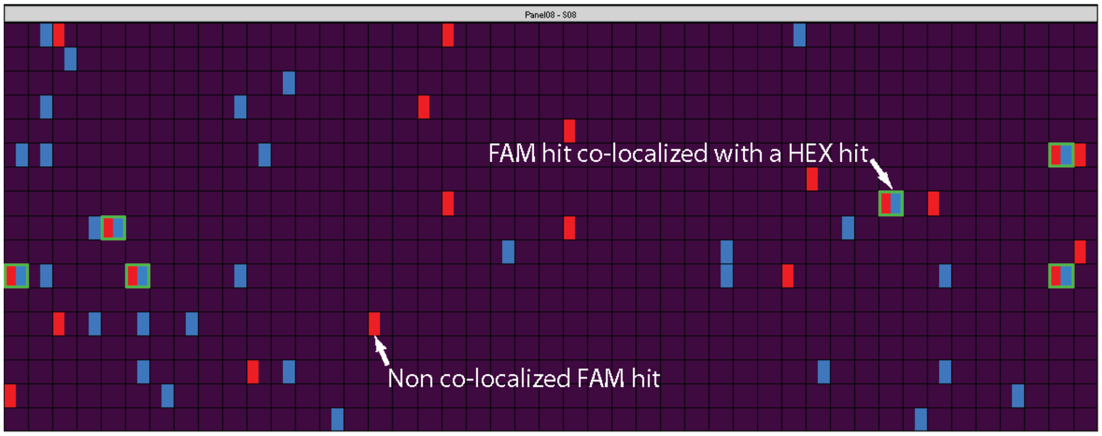

Figure 2.9. Example of microfluidic array panel readout after thresholding. Blue squares represent hits in the HEX/rRNA channel and red squares represent hits in the FAM/terminase channel. Co-localized hits are highlighted in green. In this example, spurious amplification is expected to account for ~50% of all non co-localized FAM hits based on the number of FAM hits in the no-template-control panel for this microfluidic array (7 hits).

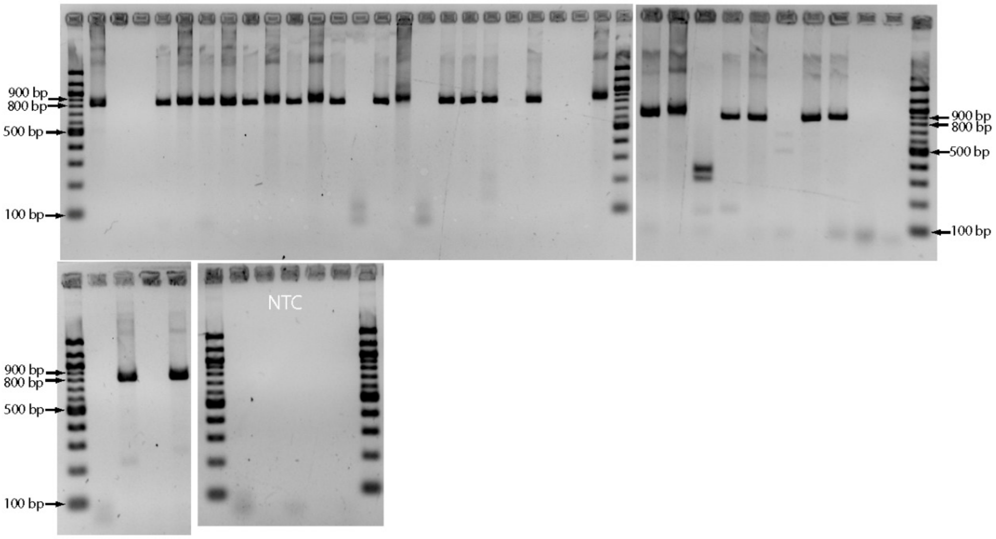

Figure 2.10. Agarose gel electrophoresis analysis of all FAM hits in a microfluidic array panel. All 38 FAM hits in panel #7 of chip B were post-amplified and analyzed by agarose gel electrophoresis. Also shown are the five no-template-control (NTC) samples for this PCR reaction. The expected amplicon size is ~820 bp (compared to a 100 bp ladder). Out of 38 reactions, 13 were negative for the template. This value is consistent with the number of FAM hits in the no-template-control panel for this microfluidic array, which was 16. The gel image was inverted, brightness was linearly scaled to maximize contrast and size was proportionally scaled to fit the figure. The microfluidic array was analyzed with the BioMark Digital PCR analysis software (Fluidigm, v.2.0.6) using a FAM threshold 0.2 and linear baseline correction.

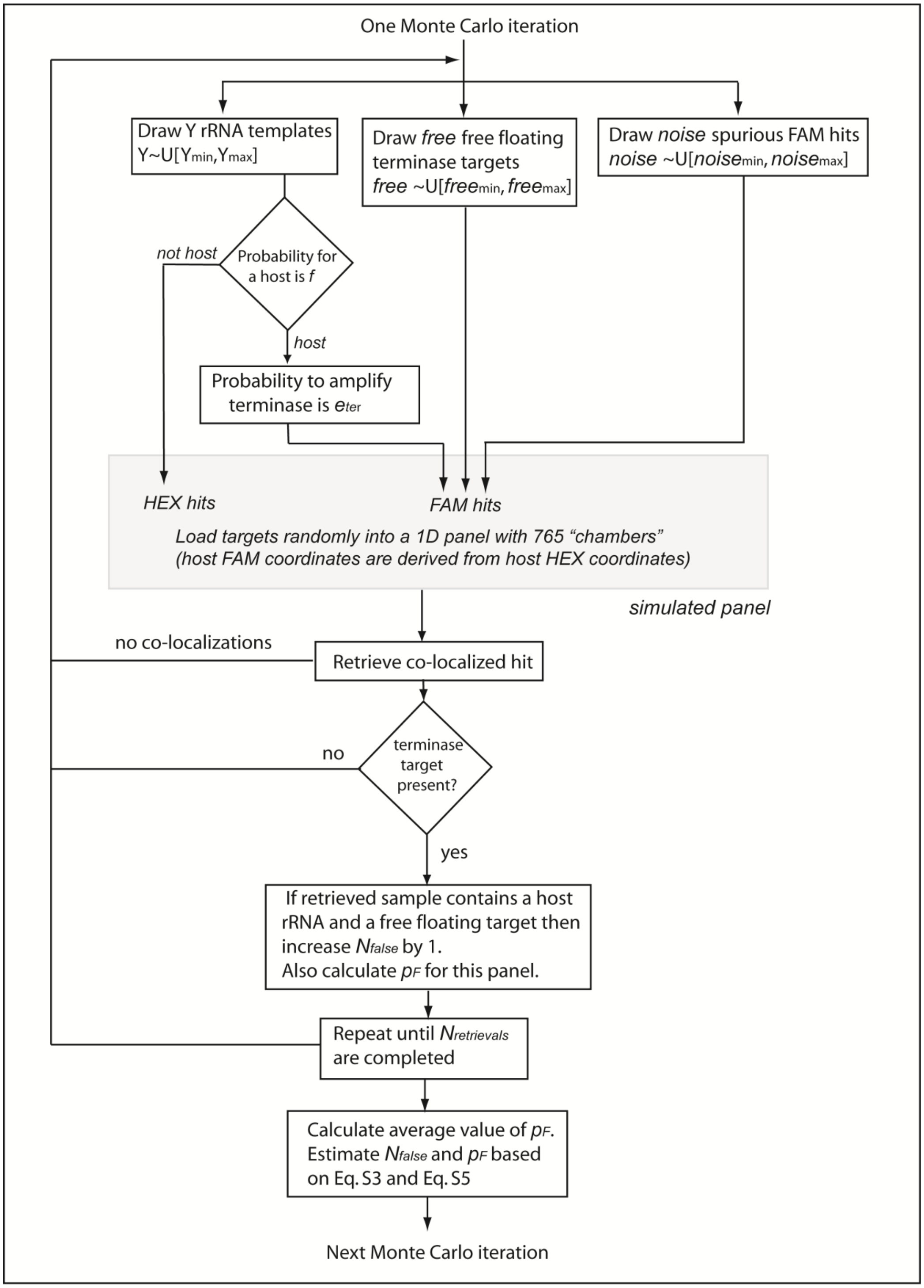
One Monte Carlo iteration
Draw Y rRNA templates $Y \sim U[Y_{min}, Y_{max}]$
Draw *free* free floating terminase targets *free* $\sim U[free_{min}, free_{max}]$
Draw *noise* spurious FAM hits *noise* $\sim U[noise_{min}, noise_{max}]$
not host
Probability for a host is *f*
host
Probability to amplify terminase is e_{ter}
HEX hits
FAM hits
Load targets randomly into a 1D panel with 765 "chambers"
(host FAM coordinates are derived from host HEX coordinates)
simulated panel
no co-localizations
Retrieve co-localized hit
no
terminase target present?
yes
If retrieved sample contains a host rRNA and a free floating target then increase N_{false} by 1.
Also calculate p_F for this panel.
Repeat until $N_{retrievals}$ are completed
Calculate average value of p_F.
Estimate N_{false} and p_F based on Eq. S3 and Eq. S5
Next Monte Carlo iteration

Figure 2.11. Schematic diagram of a Monte Carlo simulation of microfluidic array loading and sampling. See supporting text for further details.

2.9.4 Supporting tables

Table 2.2. Abundance of homologs of known viral genes in the higher termite metagenome. This table describes the number (or *abundance*, see definition in Materials and methods) of metagenome gene objects in the higher termite metagenome that were homologous to the indicated viral phage genes (E value ≤ 0.001, *abundance* ≥ 10 metagenome gene objects). This list constitutes the most abundant viral-specific genes in the metagenome (i.e., viral genes related to building a virion), using the viral RefSeq database v37 (*S41*) as a reference for known viral genes. The two highlighted rows are the portal protein and terminase protein that were found to have homologs in the ZAS prophage-like elements.

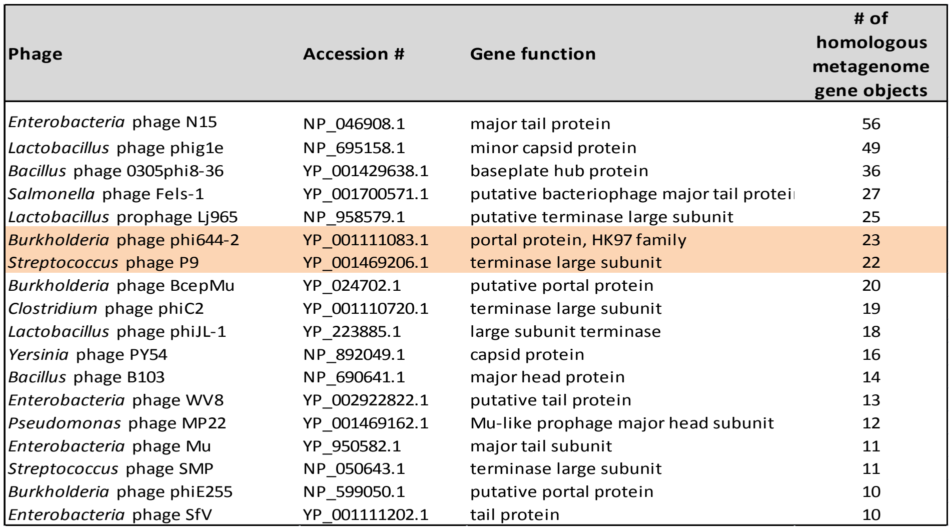

Phage	Accession #	Gene function	# of homologous metagenome gene objects
Enterobacteria phage N15	NP_046908.1	major tail protein	56
Lactobacillus phage phig1e	NP_695158.1	minor capsid protein	49
Bacillus phage 0305phi8-36	YP_001429638.1	baseplate hub protein	36
Salmonella phage Fels-1	YP_001700571.1	putative bacteriophage major tail protei	27
Lactobacillus prophage Lj965	NP_958579.1	putative terminase large subunit	25
Burkholderia phage phi644-2	YP_001111083.1	portal protein, HK97 family	23
Streptococcus phage P9	YP_001469206.1	terminase large subunit	22
Burkholderia phage BcepMu	YP_024702.1	putative portal protein	20
Clostridium phage phiC2	YP_001110720.1	terminase large subunit	19
Lactobacillus phage phiJL-1	YP_223885.1	large subunit terminase	18
Yersinia phage PY54	NP_892049.1	capsid protein	16
Bacillus phage B103	NP_690641.1	major head protein	14
Enterobacteria phage WV8	YP_002922822.1	putative tail protein	13
Pseudomonas phage MP22	YP_001469162.1	Mu-like prophage major head subunit	12
Enterobacteria phage Mu	YP_950582.1	major tail subunit	11
Streptococcus phage SMP	NP_050643.1	terminase large subunit	11
Burkholderia phage phiE255	NP_599050.1	putative portal protein	10
Enterobacteria phage SfV	YP_001111202.1	tail protein	10

Table 2.3. Similarity analysis of the termite-associated terminase gene and portal protein gene with close homologs. The following table describes the result of a BLAST analysis of the large terminase subunit gene (411 aa in length) and the portal protein gene (396 aa in length) found in *T. primitia's* prophage-like element with close homologs. Close homologs were searched for in: (1) the larger prophage-like element present in the genome of *T. azotonutricium*, (2) the metagenome of the hindgut of a *Nasutitermes sp*. termite, and (3) the viral RefSeq database v37 (*S41*). The table demonstrates that the alleles of the termite-associated phage genes were very similar to each other and highly divergent from their closest homologs found among all currently known viral genomes. Alignments were performed on the amino acid sequences.

Large terminase subunit gene	**% identity** *	**% similarity***	**Gaps***	**E value**
	T. azotonutricium			
	363/411 (89%)	385/411 (94%)	4/411 (0%)	0
	Higher termite metagenome			
	317/407 (78%)	359/407 (89%)	5/407 (1%)	0
	Viral RefSeq database *(Lactobacillus johnsonii* prophage Lj771)			
	107/415 (25%)	177/415 (42%)	64/415 (15%)	4.00E-19
Portal protein	**% identity**	**% similarity**	**Gaps**	**E value**
	T. azotonutricium			
	309/382 (81%)	348/382 (92%)	3/382 (0%)	0
	Higher termite metagenome			
	273/392 (70%)	324/392 (83%)	11/392 (2%)	1.00E-167
	Viral RefSeq database *(Streptomyces* phage mu1/6)			
	99/382 (25%)	156/382 (40%)	52/382 (13%)	6.00E-17

*Numbers divided by a forward slash correspond to the number of amino acids in each pair-wise alignment ("identity/total", "similarity/total", and "gaps/total", depending on the column).

Table 2.4. Sample collection and analysis information. Collection dates, collection sites, and dPCR execution dates for the *R. hesperus* specimens. The different colonies were on average 120 meters apart. The microfluidic array and colony labels noted here were used to label the samples throughout this report.

Chip ID	Chip designation in trees	Termite collection date	Date of chip execution	Colony	GPS coordinates
1151065015	A	11/13/2008	11/25/2008	1	34 19' 25.6"N/ 118 0' 17.9"W
1151065011	B	5/27/2009	5/29/2009	2	34 19' 31"N/118 00' 20.8"W
1151065010	C	5/27/2009	6/6/2009	2	"
1151065012	D	5/27/2009	6/7/2009	2	"
1151065017	E	5/27/2009	6/21/2009	3	34 19' 28"N/118 00' 17.5"W
1151065018	F	5/27/2009	6/22/2009	3	"
1151065019	G	5/27/2009	6/24/2009	3	"

Table 2.5. Estimated evolutionary distance between bacterial host SSU rRNA phylotypes. The number of base substitutions per site from averaging over all sequence pairs within and between host groups is shown. With the exception of samples A7 and A9 (that were composed of 784 and 810 nucleotides respectively) the SILVA (*S11*) -based alignment contained 898 unambiguous nucleotides. Distances were calculated using the Jukes-Cantor (*S70*) nucleotide substitution model in MEGA4 (*S19*). The number of repetitions appearing in Table 2.1 are based on an Operational Taxonomical Unit (OTU) cutoff of 2% assigned by DOTUR (*S71*) with the furthest neighbor sequence assignment method. The next significant OTU cutoff was 2.5%, adding a more divergent member (B4) to Host I, however due to the larger divergence and single instance of this event it cannot be statistically validated and therefore it was not included in this analysis. The distance matrix used by DOTUR was based on the above alignment and calculated in ARB (*S67*) using the Jukes-Cantor substitution model. Each bacterial host was less than 0.9% divergent on average. The maximum divergence was observed between Host III and ZAS-9 where the corrected evolutionary distance across their deduced rRNAs was measured to be 9.3%.

	Host I *(n=13)*	**Host II** *(n=8)*	**Host III** *(n=4)*	**Host IV** *(n=3)*	**ZAS-2** *(n=1)*	**ZAS-9** *(n=1)*
Host I	0.0084					
Host II	0.0822	0.0083				
Host III	0.0685	0.0544	0.005			
Host IV	0.0817	0.0841	0.087	0.0075		
ZAS-2	0.0396	0.0678	0.06	0.0712	-	
ZAS-9	0.073	0.086	0.0933	0.0865	0.0603	-

Table 2.6. Retrieved *Treponema* phylotypes from the microfluidic arrays

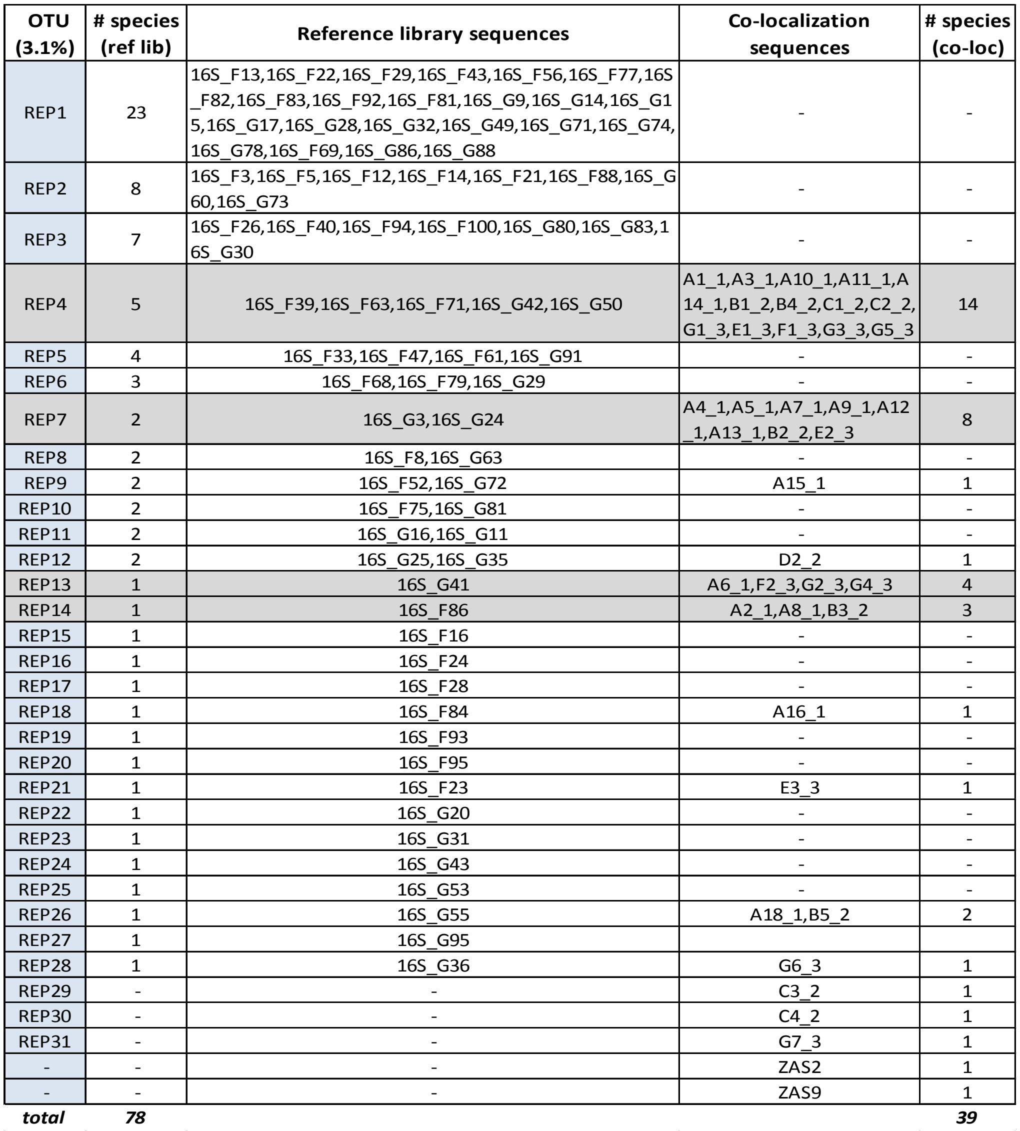

OTU (3.1%)	# species (ref lib)	Reference library sequences	Co-localization sequences	# species (co-loc)
REP1	23	16S_F13,16S_F22,16S_F29,16S_F43,16S_F56,16S_F77,16S_F82,16S_F83,16S_F92,16S_F81,16S_G9,16S_G14,16S_G15,16S_G17,16S_G28,16S_G32,16S_G49,16S_G71,16S_G74,16S_G78,16S_F69,16S_G86,16S_G88	-	-
REP2	8	16S_F3,16S_F5,16S_F12,16S_F14,16S_F21,16S_F88,16S_G60,16S_G73	-	-
REP3	7	16S_F26,16S_F40,16S_F94,16S_F100,16S_G80,16S_G83,16S_G30	-	-
REP4	5	16S_F39,16S_F63,16S_F71,16S_G42,16S_G50	A1_1,A3_1,A10_1,A11_1,A14_1,B1_2,B4_2,C1_2,C2_2,G1_3,E1_3,F1_3,G3_3,G5_3	14
REP5	4	16S_F33,16S_F47,16S_F61,16S_G91	-	-
REP6	3	16S_F68,16S_F79,16S_G29	-	-
REP7	2	16S_G3,16S_G24	A4_1,A5_1,A7_1,A9_1,A12_1,A13_1,B2_2,E2_3	8
REP8	2	16S_F8,16S_G63	-	-
REP9	2	16S_F52,16S_G72	A15_1	1
REP10	2	16S_F75,16S_G81	-	-
REP11	2	16S_G16,16S_G11	-	-
REP12	2	16S_G25,16S_G35	D2_2	1
REP13	1	16S_G41	A6_1,F2_3,G2_3,G4_3	4
REP14	1	16S_F86	A2_1,A8_1,B3_2	3
REP15	1	16S_F16	-	-
REP16	1	16S_F24	-	-
REP17	1	16S_F28	-	-
REP18	1	16S_F84	A16_1	1
REP19	1	16S_F93	-	-
REP20	1	16S_F95	-	-
REP21	1	16S_F23	E3_3	1
REP22	1	16S_G20	-	-
REP23	1	16S_G31	-	-
REP24	1	16S_G43	-	-
REP25	1	16S_G53	-	-
REP26	1	16S_G55	A18_1,B5_2	2
REP27	1	16S_G95		
REP28	1	16S_G36	G6_3	1
REP29	-	-	C3_2	1
REP30	-	-	C4_2	1
REP31	-	-	G7_3	1
-	-	-	ZAS2	1
-	-	-	ZAS9	1
total	***78***			***39***

All reference library sequences (*n*=118; 876 ± 71 bp SD) were initially classified with RDB (*S72*) and *Treponema* phylotypes (66.1%, *n*=78 with 99–100% confidence) were subsequently aligned by the SILVA incremental aligner SINA (*S11*). A distance matrix was calculated in ARB (*S67*) for the 78 reference library *Treponema* species, the 39 co-localized *Treponema* species, and ZAS-2 and ZAS-9 (*n*=119). Note that REP4 was co-localized 14 times, however one of these co-localizations, B4, was more divergent than the other ribotypes of this group (see Table 2.5) and was therefore not regarded as a repeated co-localization of Host I in Table 2.1 and Table 2.5. The distance matrix was calculated based on 780 unambiguous nucleotides (with the exception of A7, A9, rF79, rG41, rG53 that were in the range of 624–767 nucleotides) using the Jukes-Cantor (*S70*) method. Operational taxonomical units (OTUs) were then determined by DOTUR (*S71*) based on the furthest neighbor sequence assignment method using an OTU cutoff of 3.1%. This cutoff is slightly higher than the OTU cutoff used to identify the repeated co-localizations (2%) in Fig. 2.2 in order to make the statistical test for repeated co-localization more stringent. REPs corresponding to putative bacterial hosts are highlighted in gray. All *Treponema* sequences were also screened with Bellerophon v3 (*S9*) on Greengenes (*S10*) for chimeras and were found to be negative. The remaining phyla indentified by RDB to be present in the reference library were Proteobacteria (13.6%, 100% confidence), Firmicutes (6.8%, Clostridia 53–100% confidence), Tenericutes (5.9%, Mycoplasmataceae with 77–90% confidence), Bacteroidetes (3.4%, 100% confidence), Actinobacteria (3.4%, 100% confidence) and Planctomycetes (0.8%, 100% confidence). All these phyla have been observed previously in SSU rRNA libraries of *Reticulitermes speratus* (*S73*). However, from the number of rRNA targets observe in the no-template-control panels we anticipate that background amplification (see Materials and methods) should contribute to 34.1 ± 18.4% SD of the reference library sequences due to sparse loading of the panels (increasing the fraction of background amplification products). Based on retrieval of rRNA sequences from the no-template-control panel (not shown) we expect the major contributor to this fraction to be bacteria from the Proteobacteria phylum. The finding that free living prokaryotes in the termite hindgut are dominated by spirochetes is consistent with electron microscope observations showing that spirochetes can account for over 50% of the gut microbes in some termites (*S74*). The absence of bacteria belonging to the TG-1 phylum (*S75*) is an indication that large flagellates were successfully filtered out by the 5 μm pre-filter and did not lyse in this process (see Methods).

Table 2.7. Selection pressure analysis of the terminase gene. Codon-based test of purifying (negative) selection for Hosts I through IV excluding suspected recombinant sequences (B1, B2 and A13ii). d_S and d_N are the number of synonymous and nonsynonymous substitutions per number of synonymous and nonsynonymous sites respectively obtained from averaging over all sequence pairs within a given group. d_S and d_N were calculated by various methods: **NG86** — Nei-Gojobori method (*S76*) with the Jukes-Cantor (*S70*) nucleotide substitution model, **Modified NG86** (*S77*) — NG86 method with the Jukes-Cantor nucleotide substitution model, **LWL85** — Li-Wu-Luo method (*S78*), **PBL85** — Pamilo-Bianchi-Li method (*S79*), and **Kumar** — Kumar method (*S80*). For the modified NG86 method, the ratio of transitional to transversional distances per site (R) was calculated by averaging over all sequence pairs within each group using the 3rd codon position based on the Kimura 2-parameter method (*S69*). All results are based on the pairwise analysis of 235 unambiguous codon positions without gaps. Standard error estimates were obtained by a bootstrap procedure with 1000 replicates. The distribution of the test statistic (*D*) is approximated to be normal since the number of nucleotides contributing to d_S and d_N were sufficiently large (>10), allowing to test the null hypothesis using a one-tailed (Z > 0) Z test (*S80*). The P value (one-tailed Z test) for observing Z > 0 ($d_S > d_N$) by chance is shown in the table. Z is shown to be greater than zero in a statistically significant manner ($P < 10^{-7}$ for Hosts I–III and P < 0.025 for Host IV) indicating negative selection was statistically significant. n/c denotes cases in which it was not possible to estimate evolutionary distances. All analyses were carried out with MEGA4 (*S19*).

Host	Method	d_S (± S.E.)	d_N (± S.E.)	d_N/d_S	$D = d_S - d_N$ (± S.E.)	*Z = D/std(D)*	P value
I	NG86 (R=0.5)	0.57 ± 0.08	0.04 ± 0.01	0.08	0.53 ± 0.07	7.58	1.7E-14
(*n* =12)	Modified NG86 (R=2.02)	0.33 ± 0.03	0.05 ± 0.01	0.15	0.28 ± 0.03	8.94	0.0E+00
	LWL85	0.49 ± 0.06	0.04 ± 0.01	0.09	0.45 ± 0.06	7.52	2.8E-14
	PBL93	0.44 ± 0.05	0.04 ± 0.01	0.10	0.40 ± 0.05	7.42	5.7E-14
	Kumar	0.37 ± 0.04	0.04 ± 0.01	0.12	0.32 ± 0.04	8.28	0.0E+00
II	NG86 (R=0.5)	1.50 ± 0.12	0.17 ± 0.02	0.11	1.34 ± 0.12	11.18	0.0E+00
(*n* =9)	Modified NG86 (R=1.44)	0.99 ± 0.07	0.18 ± 0.02	0.18	0.81 ± 0.07	11.32	0.0E+00
	LWL85	1.48 ± 0.11	0.17 ± 0.02	0.11	1.31 ± 0.11	11.69	0.0E+00
	PBL93	1.49 ± 0.10	0.17 ± 0.02	0.11	1.32 ± 0.10	13.33	0.0E+00
	Kumar	1.14 ± 0.08	0.16 ± 0.02	0.14	0.97 ± 0.08	12.25	0.0E+00
III	NG86 (R=0.5)	0.72 ± 0.13	0.06 ± 0.01	0.08	0.66 ± 0.12	5.35	4.3E-08
(*n* =4)	Modified NG86 (R=1.80)	0.50 ± 0.06	0.06 ± 0.01	0.12	0.44 ± 0.06	6.92	2.2E-12
	LWL85	0.70 ± 0.09	0.05 ± 0.01	0.08	0.64 ± 0.10	6.75	7.2E-12
	PBL93	0.62 ± 0.09	0.06 ± 0.01	0.09	0.56 ± 0.09	6.26	1.9E-10
	Kumar	0.55 ± 0.07	0.05 ± 0.01	0.10	0.50 ± 0.08	6.63	1.7E-11
IV	NG86 (R=0.5)	n/c ± n/c	0.19 ± 0.02	n/c	n/c ± n/c	n/c	n/c
(*n* =3)	Modified NG86 (R=1.97)	1.53 ± 0.20	0.21 ± 0.03	0.14	1.32 ± 0.19	6.76	6.8E-12
	LWL85	2.30 ± 1.06	0.20 ± 0.09	0.09	2.10 ± 0.99	2.11	1.7E-02
	PBL93	1.65 ± 0.82	0.20 ± 0.09	0.12	1.45 ± 0.73	1.98	2.4E-02
	Kumar	1.94 ± 0.62	0.17 ± 0.07	0.09	1.76 ± 0.57	3.09	9.9E-04

Table 2.8. Similar terminase sequences associated with different bacterial hosts. Terminase alleles associated with different bacterial hosts having less than 10% difference between their nucleotide sequences.

Sequence 1	Sequence 2	% p-distance (705 bp)
A1_1 (Host I)	A8_1 (Host IV)	0
G1_3 (Host I)	A5_1 (Host II)	3
B1_1* (Host I)	A9ii_1 (Host II)	6.5

*Identified by RDP3 as a recombination between A9ii_1 (Host II) and A1_1 (Host I). See also Fig. 2.8.

Table 2.9. P values for the P Test comparing terminase alleles by bacterial host. The P Test (*S97*) estimates the similarity between communities as the number of parsimony changes that would be required to explain the distribution of sequences between the different samples in the tree (samples here were grouped by bacterial host). The P value is the fraction of trials in which the true tree requires fewer changes than trees in which the sample assignments have been randomized (*S98*). The P test was implemented in Fast UniFrac (*S99*) selecting the "P Test Significance" option, comparing "Each pair of samples" using *n*=1000 random permutations. The analysis was performed on the phylogenetic tree in Fig. 2.2 applying midpoint rooting. P values shown have been corrected for multiple comparisons using the Bonferroni correction.

	Host II	Host III	Host IV
Host I	≤0.001	≤0.001	0.024
Host II	-	0.018	1
Host III	-	-	0.204

Table 2.10. P values for the P Test comparing terminase alleles by colonies. Samples here were grouped by termite colony. P values shown have been corrected for multiple comparisons using the Bonferroni correction. *n*=1000 random permutations were used to calculate P Values. See Table 2.9 for further details.

	Colony 2	Colony 3
Colony 1	0.399	0.927
Colony 2	-	0.537

Table 2.11. Sequences analyzed in this study. Accession numbers of the uncultured treponemes associated with Phage Host I through IV in Fig. 2.2 were AF068338, AB192197, AB192140, and AB192202, respectively.

Clone ID	Termite/bacterium species	Location/Source	Method	Accession (NCBI/JGI)	Figure	Reference
Terminase gene – isolates						
ZAS2i	*Z. angusticollis /T. primitia*	California	Isolate		2.2,2.5,2.6,2.8	this study
ZAS2ii	*Z. angusticollis /T. primitia*	California	Isolate		2.5,,2.8	this study
ZAS9i	*Z. angusticollis /T. azotonutricium*	California	Isolate		2.5,,2.8	this study
ZAS9ii	*Z. angusticollis /T. azotonutricium*	California	Isolate		2.2,2.5,2.6	this study
Terminase gene - co-localization						
A1_1	*Reticulitermes hesperus*	California	Digital PCR	HQ202808	2.2,2.5,2.6	this study
A3_1	*Reticulitermes hesperus*	California	Digital PCR	HQ187752	2.2,2.5,2.6	this study
A10_1	*Reticulitermes hesperus*	California	Digital PCR	HQ187760	2.2,2.5,2.6	this study
A11_1	*Reticulitermes hesperus*	California	Digital PCR	HQ187761	2.2,2.5,2.6	this study
A14_1	*Reticulitermes hesperus*	California	Digital PCR	HQ187765	2.2,2.5,2.6	this study
B1_2	*Reticulitermes hesperus*	California	Digital PCR	HQ187766	2.5,,2.8	this study
C1_2	*Reticulitermes hesperus*	California	Digital PCR	HQ187769	2.2,2.5,2.6	this study
C2_2	*Reticulitermes hesperus*	California	Digital PCR	HQ187770	2.2,2.5,2.6	this study
E1_3	*Reticulitermes hesperus*	California	Digital PCR	HQ187771	2.2,2.5,2.6	this study
F1_3	*Reticulitermes hesperus*	California	Digital PCR	HQ187774	2.2,2.5,2.6	this study
G1_3	*Reticulitermes hesperus*	California	Digital PCR	HQ187776	2.2,2.5,2.6	this study
G3_3	*Reticulitermes hesperus*	California	Digital PCR	HQ187778	2.2,2.5,2.6	this study
G5_3	*Reticulitermes hesperus*	California	Digital PCR	HQ187780	2.2,2.5,2.6	this study
A4_1	*Reticulitermes hesperus*	California	Digital PCR	HQ187753	2.2,2.5,2.6	this study
A5_1	*Reticulitermes hesperus*	California	Digital PCR	HQ187754	2.2,2.5,2.6	this study
A7_1	*Reticulitermes hesperus*	California	Digital PCR	HQ187756	2.2,2.5,2.6	this study
A9i_1	*Reticulitermes hesperus*	California	Digital PCR	HQ187758	2.2,2.5,2.6	this study
A9ii_1	*Reticulitermes hesperus*	California	Digital PCR	HQ187759	2.2,2.5,2.6	this study
A12_1	*Reticulitermes hesperus*	California	Digital PCR	HQ187762	2.2,2.5,2.6	this study
A13i_1	*Reticulitermes hesperus*	California	Digital PCR	HQ187763	2.2,2.5,2.6	this study
A13ii_1	*Reticulitermes hesperus*	California	Digital PCR	HQ187764	2.5,,2.8	this study
B2_2	*Reticulitermes hesperus*	California	Digital PCR	HQ187767	2.5,,2.8	this study
E2i_3	*Reticulitermes hesperus*	California	Digital PCR	HQ187772	2.2,2.5,2.6	this study
E2ii_3	*Reticulitermes hesperus*	California	Digital PCR	HQ187773	2.2,2.5,2.6	this study
A6_1	*Reticulitermes hesperus*	California	Digital PCR	HQ187755	2.2,2.5,2.6	this study
F2_3	*Reticulitermes hesperus*	California	Digital PCR	HQ187775	2.2,2.5,2.6	this study
G2_3	*Reticulitermes hesperus*	California	Digital PCR	HQ187777	2.2,2.5,2.6	this study
G4_3	*Reticulitermes hesperus*	California	Digital PCR	HQ187779	2.2,2.5,2.6	this study
A2_1	*Reticulitermes hesperus*	California	Digital PCR	HQ187751	2.5,,2.8	this study

A8_1	*Reticulitermes hesperus*	California	Digital PCR	HQ187757	2.5,,2.8	this study
B3_2	*Reticulitermes hesperus*	California	Digital PCR	HQ187768	2.5,,2.8	this study
Terminase gene - close relatives						
H1	*Nasutitermes sp.*	Costa Rica	Metagenome	2004118157	2.2,2.5,2.8	(*S5*)
H2	*Nasutitermes sp.*	Costa Rica	Metagenome	2004126816	2.2,2.5,2.8	(*S5*)
H3	*Nasutitermes sp.*	Costa Rica	Metagenome	2004144277	2.2,2.5,2.8	(*S5*)
H4	*Nasutitermes sp.*	Costa Rica	Metagenome	2004144007	2.2,2.5,2.8	(*S5*)
H5	*Nasutitermes sp.*	Costa Rica	Metagenome	2004132071	2.5,,2.8	(*S5*)
H6	*Nasutitermes sp.*	Costa Rica	Metagenome	2004107522	2.2,2.5,2.8	(*S5*)
H7	*Nasutitermes sp.*	Costa Rica	Metagenome	2004111244	2.2,2.5,2.8	(*S5*)
H8	*Nasutitermes sp.*	Costa Rica	Metagenome	2004124547	2.2,2.5,2.8	(*S5*)
H9	*Nasutitermes sp.*	Costa Rica	Metagenome	2004134785	2.2,2.5,2.8	(*S5*)
H10	*Nasutitermes sp.*	Costa Rica	Metagenome	2004136622	2.5,,2.8	(*S5*)
Terminase gene - non termite related						
T4	Phage isolate		Isolate	NP_049776.1	2.5,2.6	(*S81*)
Vic	*Victivallis vadensis ATCC BAA-548*	Feces, human	Isolate	ZP_06243301.1	2.5	-
Sino	*Sinorhizobium medicae WSM419*	Plant root, Soil (Sardinia)	Isolate	YP_001327565.1	2.5	(*S82*)
Gluc	*Gluconobacter oxydans 621H*	Fruits, Plants, Wine (Germany)	Isolate	YP_191628.1	2.5	(*S83*)
Nov	*Novosphingobium aromaticivorans DSM 12444*	Fresh water, Soil (S. Carolina)	Isolate	YP_497986.1	2.5	-
Mat1	Hypersaline mat	Mexico	Metagenome	2004359243	2.5	(*S84*)
Mat2	Hypersaline mat	Mexico	Metagenome	2004346681	2.5	(*S84*)
Mat3	Hypersaline mat	Mexico	Metagenome	2004362568	2.5	(*S84*)
SSU rRNA gene – isolates						
ZAS2	*Z. angusticollis /T. primitia*	California	Isolate	AF093252	2.2,2.7	(*S32*)
ZAS9	*Z. angusticollis /T. azotonutricium*	California	Isolate	AF320287	2.2,2.7	(*S33*)
SSU rRNA gene - co-localization and reference library						
A1_1	*Reticulitermes hesperus*	California	Digital PCR	HQ187712	2.2,2.7	this study
A3_1	*Reticulitermes hesperus*	California	Digital PCR	HQ187722	2.2,2.7	this study
A10_1	*Reticulitermes hesperus*	California	Digital PCR	HQ187713	2.2,2.7	this study
A11_1	*Reticulitermes hesperus*	California	Digital PCR	HQ187714	2.2,2.7	this study
A14_1	*Reticulitermes hesperus*	California	Digital PCR	HQ187717	2.2,2.7	this study
B1_2	*Reticulitermes hesperus*	California	Digital PCR	HQ187729	2.2,2.7	this study
C1_2	*Reticulitermes hesperus*	California	Digital PCR	HQ187734	2.2,2.7	this study
C2_2	*Reticulitermes hesperus*	California	Digital PCR	HQ187735	2.2,2.7	this study
E1_3	*Reticulitermes hesperus*	California	Digital PCR	HQ187739	2.2,2.7	this study
F1_3	*Reticulitermes hesperus*	California	Digital PCR	HQ187742	2.2,2.7	this study
G1_3	*Reticulitermes hesperus*	California	Digital PCR	HQ187744	2.2,2.7	this study
G3_3	*Reticulitermes hesperus*	California	Digital PCR	HQ187746	2.2,2.7	this study

G5_3	*Reticulitermes hesperus*	California	Digital PCR	HQ187748	2.2,2.7	this study
A4_1	*Reticulitermes hesperus*	California	Digital PCR	HQ187723	2.2,2.7	this study
A5_1	*Reticulitermes hesperus*	California	Digital PCR	HQ187724	2.2,2.7	this study
A7_1	*Reticulitermes hesperus*	California	Digital PCR	HQ187726	2.2,2.7	this study
A9_1	*Reticulitermes hesperus*	California	Digital PCR	HQ187728	2.2,2.7	this study
A12_1	*Reticulitermes hesperus*	California	Digital PCR	HQ187715	2.2,2.7	this study
A13_1	*Reticulitermes hesperus*	California	Digital PCR	HQ187716	2.2,2.7	this study
B2_2	*Reticulitermes hesperus*	California	Digital PCR	HQ187730	2.2,2.7	this study
E2_3	*Reticulitermes hesperus*	California	Digital PCR	HQ187740	2.2,2.7	this study
A6_1	*Reticulitermes hesperus*	California	Digital PCR	HQ187725	2.2,2.7	this study
F2_3	*Reticulitermes hesperus*	California	Digital PCR	HQ187743	2.2,2.7	this study
G2_3	*Reticulitermes hesperus*	California	Digital PCR	HQ187745	2.2,2.7	this study
G4_3	*Reticulitermes hesperus*	California	Digital PCR	HQ187747	2.2,2.7	this study
A2_1	*Reticulitermes hesperus*	California	Digital PCR	HQ187721	2.2,2.7	this study
A8_1	*Reticulitermes hesperus*	California	Digital PCR	HQ187727	2.2,2.7	this study
B3_2	*Reticulitermes hesperus*	California	Digital PCR	HQ187731	2.2,2.7	this study
A15_1	*Reticulitermes hesperus*	California	Digital PCR	HQ187718	2.7	this study
D2_2	*Reticulitermes hesperus*	California	Digital PCR	HQ187738	2.7	this study
A16_1	*Reticulitermes hesperus*	California	Digital PCR	HQ187719	2.7	this study
E3_3	*Reticulitermes hesperus*	California	Digital PCR	HQ187741	2.7	this study
A18_1	*Reticulitermes hesperus*	California	Digital PCR	HQ187720	2.7	this study
B5_2	*Reticulitermes hesperus*	California	Digital PCR	HQ187733	2.7	this study
G6_3	*Reticulitermes hesperus*	California	Digital PCR	HQ187749	2.7	this study
C3_2	*Reticulitermes hesperus*	California	Digital PCR	HQ187736	2.7	this study
C4_2	*Reticulitermes hesperus*	California	Digital PCR	HQ187737	2.7	this study
G7_3	*Reticulitermes hesperus*	California	Digital PCR	HQ187750	2.7	this study
B4_1	*Reticulitermes hesperus*	California	Digital PCR	HQ187732	2.7	this study
rF100	*Reticulitermes hesperus*	California	Digital PCR	HQ187634	2.7	this study
rF12	*Reticulitermes hesperus*	California	Digital PCR	HQ187635	2.7	this study
rF13	*Reticulitermes hesperus*	California	Digital PCR	HQ187636	2.7	this study
rF14	*Reticulitermes hesperus*	California	Digital PCR	HQ187637	2.7	this study
rF16	*Reticulitermes hesperus*	California	Digital PCR	HQ187638	2.7	this study
rF21	*Reticulitermes hesperus*	California	Digital PCR	HQ187639	2.7	this study
rF22	*Reticulitermes hesperus*	California	Digital PCR	HQ187640	2.7	this study
rF23	*Reticulitermes hesperus*	California	Digital PCR	HQ187641	2.7	this study
rF24	*Reticulitermes hesperus*	California	Digital PCR	HQ187642	2.7	this study
rF26	*Reticulitermes hesperus*	California	Digital PCR	HQ187643	2.7	this study
rF28	*Reticulitermes hesperus*	California	Digital PCR	HQ187644	2.7	this study
rF29	*Reticulitermes hesperus*	California	Digital PCR	HQ187645	2.7	this study
rF3	*Reticulitermes hesperus*	California	Digital PCR	HQ187646	2.7	this study
rF33	*Reticulitermes hesperus*	California	Digital PCR	HQ187647	2.7	this study

rF39	*Reticulitermes hesperus*	California	Digital PCR	HQ187648	2.7	this study
rF40	*Reticulitermes hesperus*	California	Digital PCR	HQ187649	2.7	this study
rF43	*Reticulitermes hesperus*	California	Digital PCR	HQ187650	2.7	this study
rF47	*Reticulitermes hesperus*	California	Digital PCR	HQ187651	2.7	this study
rF5	*Reticulitermes hesperus*	California	Digital PCR	HQ187652	2.7	this study
rF52	*Reticulitermes hesperus*	California	Digital PCR	HQ187653	2.7	this study
rF56	*Reticulitermes hesperus*	California	Digital PCR	HQ187654	2.7	this study
rF61	*Reticulitermes hesperus*	California	Digital PCR	HQ187655	2.7	this study
rF63	*Reticulitermes hesperus*	California	Digital PCR	HQ187656	2.7	this study
rF68	*Reticulitermes hesperus*	California	Digital PCR	HQ187657	2.7	this study
rF69	*Reticulitermes hesperus*	California	Digital PCR	HQ187658	2.7	this study
rF71	*Reticulitermes hesperus*	California	Digital PCR	HQ187659	2.7	this study
rF75	*Reticulitermes hesperus*	California	Digital PCR	HQ187660	2.7	this study
rF77	*Reticulitermes hesperus*	California	Digital PCR	HQ187661	2.7	this study
rF79	*Reticulitermes hesperus*	California	Digital PCR	HQ187662	2.7	this study
rF8	*Reticulitermes hesperus*	California	Digital PCR	HQ187663	2.7	this study
rF81	*Reticulitermes hesperus*	California	Digital PCR	HQ187664	2.7	this study
rF82	*Reticulitermes hesperus*	California	Digital PCR	HQ187665	2.7	this study
rF83	*Reticulitermes hesperus*	California	Digital PCR	HQ187666	2.7	this study
rF84	*Reticulitermes hesperus*	California	Digital PCR	HQ187667	2.7	this study
rF86	*Reticulitermes hesperus*	California	Digital PCR	HQ187668	2.7	this study
rF88	*Reticulitermes hesperus*	California	Digital PCR	HQ187669	2.7	this study
rF92	*Reticulitermes hesperus*	California	Digital PCR	HQ187670	2.7	this study
rF93	*Reticulitermes hesperus*	California	Digital PCR	HQ187671	2.7	this study
rF94	*Reticulitermes hesperus*	California	Digital PCR	HQ187672	2.7	this study
rF95	*Reticulitermes hesperus*	California	Digital PCR	HQ187673	2.7	this study
rG11	*Reticulitermes hesperus*	California	Digital PCR	HQ187674	2.7	this study
rG14	*Reticulitermes hesperus*	California	Digital PCR	HQ187675	2.7	this study
rG15	*Reticulitermes hesperus*	California	Digital PCR	HQ187676	2.7	this study
rG16	*Reticulitermes hesperus*	California	Digital PCR	HQ187677	2.7	this study
rG17	*Reticulitermes hesperus*	California	Digital PCR	HQ187678	2.7	this study
rG20	*Reticulitermes hesperus*	California	Digital PCR	HQ187679	2.7	this study
rG24	*Reticulitermes hesperus*	California	Digital PCR	HQ187680	2.7	this study
rG25	*Reticulitermes hesperus*	California	Digital PCR	HQ187681	2.7	this study
rG28	*Reticulitermes hesperus*	California	Digital PCR	HQ187682	2.7	this study
rG29	*Reticulitermes hesperus*	California	Digital PCR	HQ187683	2.7	this study
rG3	*Reticulitermes hesperus*	California	Digital PCR	HQ187684	2.7	this study
rG30	*Reticulitermes hesperus*	California	Digital PCR	HQ187685	2.7	this study
rG31	*Reticulitermes hesperus*	California	Digital PCR	HQ187686	2.7	this study
rG32	*Reticulitermes hesperus*	California	Digital PCR	HQ187687	2.7	this study
rG35	*Reticulitermes hesperus*	California	Digital PCR	HQ187688	2.7	this study

rG36	*Reticulitermes hesperus*	California	Digital PCR	HQ187689	2.7	this study
rG41	*Reticulitermes hesperus*	California	Digital PCR	HQ187690	2.7	this study
rG42	*Reticulitermes hesperus*	California	Digital PCR	HQ187691	2.7	this study
rG43	*Reticulitermes hesperus*	California	Digital PCR	HQ187692	2.7	this study
rG49	*Reticulitermes hesperus*	California	Digital PCR	HQ187693	2.7	this study
rG50	*Reticulitermes hesperus*	California	Digital PCR	HQ187694	2.7	this study
rG53	*Reticulitermes hesperus*	California	Digital PCR	HQ187695	2.7	this study
rG55	*Reticulitermes hesperus*	California	Digital PCR	HQ187696	2.7	this study
rG60	*Reticulitermes hesperus*	California	Digital PCR	HQ187697	2.7	this study
rG63	*Reticulitermes hesperus*	California	Digital PCR	HQ187698	2.7	this study
rG71	*Reticulitermes hesperus*	California	Digital PCR	HQ187699	2.7	this study
rG72	*Reticulitermes hesperus*	California	Digital PCR	HQ187700	2.7	this study
rG73	*Reticulitermes hesperus*	California	Digital PCR	HQ187701	2.7	this study
rG74	*Reticulitermes hesperus*	California	Digital PCR	HQ187702	2.7	this study
rG78	*Reticulitermes hesperus*	California	Digital PCR	HQ187703	2.7	this study
rG80	*Reticulitermes hesperus*	California	Digital PCR	HQ187704	2.7	this study
rG81	*Reticulitermes hesperus*	California	Digital PCR	HQ187705	2.7	this study
rG83	*Reticulitermes hesperus*	California	Digital PCR	HQ187706	2.7	this study
rG86	*Reticulitermes hesperus*	California	Digital PCR	HQ187707	2.7	this study
rG88	*Reticulitermes hesperus*	California	Digital PCR	HQ187708	2.7	this study
rG9	*Reticulitermes hesperus*	California	Digital PCR	HQ187709	2.7	this study
rG91	*Reticulitermes hesperus*	California	Digital PCR	HQ187710	2.7	this study
rG95	*Reticulitermes hesperus*	California	Digital PCR	HQ187711	2.7	this study
SSU rRNA gene - close relatives and other termite related						
unc Trep clone RFS84	*Reticulitermes flavipes*	Michigan	PCR	AF068428	2.7	(*S64*)
unc Trep clone RFS99	*Reticulitermes flavipes*	Michigan	PCR	AF068424	2.7	(*S64*)
unc Trep clone RFS94	*Reticulitermes flavipes*	Michigan	PCR	AF068423	2.7	(*S64*)
unc Trep clone RFS21	*Reticulitermes flavipes*	Michigan	PCR	AF068338	2.7	(*S64*)
unc Trep clone RFS12	*Reticulitermes flavipes*	Michigan	PCR	AF068335	2.7	(*S64*)
unc Trep clone RFS2	*Reticulitermes flavipes*	Michigan	PCR	AF068429	2.7	(*S64*)
unc Trep sp.	*Reticulitermes speratus*	Asia	PCR	AB192140	2.7	(*S85*)
unc Trep sp.	*Reticulitermes speratus*	Asia	PCR	AB192197	2.7	(*S85*)
unc Trep sp.	*Reticulitermes speratus*	Asia	PCR	AB192202	2.7	(*S85*)
unc Trep sp.	*Reticulitermes speratus*	Asia	PCR	AB192142	2.7	(*S85*)
unc Trep sp.	*Reticulitermes sp.*	Asia	PCR	AB192251	2.7	(*S85*)
unc Trep sp.	*Reticulitermes sp.*	Asia	PCR	AB192248	2.7	(*S85*)
unc Trep sp.	*Reticulitermes sp.*	Asia	PCR	AB192247	2.7	(*S85*)
unc Trep sp.	*Reticulitermes speratus*	Asia	PCR	AB088870	2.7	(*S73*)
unc Trep sp.	*Reticulitermes speratus*	Asia	PCR	AB088896	2.7	(*S73*)
unc Trep sp.	*Reticulitermes speratus*	Asia	PCR	AB088915	2.7	(*S73*)
unc Trep sp.	*Reticulitermes speratus*	Asia	PCR	AB088876	2.7	(*S73*)

unc Trep sp.	*Reticulitermes speratus*	Asia	PCR	AB088895	2.7	(*S73*)
unc Trep sp.	*Reticulitermes speratus*	Asia	PCR	AB088866	2.7	(*S73*)
unc Trep sp.	*Reticulitermes speratus*	Asia	PCR	AB088874	2.7	(*S73*)
unc Trep sp.	*Reticulitermes speratus*	Asia	PCR	AB088890	2.7	(*S73*)
unc Trep sp.	*Reticulitermes speratus*	Asia	PCR	AB088878	2.7	(*S73*)
unc Trep sp.	*Reticulitermes speratus*	Asia	PCR	AB088909	2.7	(*S73*)
unc Trep clone HsDiSp314	*Hodotermopsis sjoestedti*	Asia	PCR	AB032005	2.7	(*S86*)
SSU rRNA gene - non termite related						
Treponema vincentii (D2A-2)		Oral cavity	isolate	AY119690	2.7	(*S87*)
Treponema denticola (ATCC 35405)		Oral cavity	isolate	AE017226	2.7	(*S88*)
Treponema pallidum (Nichols)		Human genital tract	isolate	AE000520	2.7	(*S89*)
Treponema zioleckii (kT)		Sheep rumen	isolate	DQ065758	2.7	(*S90*)
Treponema socranskii (socranskii)		Oral cavity	isolate	AF033306	2.7	(*S91*)
Treponema succinifaciens		Pig colon	isolate	M57738	2.7	(*S92*)
Brevinema andersonii		Shrews and mice	isolate	L31543	2.7	(*S93*)
Borrelia burgdorferi (DK7)		Ticks, deer and humans	isolate	X85195	2.7	(*S94*)
Spirochaeta aurantia (M1)		Fresh water	isolate	AY599019	2.7	(*S95*)
Escherichia coli K-12 MG1655		-	isolate	U00096	2.7	(*S96*)

Table 2.12. Analysis of all FAM hits for a number of microfluidic array panels. For several microfluidic array panels, all chambers exhibiting amplification in the FAM fluorescence channel were retrieved, post-amplified and analyzed by agarose gel electrophoresis. In this table we show the total number of chambers that exhibited FAM fluorescence on the given panel ("Total FAM hits"), the number of false positives based on analysis by agarose gel electrophoresis ("# of false positives"), the mean number of false positives per array ("Mean # of false positives"), and the average number of chambers that exhibited FAM fluorescence in the no-template-control panel on the same array ("# of FAM hits in NTC panel"). The mean number of false positive hits agrees well with the number of hits in the corresponding no-template-control panel indicating the latter is a good predictor of the former. See supporting text for further details.

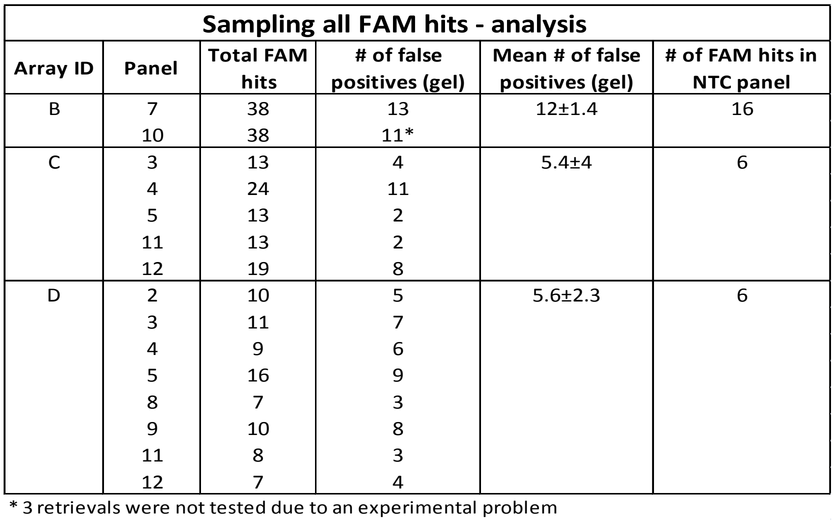

Sampling all FAM hits - analysis					
Array ID	**Panel**	**Total FAM hits**	**# of false positives (gel)**	**Mean # of false positives (gel)**	**# of FAM hits in NTC panel**
B	7	38	13	12±1.4	16
	10	38	11*		
C	3	13	4	5.4±4	6
	4	24	11		
	5	13	2		
	11	13	2		
	12	19	8		
D	2	10	5	5.6±2.3	6
	3	11	7		
	4	9	6		
	5	16	9		
	8	7	3		
	9	10	8		
	11	8	3		
	12	7	4		

* 3 retrievals were not tested due to an experimental problem

Table 2.13. Definition of variables used in the microfluidic array statistical model. See supporting text for further details.

Variable	Definition	Estimation method
X	Number of FAM hits per panel	Measured
Y	Number of HEX hits per panel	Measured
I	Number of wells per panel with both a FAM hit and a HEX hit (i.e. co-localization)	Measured
noise	Number of FAM hits that are due to spurious amplification	Measured
f_S	Frequency of ribotype ***S*** on the chip	Measured
$\varepsilon_{ter/16S}$	Terminase/16S primer efficiency	Measured
X_f	Number of non co-localized FAM events	$X_f = X - I$
p_{ter}	The probability that a given well will contain a free floating terminase target	Eq. S1
I_{S}	Average number of free floating terminase targets to co-localize with a *particular* 16S rRNA ribotype ***S*** on a panel	Eq. S2a
$I_{\text{all 16S-ter}}$	Average number of any terminase target to co-localize with any 16S rRNA target on a panel	Eq. S2b
p_F	Probability that a successful retrieval from a panel contains a particular ribotype ***S*** and any terminase gene by chance	Eq. S3
X_T	Sum of the total number of free floating terminase targets and spurious targets	Eq. S4
N_{false}	Expected number of false co-localizations in the dataset	Eq. S5
p_S	Probability that a successful retrieval will contain host ***S***	Eq. S6

Table 2.14. Statistics for all sampled panels. This table lists for each ribotype in Fig. 2.2 the panel from which the ribotype was retrieved, the number of FAM hits *X* on that panel, the number of HEX hits *Y* on that panel, their intersection *I*, the number of FAM hits found in the no-target-control-panel for the microfluidic array containing the given panel (*noise*), the frequency of this host in the reference rRNA library, f_s (based on Table 2.6), the estimated probability for false co-localization p_F (Eq. S3), and the P value (one-tailed test, *n*=41) for each host for obtaining at least the number of observed co-localizations by chance (based on the data in Table 2.1). The statistical test to determine the P value is explained in the supporting text. Chip analysis was performed using the Fluidigm Digital PCR Analysis software v.2.1.1 with the linear baseline correction. See supporting text for further details.

#	Retrieval ID (*n*=41)	Host	chip	panel	X (FAM)	Y (HEX)	I	*noise* (FAM)	X$_T$-*noise*	p_{ter}	$I_{all16S\text{-}ter}$	f_S	p_F	P value (*n*=41)
1	A1_1	I	A	3	22	38	2	15	6.0	7.9E-03	1.3	4.2%	7.77E-03	5.45E-18
2	A3_1	I	A	5	33	66	8	15	12.4	1.6E-02	6.7			
3	A10_1	I	A	8	40	59	12	15	15.3	2.0E-02	10.8			
4	A11_1	I	A	9	34	46	9	15	11.6	1.5E-02	8.1			
5	A14_1	I	A	10	30	46	11	15	5.2	6.8E-03	10.1			
6	B1_2	I	B	10	42	52	5	20	19.7	2.6E-02	3.6			
7	C1_2	I	C	11	13	55	3	6	4.8	6.2E-03	2.6			
8	C2_2	I	C	5	13	69	4	6	3.9	5.1E-03	3.5			
9	E1_3	I	E	2	14	21	2	5	7.3	9.6E-03	1.9			
10	F1_3	I	F	3	22	32	2	7	13.9	1.8E-02	1.7			
11	G1_3	I	G	3	12	51	4	6	2.6	3.4E-03	3.6			
12	G3_3	I	G	8	17	33	2	6	9.7	1.3E-02	1.7			
13	G5_3	I	G	11	14	26	1	6	7.5	9.7E-03	0.8			
14	A4_1	II	A	6	54	79	10	15	34.1	4.5E-02	8.5	1.7%	3.11E-03	7.63E-13
15	A5_1	II	A	6	54	79	10	15	34.1	4.5E-02	8.5			
16	A7_1	II	A	8	40	59	12	15	15.3	2.0E-02	10.8			
17	A9_1	II	A	8	40	59	12	15	15.3	2.0E-02	10.8			
18	A12_1	II	A	10	30	46	11	15	5.2	6.8E-03	10.1			
19	A13_1	II	A	10	30	46	11	15	5.2	6.8E-03	10.1			
20	B2_2	II	B	10	42	52	5	20	19.7	2.6E-02	3.6			
21	E2_3	II	E	2	14	21	2	5	7.3	9.6E-03	1.9			
22	A6_1	III	A	7	40	66	8	15	20.0	2.6E-02	6.7	0.9%	1.55E-03	5.65E-07
23	F2_3	III	F	8	21	34	6	7	8.7	1.1E-02	5.7			
24	G2_3	III	G	4	20	53	3	6	12.3	1.6E-02	2.6			
25	G4_3	III	G	10	19	36	2	6	11.8	1.5E-02	1.7			
26	A2_1	IV	A	4	46	129	17	15	19.9	2.6E-02	14.5	0.9%	1.55E-03	3.83E-05
27	A8_1	IV	A	8	40	59	12	15	15.3	2.0E-02	10.8			
28	B3_2	IV	B	10	42	52	5	20	19.7	2.6E-02	3.6			
29	A15_1	-	A	4	46	129	17	15	19.9	2.6E-02	14.5	-	-	-
30	A16_1	-	A	5	33	66	8	15	12.4	1.6E-02	6.7	-	-	-
31	A17_1	-	A	10	30	46	11	15	5.2	6.8E-03	10.1	-	-	-
32	A18_1	-	A	11	27	84	7	15	7.5	9.8E-03	5.4	-	-	-
33	B5_2	-	B	7	46	53	11	20	17.6	2.3E-02	9.6	-	-	-
34	B4_2	-	B	7	46	53	11	20	17.6	2.3E-02	9.6	-	-	-
35	C3_2	-	C	11	13	55	3	6	4.8	6.2E-03	2.6	-	-	-
36	C4_2	-	C	11	13	55	3	6	4.8	6.2E-03	2.6	-	-	-
37	D1_2	-	D	4	9	24	1	8	0.3	3.4E-04	0.7	-	-	-
38	D2_2	-	D	3	11	26	1	8	2.4	3.1E-03	0.7	-	-	-
39	E3_3	-	E	11	12	24	2	5	5.3	7.0E-03	1.8	-	-	-
40	G6_3	-	G	4	20	53	3	6	12.3	1.6E-02	2.6	-	-	-
41	G7_3	-	G	4	20	53	3	6	12.3	1.6E-02	2.6	-	-	-

2.9.5 References

*S*1. E. Ottesen, J. Hong, S. Quake, J. Leadbetter, *Science* **314**, 1464 (2006).

*S*2. E. Ottesen, PhD thesis, California Institute of Technology (2008).

*S*3. J. Austin, A. Szalanski, B. Cabrera, *Ann. Entomol. Soc. Am.* **97**, 548 (2004).

*S*4. M. Ohkuma et al., *Mol. Phylogenet. Evol.* **31**, 701 (2004).

*S*5. F. Warnecke et al., *Nature* **450**, 560 (2007).

*S*6. K. Maekawa, N. Lo, O. Kitade, T. Miura, T. Matsumoto, *Mol. Phylogenet. Evol.* **13**, 360 (1999).

*S*7. H. Liu, A. Beckenbach, *Mol. Phylogenet. Evol.* **1**, 41 (1992).

*S*8. K. Ashelford, N. Chuzhanova, J. Fry, A. Jones, A. Weightman, *Appl. Environ. Microbiol.* **71**, 7724 (2005).

*S*9. T. Huber, G. Faulkner, P. Hugenholtz, *Bioinformatics* **20**, 2317 (2004).

*S*10. T. DeSantis et al., *Appl. Environ. Microbiol.* **72**, 5069 (2006).

*S*11. E. Pruesse et al., *Nucleic Acids Res.* **35**, 7188 (2007).

*S*12. W. Ludwig et al., *Nucleic Acids Res.* **32**, 1363 (2004).

*S*13. D. Posada, *Mol. Biol. Evol.* **25**, 1253 (2008).

*S*14. S. Guindon, O. Gascuel, *Syst. Biol.* **52**, 696 (2003).

*S*15. K. Tamura, M. Nei, *Mol. Biol. Evol.* **10**, 512 (1993).

*S*16. J. Felsenstein, *Phylogeny inference package (PHYLIP), Version 3.6 a3* (2002).

*S*17. W. Fitch, E. Margoliash, *Science* **155**, 279 (1967).

*S*18. J. Thompson, D. Higgins, T. Gibson, *Nucleic Acids Res.* **22**, 4673 (1994).

*S*19. K. Tamura, J. Dudley, M. Nei, S. Kumar, *Mol. Biol. Evol.* **24**, 1596 (2007).

*S*20. L. Heath, E. Van Der Walt, A. Varsani, D. Martin, *J. Virol.* **80**, 11827 (2006).

*S*21. M. Padidam, S. Sawyer, C. Fauquet, *Virology* **265**, 218 (1999).

*S*22. J. Smith, *J. Mol. Evol.* **34**, 126 (1992).

*S*23. D. Martin, E. Rybicki, *Bioinformatics* **16**, 562 (2000).

*S*24. D. Posada, *Mol. Biol. Evol.* **19**, 708 (2002).

*S*25. D. Posada, K. Crandall, *Proc. Natl. Acad. Sci. USA* **98**, 13757 (2001).

*S*26. M. O. Salminen, J. K. Carr, D. S. Burke, F. E. McCutchan, *AIDS Res. Hum. Retroviruses* **11**, 1423 (1995).

*S*27. M. Salminen, D. Marin, in *The Phylogenetic Handbook: A Practical Approach to Phylogenetic Analysis and Hypothesis Testing,* P. Lemey, M. Salemi, A. Vandamme, Eds. (Cambridge University Press; 2nd edition, 2010), pp. 519-548.

*S*28. D. Huson, D. Bryant, *Mol. Biol. Evol.* **23**, 254 (2006).

*S*29. N. Tao et al., *FINDMODEL: a tool to select the best-fit model of nucleotide substitution*, M.S. thesis, University of New Mexico (2005).

*S*30. K. Strimmer, A. Von Haeseler, *Proc. Natl. Acad. Sci. USA* **94**, 6815 (1997).

*S*31. H. Schmidt, A. von Haeseler, in *The Phylogenetic Handbook: A Practical Approach to Phylogenetic Analysis and Hypothesis Testing,* P. Lemey, M. Salemi, A. Vandamme, Eds. (Cambridge University Press; 2nd edition, 2010), pp. 181-209.

*S*32. J. Leadbetter, T. Schmidt, J. Graber, J. Breznak, *Science* **283**, 686 (1999).

*S*33. T. Lilburn et al., *Science* **292**, 2495 (2001).

*S*34. T. Rose et al., *Nucleic Acids Res.* **26**, 1628 (1998).

*S*35. Y. Zhang et al., *Nucleic Acids Res.* **31**, doi: 10.1093/nar/gng123 (2003).

*S*36. C. Corless et al., *J. Clin. Microbiol.* **38**, 1747 (2000).

*S*37. S. Pond, S. Muse, *HyPhy: hypothesis testing using phylogenies*. Statistical Methods in Molecular Evolution (Springer, 2005), pp. 125-181.

*S*38. S. Pond, S. Muse, in *The Phylogenetic Handbook: A Practical Approach to Phylogenetic Analysis and Hypothesis Testing,* P. Lemey, M. Salemi, A. Vandamme, Eds. (Cambridge University Press; 2nd edition, 2010), pp. 419-490.

*S*39. S. Muse, B. Gaut, *Mol. Biol. Evol.* **11**, 715 (1994).

*S*40. S. Altschul et al., *Nucleic Acids Res.* **25**, 3389 (1997).

*S*41. K. Pruitt, T. Tatusova, D. Maglott, *Nucleic Acids Res.* **33**, D501 (2005).

*S*42. S. Casjens, *Mol. Microbiol.* **49**, 277 (2003).

*S*43. S. Dube, J. Qin, R. Ramakrishnan, *PLoS ONE* **3**, doi:10.1371/journal.pone.0002876 (2008).

*S*44. L. Black, *Bioessays* **17**, 1025 (1995).

*S*45. S. Casjens et al., *J. Bacteriol.* **187**, 1091 (2005).

*S*46. H. Ackermann, *Adv. Virus Res.* **51**, 135 (1999).

*S*47. S. R. Casjens, *Res. Microbiol.* **159**, 340 (2008).

*S*48. J. Lawrence, G. Hatfull, R. Hendrix, *J. Bacteriol.* **184**, 4891 (2002).

*S*49. M. Daw, F. Falkiner, *Micron* **27**, 467 (1996).

*S*50. K. Nakayama et al., *Mol. Microbiol.* **38**, 213 (2000).

*S*51. Y. Michel-Briand, C. Baysse, *Biochimie* **84**, 499 (2002).

*S*52. A. Lang, J. Beatty, *Proc. Natl. Acad. Sci. USA* **97**, 859 (2000).

*S*53. A. Lang, J. Beatty, *Arch. Microbiol.* **175**, 241 (2001).

*S*54. A. Lang, J. Beatty, *Trends Microbiol.* **15**, 54 (2007).

*S*55. M. Mitchell, S. Matsuzaki, S. Imai, V. Rao, *Nucleic Acids Res.* **30**, 4009 (2002).

*S*56. A. Davison, *Virology* **186**, 9 (1992).

*S*57. E. Koonin, T. Senkevich, V. Dolja, *Biol. Direct* **1**, 29 (2006).

*S*58. M. Baker, W. Jiang, F. Rixon, W. Chiu, *J. Virol.* **79**, 14967 (2005).

*S*59. S. Kanamaru, K. Kondabagil, M. Rossmann, V. Rao, *J. Biol. Chem.* **279**, 40795 (2004).

*S*60. A. Marchler-Bauer et al., *Nucleic Acids Res.* **33**, D192 (2005).

*S*61. R. Edgar, *BMC bioinformatics* **5**, 113 (2004).

*S*62. V. Rao, M. Feiss, *Annu. Rev. Genet.* **42**, 647 (2008).

*S*63. S. Sun et al., *Cell* **135**, 1251 (2008).

*S*64. S. Lilburn, *Environ. Microbiol.* **1**, 331 (1999).

*S*65. J. Breznak, J. Leadbetter, *Prokaryotes* **7**, 318 (2006).

*S*66. B. Paster et al., *J. Bacteriol.* **173**, 6101 (1991).

*S*67. W. Ludwig, O. Strunk, R. Westram, L. Richter, H. Meier, *Nucleic Acids Res.* **32**, 1363 (2004).

*S*68. D. Bryant, V. Moulton, *Mol. Biol. Evol.* **21**, 255 (2004).

*S*69. M. Kimura, *J. Mol. Evol.* **16**, 111 (1980).

S70. T. Jukes, C. Cantor, *Mammalian protein metabolism* **3**, 21 (1969).

S71. P. Schloss, J. Handelsman, *Appl. Environ. Microbiol.* **71**, 1501 (2005).

*S*72. J. Cole et al., *Nucleic Acids Res.* **37**, doi: 10.1093/nar/gkn879 (2008).

*S*73. Y. Hongoh, M. Ohkuma, T. Kudo, *FEMS Microbiol. Ecol.* **44**, 231 (2003).

*S*74. B. Paster et al., *Appl. Environ. Microbiol.* **62**, 347 (1996).

*S*75. W. Ikeda-Ohtsubo, M. Desai, U. Stingl, A. Brune, *Microbiology* **153**, 3458 (2007).

*S*76. M. Nei, T. Gojobori, *Mol. Biol. Evol.* **3**, 418 (1986).

*S*77. J. Zhang, H. Rosenberg, M. Nei, *Proc. Natl. Acad. Sci. USA* **95**, 3708 (1998).

*S*78. W. Li, C. Wu, C. Luo, *Mol. Biol. Evol.* **2**, 150 (1985).

*S*79. P. Pamilo, N. Bianchi, *Mol. Biol. Evol.* **10**, 271 (1993).

*S*80. M. Nei, S. Kumar, *Molecular evolution and phylogenetics* (Oxford University Press, USA, 2000).

*S*81. E. Miller et al., *Microbiol. Mol. Biol. Rev.* **67**, 86 (2003).

*S*82. W. Reeve et al., *Standards in Genomic Sciences* **2**, 77 (2010).

*S*83. C. Prust et al., *Nat. Biotechnol.* **23**, 195 (2005).

*S*84. V. Kunin et al., *Mol. syst. biol.* **4**, 198 (2008).

*S*85. Y. Hongoh et al., *Appl. Environ. Microbiol.* **71**, 6590 (2005).

*S*86. T. Iida, M. Ohkuma, K. Ohtoko, T. Kudo, *FEMS Microbiol. Ecol.* **34**, 17 (2000).

*S*87. A. Edwards, D. Dymock, M. Woodward, H. Jenkinson, *Microbiology* **149**, 1083 (2003).

*S*88. R. Seshadri et al., *Proc. Natl. Acad. Sci. USA* **101**, 5646 (2004).

*S*89. C. Fraser et al., *Science* **281**, 375 (1998).

*S*90. M. Piknova et al., *FEMS Microbiol. Lett.* **289**, 166 (2008).

*S*91. B. Paster, F. Dewhirst, B. Coleman, C. Lau, R. Ericson, *Int. J. Syst. Evol. Micr.* **48**, 713 (1998).

*S*92. T. Stanton et al., *Int. J. Syst. Bacteriol.* **41**, 50 (1991).

*S*93. D. Defosse, R. Johnson, B. Paster, F. Dewhirst, G. Fraser, *Int. J. Syst. Evol. Micr.* **45**, 78 (1995).

*S*94. M. Theisen et al., *J. Bacteriol.* **177**, 3036 (1995).

*S*95. R. McLaughlin, D. Secko, C. Paul, A. Kropinski, *Can. J. Microbiol.* **50**, 967 (2004).

*S*96. W. Kang, T. Icho, S. Isono, M. Kitakawa, K. Isono, *Mol. Gen. Genet.* **217**, 281 (1989).

S97. A. P. Martin, *Appl. Environ. Microbiol.* **68**, 3673 (2002).

S98. C. Lozupone, M. Hamady, R. Knight, *BMC bioinformatics* **7**, 371 (2006).

S99. M. Hamady, C. Lozupone, R. Knight, *The ISME journal* **4**, 17 (2009).